MULTITERMINAL SOURCE CODING: SUM-RATE LOSS, CODE DESIGNS, AND APPLICATIONS TO VIDEO SENSOR NETWORKS

A Dissertation

by

YANG YANG

Submitted to the Office of Graduate Studies of
Texas A&M University
in partial fulfillment of the requirements for the degree of

DOCTOR OF PHILOSOPHY

December 2008

Major Subject: Electrical Engineering

MULTITERMINAL SOURCE CODING: SUM-RATE LOSS, CODE DESIGNS, AND APPLICATIONS TO VIDEO SENSOR NETWORKS

A Dissertation

by

YANG YANG

Submitted to the Office of Graduate Studies of
Texas A&M University
in partial fulfillment of the requirements for the degree of

DOCTOR OF PHILOSOPHY

Approved by:

Chair of Committee,	Zixiang Xiong
Committee Members,	Costas N. Georghiades
	Mosong Cheng
	Wei Zhao
Head of Department,	Costas N. Georghiades

December 2008

Major Subject: Electrical Engineering

ABSTRACT

Multiterminal Source Coding: Sum-Rate Loss,
Code Designs, and Applications to Video Sensor Networks. (December 2008)
Yang Yang, B.S., Tsinghua University;
M.S., Texas A&M University
Chair of Advisory Committee: Dr. Zixiang Xiong

Driven by a host of emerging applications (e.g., sensor networks and wireless video), distributed source coding (i.e., Slepian-Wolf coding, Wyner-Ziv coding and various other forms of multiterminal source coding), has recently become a very active research area.

This dissertation focuses on multiterminal (MT) source coding problem, and consists of three parts. The first part studies the sum-rate loss of an important special case of quadratic Gaussian multi-terminal source coding, where all sources are *positively symmetric* and all target distortions are *equal*. We first give the minimum sum-rate for joint encoding of Gaussian sources in the symmetric case, and then show that the supremum of the sum-rate loss due to distributed encoding in this case is $\frac{1}{2}\log_2\frac{5}{4} = 0.161$ b/s when $L = 2$ and increases in the order of $\frac{\sqrt{L}}{2}\log_2 e$ b/s as the number of terminals L goes to infinity. The supremum sum-rate loss of 0.161 b/s in the symmetric case equals to that in general quadratic Gaussian two-terminal source coding without the symmetric assumption. It is conjectured that this equality holds for any number of terminals.

In the second part, we present two practical MT coding schemes under the framework of Slepian-Wolf coded quantization (SWCQ) for both direct and indirect MT problems. The first, *asymmetric* SWCQ scheme relies on quantization and Wyner-Ziv coding, and it is implemented via source splitting to achieve any point on the sum-rate bound. In the second, conceptually simpler scheme, *symmetric* SWCQ, the two quantized sources are compressed using symmetric Slepian-Wolf coding via a channel code partitioning technique

that is capable of achieving any point on the Slepian-Wolf sum-rate bound. Our practical designs employ trellis-coded quantization and turbo/LDPC codes for both asymmetric and symmetric Slepian-Wolf coding. Simulation results show a gap of only 0.139-0.194 bit per sample away from the sum-rate bound for both direct and indirect MT coding problems.

The third part applies the above two MT coding schemes to two practical sources, i.e., stereo video sequences to save the sum rate over independent coding of both sequences. Experiments with both schemes on stereo video sequences using H.264, LDPC codes for Slepian-Wolf coding of the motion vectors, and scalar quantization in conjunction with LDPC codes for Wyner-Ziv coding of the residual coefficients give slightly smaller sum rate than separate H.264 coding of both sequences at the same video quality.

To my parents

ACKNOWLEDGMENTS

I would like to express my deepest gratitude to Dr. Zixiang Xiong for his great patience and enlightening guidance. He was always a source of encouragement throughout my graduate studies. I would like to thank Dr. Wei Zhao for all his kind help without which I could not be where I am today. I would also like to thank Dr. Costas N. Georghiades, and Dr. Mosong Cheng for serving on my committee. I want to thank my colleagues in the Multimedia Laboratory for sharing their insightful knowledge with me. I am especially grateful to Dr. Vladimir Stanković, Samuel Cheng, and Angelos D. Liveris for their many helpful suggestions and assistance. I also want to express my hearty appreciation to my parents, who gave me not only life, but all their love.

TABLE OF CONTENTS

CHAPTER Page

Page

LIST OF TABLES

LIST OF FIGURES

FIGURE Page

FIGURE Page

CHAPTER I

INTRODUCTION

In many emerging applications (e.g., distributed sensor networks), multiple correlated sources need to be separately compressed at distributed terminals and transmitted to a central unit. Due to complexity and power constraints, the transmitters are often not allowed to communicate with each other. This gives rise to the problem of *multiterminal source coding* [4], which has thirty years of history.

Multiterminal (MT) source coding is a distributed source coding problem. Distributed source coding was started by Slepian and Wolf in 1973 [47], who considered separate lossless compression of two correlated sources, and showed the surprising result that separate encoding and joint decoding suffer no rate loss compared to the case when the sources are compressed jointly. Their seminal work [47] was subsequently extended to other distributed source coding scenarios. In 1976, Wyner and Ziv [62] extended one special case of Slepian-Wolf (SW) coding, namely, lossless source coding with decoder side information, to *lossy* source coding with decoder side information. Unlike SW coding, there is in general a rate loss with Wyner-Ziv (WZ) coding [62] compared to the lossy source coding problem when side information is also available at the encoder. An exception occurs when the source and side information are jointly Gaussian and the distortion measure is mean-squared error (MSE).

Soon after the celebrated works of Slepian and Wolf [47] and Wyner and Ziv [62], Berger [4] introduced the general problem of MT source coding by considering a more general case of separate *lossy* source coding of two (or more) sources[1]. Two classes of MT

The journal model is *IEEE Transactions on Automatic Control.*

[1]One can loosely think of MT source coding as the lossy version of SW coding.

source coding problems have been studied in the literature. In the original work of Berger and Tung [4, 55], the case where each encoder observes *directly* its source was considered; later, Yamamoto and Itoh [64] and Flynn and Gray [17] focused on another scenario where each encoder cannot observe directly the source that is to be reconstructed at the decoder, but is rather provided only with a noisy version. These two classes are distinguished as the *direct* and *indirect* (or *remote*) MT source coding problem, respectively. Note that in the latter case, often referred to as the CEO problem [36, 57], a single source is to be reconstructed at the decoder.

Theoretical study of the MT source coding problem amounts to determining the achievable rate region (i.e., all possible compression rate tuples) under distortion constraint(s) on the source(s). Finding the achievable rate region for general MT source coding is a difficult task and still remains open. Only inner and outer bounds[2] for both MT coding problems have been provided [4, 17, 55, 64].

Owing to the difficulty of the general MT source coding problem, researchers have focused on the *quadratic Gaussian* setup with Gaussian source(s) and MSE distortion measure. Theoretical results on the quadratic Gaussian MT source coding problem appeared in [4, 35, 55] for the direct setting and in [8, 36, 37, 40, 57] for the indirect/CEO setting. However, even for this special case, the achievable rate region was unknown until recently. The indirect/CEO problem (with arbitrary number of encoders) was solved independently by Oohama [37] in 1999 (and published recently in [38]) and Prabhakaran *et al.* [40], using the entropy power inequality [12]. But the direct MT source coding problem is more challenging because it requires the reconstruction of a *vector source* instead of a single remote source, and the lack of a vector version of the entropy power inequality has prevented the generalization of the proofs of [38, 40]. Consequently, the exact achievable rate region is

[2]All rate points within the inner bound are achievable, while those outside the outer bound are not.

still unknown for the direct MT source coding problem with arbitrary number of encoders. However, for the case with two encoders, Wagner *et al.* [58] made the connection in 2005 between the direct and indirect MT source coding problems (via a so-called μ-sum problem) and showed tightness of the Berger-Tung achievable bound [4, 55] by proving the converse.

It is interesting to investigate the exact sum-rate loss of distributed encoding as compared to joint encoding (and decoding) of Gaussian sources. To this end, In the first part of this dissertation, we study the minimum sum-rate for the joint encoding case. For general jointly Gaussian sources (without the symmetric assumption), the optimal joint encoding strategy is to first transform the sources into independent unit-variance Gaussian sources and then apply classical source coding on the transformed sources. Interestingly, our results indicate that the optimal transform varies with different target distortions, and is not always the Karhunen-Loéve transform (KLT) of the sources, and the minimum sum-rate of joint encoding can be obtained by solving an optimization problem over all achievable distortion matrices $\mathcal{D}$ (defined as the covariance matrix of the sources given the transmitted messages). Although we are not able to explicitly solve this optimization problem for general jointly Gaussian sources and target distortions, for the symmetric case we are interested in, the minimum sum-rate can be written in exact form and the KLT is always optimal. We also show that the supremum (i.e., the least upper bound, which is not achievable) of the sum-rate loss is only $\frac{1}{2}\log_2\frac{5}{4} = 0.161$ bit per sample (b/s) for quadratic Gaussian two-terminal source coding *with or without our symmetric assumption*. Moreover, our results indicate that for the quadratic Gaussian MT source coding problem with more than two positively symmetric sources and equal target distortions, the supremum of the sum-rate loss increases in the order of $\frac{\sqrt{L}}{2}\log_2 e$, where L is the number of terminals. We conjecture that for any integer $L > 2$, the supremum sum-rate loss in the symmetric case equals to that in general quadratic Gaussian MT source coding.

This conjecture is numerically verified for $L = 3$ and 4.

With the precise rate regions for both the direct and indirect quadratic Gaussian MT problems with two encoders recently provided in [38, 40, 58], now is the time to study practical code designs that are capable of achieving any point in these regions. Compared to the body of theoretical works on MT source coding problems, research on practical code designs is still in its infancy. Targeting the tight sum-rate bound for the two-encoder quadratic Gaussian CEO problem [38, 40], Pradhan and Ramchandran [42] provided a code design based on generalized coset codes, with fixed-rate scalar quantizers and trellis codes. Although capable of trading off transmission rates between the two encoders, the design in [42] performs relatively far away from the theoretical limits, especially at low rates. Motivated by the fact that WZ coding [62] is a special case of MT coding, in an earlier work [66], we proposed an asymmetric coding system for the CEO problem that essentially relies on WZ coding. Although the scheme in [66] gives better results than those of [42], it is limited to approaching the two corner points of the achievable rate region only.

In the second part of this dissertation, we focus on practical code designs for the quadratic Gaussian direct and indirect MT problems with two encoders. Generally speaking, MT source coding is a joint source-channel coding problem: first, its lossy nature necessitates quantization of the sources; second, the distributed nature of the encoders calls for compression (after quantization) by SW coding, which is commonly implemented by a channel code. More importantly, one of the conclusions of the theoretical works of [38, 40, 58] is that vector quantization (VQ) plus SW coding is indeed optimal for the quadratic Gaussian MT source coding *with two terminals*[3]. Following this guiding principle, we propose a framework called Slepian-Wolf coded quantization (SWCQ) for practical MT source coding. Unlike nested lattice codes suggested by Zamir *et al.* [76] and

[3]We point out that separate VQ and SW coding is in general not optimal for MT source coding.

generalized coset codes used by Pradhan and Ramchandran [42], which are essentially nested source-channel codes, SWCQ explicitly separates the SW coding component from the vector quantizers at the encoder (while employing joint estimation/reconstruction at the decoder). This approach not only allows us to design a good source code and a good channel code individually, but also enables us to evaluate the practical performance loss due to source coding and channel coding separately. Moreover, SWCQ is very general as it applies to both direct and indirect MT source coding problems. It also generalizes similar approaches recently developed in [28, 65] for WZ coding.

Slepian and Wolf [47] showed that the separate compression of two correlated sources can be near lossless at the total rate of their joint entropy. In particular, when one source is available only at the decoder as *side information*, the other source can still be near-losslessly compressed at the rate of its conditional entropy given the decoder side information. This special case corresponds to the two *corner points* of the SW rate region, and is called *asymmetric* SW coding; on the other hand, *symmetric* (or more precisely, *non-asymmetric*) SW coding attempts to approach any point between the two corner points. Correspondingly, two classes of SW code designs exist in the literature. *Asymmetric SW code designs* based on coset codes [41], turbo codes [1, 2, 20, 30] and low-density parity-check (LDPC) codes [29, 54] were developed for binary sources. The main idea [61] is to compress a binary input source sequence to the *syndrome* of a linear channel code for the "virtual" correlation channel between the source and the decoder side information, and find the binary sequence with the same syndrome that is closest to the side information at the decoder. This syndrome-based method can approach one of the two corner points of the SW rate region if the employed channel code approaches the capacity of the "virtual" correlation channel.

In practical applications (e.g., sensor networks), it is preferable for the encoders to be able to operate at flexible rates. This necessitates *symmetric SW coding*. The most

straightforward approach is time-sharing between the two corner points. However, time-sharing might not be practical because it requires synchronization between the encoders. An alternative is the *source splitting* approach introduced by Rimoldi and Urbanke [46]. By "splitting" one source into two subsources, arbitrary point on the two-terminal SW rate region can be mapped to the corner point of a three-terminal SW rate region, which can be approached using asymmetric SW coding. A drawback of source splitting is that it increases coding complexity and introduces extra error propagations. Recently, Pradhan and Ramchandran [42] suggested a method for symmetric SW coding based on partitioning a single parity-check code. Following this idea, in [49], a practical code design method for symmetric SW coding of uniform binary sources was developed; assuming binary symmetric correlation channel between two sources, the designs of [49] with irregular repeat-accumulate codes [25] and turbo codes [5] give results that are very close to the SW limit.

Combining trellis coded quantization (TCQ) [33], as the most powerful source coding technique, with asymmetric and symmetric SW coding, respectively, we present in this dissertation two practical designs under the SWCQ framework for both direct and indirect quadratic Gaussian MT source coding with two encoders. The first *asymmetric SWCQ* scheme employs quantization (i.e., TCQ), asymmetric SW coding, and source splitting to realize MT source coding with two encoders. More precisely, our MT source code design is "split" into one classic source coding component and two WZ coding components. While classic source coding relies on entropy-coded VQ, WZ coding is implemented by combining TCQ and turbo/LDPC codes (for asymmetric SW coding).

In our second *symmetric SWCQ* scheme, the outputs of two TCQs are compressed using symmetric SW coding, which is based on the concept of channel code partitioning [49] for arbitrary rate allocation between the two encoders. Exploiting the joint statistics of the quantized sources, we develop a multi-level channel coding framework for symmetric SW coding. Furthermore, arithmetic coding [3] is employed at each encoder to exploit the

cross-bit-plane correlation in each of the quantized sources for further compression.

To demonstrate the effectiveness of our proposed SWCQ framework, we show that, assuming ideal source coding and ideal SW coding (realized, for example, via capacity-achieving channel coding), both asymmetric SWCQ and symmetric SWCQ can achieve *any* point on the sum-rate bound of the rate region for both direct and indirect MT source coding. We also perform high-rate performance analysis of SWCQ under practical TCQ and ideal SW coding. Practical designs using TCQ and turbo/LDPC codes for asymmetric SW coding, and TCQ, arithmetic coding, and turbo/LDPC code for symmetric SW coding perform only 0.139-0.194 bit per sample (b/s) away from the sum-rate bounds of quadratic Gaussian MT source coding.

In the third part of this dissertation, we examine MT video coding of two correlated sequences captured by calibrated cameras with known intrinsic (e.g., focal length and pixel width) and extrinsic 3D geometric parameters (e.g., relative positions). They are often referred to as *stereo video sequences*. The two encoders, one at each camera, cannot communicate with each other. Each encoder compresses its captured video before sending it to the joint decoder for stereo video reconstruction.

In general, effective coding of a single/monocular video sequence necessitates exploitation of both spatial and temporal redundancies within the sequence. H.264/AVC [59] provides the currently most efficient solution by using motion estimation/compensation to strip off the temporal redundancy between frames, the DCT of the resulting motion-compensated residual frames for energy compaction and de-correlation, and variable-length coding for compression.

For stereo video sequences, the compression efficiency can be further improved by exploiting the inter-sequence correlation (as done in the MPEG-2 stereo video coding standard [34]) in a joint encoding setup. This leads us to stereo matching [50] *at the encoder side*, which is a fundamental problem in stereo vision, and has been extensively studied

in the past by many researchers. For MT video coding, since the correlation between the two video sequences is not known *a priori*, correlation modeling is one of the key issues; although the encoders cannot communicate with each other, the 3D geometric information of the cameras can still help exploit the binocular correlation between the stereo pair *at the decoder*.

We describe in this dissertation two MT video coders, each capable of outperforming separate H.264/AVC coding of two stereo sequences. The first coder shares the basic structure of SWCQ developed in [69] for MT source coding of two Gaussian sources. Specifically, the left video sequence is compressed by the left encoder using H.264/AVC and a reconstructed version is available at the joint decoder. Then, the first I-frame of the right sequence is successively coded: a low-quality version is generated by H.264/AVC Intra coding and sent to the decoder to obtain a rough disparity map, which is combined with the decoded left I-frame to generate decoder side information for SW coding of the refinement bit stream of the right I-frame. With a better quality right I-frame, the disparity map between the left and right I-frames are refined at the decoder to serve as an initial point-to-point correspondence for the subsequent P-frames of the right sequence. The joint decoder subsequently generates side informations for both the motion vectors and the motion-compensated residual frames of the right sequence on the fly by imposing an "identical motion constraint", which means the corresponding points in the left and right scenes must have identical 3D motions. With side information available at the decoder, motion vectors for the P-frames of the right sequence are SW coded by LDPC codes, and the corresponding motion-compensated residual frames are WZ coded [62] via SWCQ.

The second coder employs the source splitting idea of [46] in conjunction with SWCQ [69]. The goal is to allow flexible rate allocation between the two video sequences. Specifically, the two sources are first coded with lower quality and the resulting bitstreams are transmitted to the decoder to generate a rough disparity map, which is used to compute a

side information of the first source by warping the low-quality second source. Then the residual frame of the first source is refined via SWCQ. Now the decoder comes back to warp the decoded high-quality first source to generate a side information of the second source, which is in turn used for refining the residual frames of the second source. This way, the two encoders are able to control the quality of the four quantized versions (one coarse version and one finer version for each source) and arbitrarily allocate rates between the two encoders.

Unlike approaches (e.g., in [43, 71]) that emphasize low-complexity encoding, this work aims to show for the first time that MT video coding can outperform independent coding with standard approaches (e.g., H.264/AVC) at the same sum rate, thus making the nascent field of distributed video coding viable. With H.264/AVC being a very powerful video compression standard, our solution for MT video coding is to use the disparity maps generated by the stereo matching algorithm to explore the joint statistics between component H.264/AVC bit streams (e.g., motion vector bits and texture bits) of the left and right sequences. Instead of using the entropy coder of H.264/AVC for the right sequence, we employ SW coding (or conditional entropy coding) based on the joint statistics. Since conditioning reduces entropy, the compression performance of our proposed schemes with SW coding is guaranteed (in theory) to be no worse than that of separate H.264/AVC compression. In our implementation of MT video coding, although inaccurate correlation modeling and rate loss with practical SW coding hurt the overall performance, we are able to achieve savings, albeit very small, in terms of the sum rate over separate H.264/AVC coding.

In summary, the main contributions of this dissertation are:

1. Exact form of minimum sum-rate for joint encoding of Gaussian sources in the symmetric case,

2. Proof that the supremum of the sum-rate loss due to distributed encoding in this case

is $\frac{1}{2}\log_2\frac{5}{4} = 0.161$ b/s when $L = 2$ and increases in the order of $\frac{\sqrt{L}}{2}\log_2 e$ b/s as the number of terminals L goes to infinity.

3. Conjecture that for any number of terminals, the supremum sum-rate loss in the symmetric case equals to that in general quadratic Gaussian two-terminal source coding without the symmetric assumption. It is conjectured that this equality holds.

4. The SWCQ framework based on separate vector quantization and SW coding for the quadratic Gaussian direct and indirect MT source coding problems with *two* encoders,

5. Demonstration of optimality of SWCQ for quadratic Gaussian MT source coding in the sense of being able to approach arbitrary points on the sum-rate bounds, assuming ideal source coding and ideal SW coding,

6. High-rate performance analysis of SWCQ for MT source coding under practical TCQ and ideal SW coding,

7. Characterization of the joint behavior of two independently dithered TCQ quantizers with independent identically distributed (i.i.d.) dither sequences; the quantization noises of the two quantizers are shown to be (nearly) independent, which is required by optimality of an MT source coding scheme,

8. An efficient multi-level symmetric SW code design that extends channel code partitioning approach for binary sources [49] to arbitrary correlation models among the sources; this design is capable of exploiting the joint statistics of the quantization indices and incorporating the statistics into the decoding algorithm.

9. Practical asymmetric and symmetric MT code designs with dithered TCQ and multi-level asymmetric/symmetric SW coding that come much closer to the sum-rate bounds

of direct and indirect MT problems with two encoders than the design of [42].

10. Two MT video coders that are capable of saving sum rate over independent H.264/AVC coding of stereo video sequences.

Notation-wise, random variables are denoted by capital letters, e.g., X. They take values x from alphabet $\mathcal{X}$. Random vectors are denoted by capital letters superscripted by their lengths, e.g., X^n. All channel codes are binary. Matrices are denoted by bold-face upper-case letters. $\boldsymbol{I}_k$ is the $k \times k$ identity matrix and $\boldsymbol{O}_{k_1 \times k_2}$ the $k_1 \times k_2$ all-zero matrix. All logarithms are of base two.

CHAPTER II

THEORETICAL LIMITS OF MT SOURCE CODING

In this section, we review theoretical bounds of direct and indirect MT source coding.

A. Direct MT source coding

The direct MT source coding setup is depicted in Fig. 1. The encoders observe sources Y_1 and Y_2, which take values in $\mathcal{Y}_1 \times \mathcal{Y}_2$, and are drawn i.i.d. from the joint probability density function (p.d.f.) $f_{Y_1,Y_2}(y_1, y_2)$. Each sequence of n source samples is grouped as a *source block* Y_1^n and Y_2^n, where $Y_1^n = \{Y_{1,i}\}_1^n, Y_2^n = \{Y_{2,i}\}_1^n$. Two encoder functions

$$\begin{aligned} \phi_1 : \quad & \mathcal{Y}_1^n \to \{1, 2, ..., 2^{nR_1}\}, \\ \phi_2 : \quad & \mathcal{Y}_2^n \to \{1, 2, ..., 2^{nR_2}\} \end{aligned} \tag{2.1}$$

separately compress Y_1^n and Y_2^n to W_1 and W_2 at rates R_1 and R_2, respectively. A decoder function

$$\varphi : \{1, 2, ..., 2^{nR_1}\} \times \{1, 2, ..., 2^{nR_2}\} \to \mathcal{Y}_1^n \times \mathcal{Y}_2^n \tag{2.2}$$

reconstructs the source block as $\{\hat{Y}_1^n, \hat{Y}_2^n\}$ based on the received W_1 and W_2.

For a distortion pair (D_1, D_2) and a given distortion measure $d(\cdot, \cdot)$, a rate pair (R_1, R_2) is *achievable* if for any $\epsilon > 0$, there exists a large enough n and a triple $(\phi_1, \phi_2, \varphi)$ such that the distortion constraints

$$\begin{aligned} \frac{1}{n}\sum_{i=1}^{n} E[d(Y_{1,i}, \hat{Y}_{1,i})] \quad &\leq \quad D_1 + \epsilon, \\ \frac{1}{n}\sum_{i=1}^{n} E[d(Y_{2,i}, \hat{Y}_{2,i})] \quad &\leq \quad D_2 + \epsilon \end{aligned} \tag{2.3}$$

are satisfied. The *achievable rate region* $\mathcal{R}^{\star}(D_1, D_2)$ is the convex hull of the set of all achievable rate pairs (R_1, R_2).

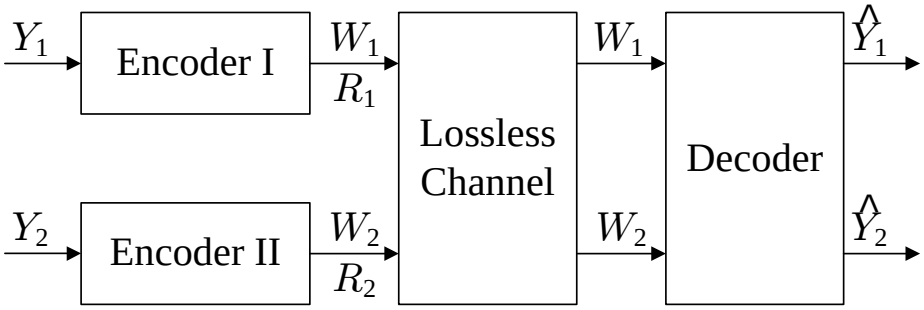

Fig. 1. Two-terminal direct MT source coding.

The exact achievable rate region for the direct MT source coding problem is still unknown. Only inner and outer rate regions are provided. For auxiliary random variables Z_1 and Z_2 let

$$\begin{aligned}\tilde{\mathcal{R}}(Z_1, Z_2) \;=\; & \{(R_1, R_2) : R_i \geq I(Y_1Y_2; Z_i|Z_j), i, j = 1, 2, i \neq j, \\ & R_1 + R_2 \geq I(Y_1Y_2; Z_1Z_2)\},\end{aligned} \tag{2.4}$$

then the inner rate region is given by [4, 55, 64]

$$\begin{aligned}\hat{\mathcal{R}}(D_1, D_2) \;=\; & \mathrm{conv}\{\tilde{\mathcal{R}}(Z_1, Z_2) : Z_1 \to Y_1 \to Y_2 \to Z_2, \\ & \exists\, \varphi(Z_1^n, Z_2^n) \text{ satisfying } (3.5)\},\end{aligned} \tag{2.5}$$

while the outer rate region is [4, 55, 64]

$$\begin{aligned}\check{\mathcal{R}}(D_1, D_2) \;=\; & \mathrm{conv}\{\tilde{\mathcal{R}}(Z_1, Z_2) : Z_1 \to Y_1 \to Y_2, Z_2 \to Y_2 \to Y_1, \\ & \exists\, \varphi(Z_1^n, Z_2^n) \text{ satisfying } (3.5)\},\end{aligned} \tag{2.6}$$

where $\mathrm{conv}(\cdot)$ represents convex closure. Let $\partial\hat{\mathcal{R}}(D_1, D_2)$ be the set of all boundary points of the rate region $\hat{\mathcal{R}}(D_1, D_2)$; likewise, let $\partial\check{\mathcal{R}}(D_1, D_2)$ be the set of all boundary points

of the rate region $\check{\mathcal{R}}(D_1, D_2)$. We call $\partial\hat{\mathcal{R}}(D_1, D_2)$ the *inner bound*, and $\partial\check{\mathcal{R}}(D_1, D_2)$ the *outer bound*.

For the direct Gaussian MT source coding problem with MSE distortion measure $d(\cdot, \cdot)$, where the sources (Y_1, Y_2) are jointly Gaussian random variables with variances $(\sigma^2_{y_1}, \sigma^2_{y_2})$ and correlation coefficient $\rho = \frac{E[Y_1 Y_2]}{\sigma_{y_1}\sigma_{y_2}}$, the Berger-Tung (BT) inner rate region (2.5) becomes [35]

$$\hat{\mathcal{R}}^{BT}(D_1, D_2) = \hat{\mathcal{R}}_1^{BT}(D_1, D_2) \cap \hat{\mathcal{R}}_2^{BT}(D_1, D_2) \cap \hat{\mathcal{R}}_{12}^{BT}(D_1, D_2), \tag{2.7}$$

where

$$\hat{\mathcal{R}}_i^{BT}(D_1, D_2) = \{(R_1, R_2) : R_i \geq \frac{1}{2}\log^+[(1 - \rho^2 + \rho^2 2^{-2R_j})\frac{\sigma^2_{y_i}}{D_i}]\}, i, j = 1, 2, i \neq j, \tag{2.8}$$

$$\hat{\mathcal{R}}_{12}^{BT}(D_1, D_2) = \{(R_1, R_2) : R_1 + R_2 \geq \frac{1}{2}\log^+[(1 - \rho^2)\frac{\beta_{max}\sigma^2_{y_1}\sigma^2_{y_2}}{2D_1 D_2}]\}, \tag{2.9}$$

with $\beta_{max} = 1 + \sqrt{1 + \frac{4\rho^2 D_1 D_2}{(1-\rho^2)^2\sigma^2_{y_1}\sigma^2_{y_2}}}$, and $\log^+ x = \max\{\log x, 0\}$.

Recently, the achievable BT rate region $\hat{\mathcal{R}}^{BT}(D_1, D_2)$ is shown to be tight [58] for the two-terminal direct Gaussian MT source coding problem, that is, $\hat{\mathcal{R}}^{BT}(D_1, D_2) = \mathcal{R}^{\star}(D_1, D_2)$. The boundary of the rate region $\hat{\mathcal{R}}^{BT}(D_1, D_2)$ consists of a diagonal line segment and two curved portions (see Fig. 2 for an example) if and only if (*iff*) [58]

$$\rho^2\frac{D_1}{\sigma^2_{y_1}} + 1 - \rho^2 > \frac{D_2}{\sigma^2_{y_2}} \quad \text{and} \quad \rho^2\frac{D_2}{\sigma^2_{y_2}} + 1 - \rho^2 > \frac{D_1}{\sigma^2_{y_1}}. \tag{2.10}$$

Under this constraint, the set of all achievable rate pairs that minimize the sum-rate $R = R_1 + R_2$ is called the *sum-rate bound* and will be denoted as $\partial\hat{\mathcal{R}}_{12}^{BT}(D_1, D_2)$.

In the special case when $D_1 = D_2 = D$ and $\sigma^2_{y_1} = \sigma^2_{y_2} = \sigma^2_y$, the sum-rate bound

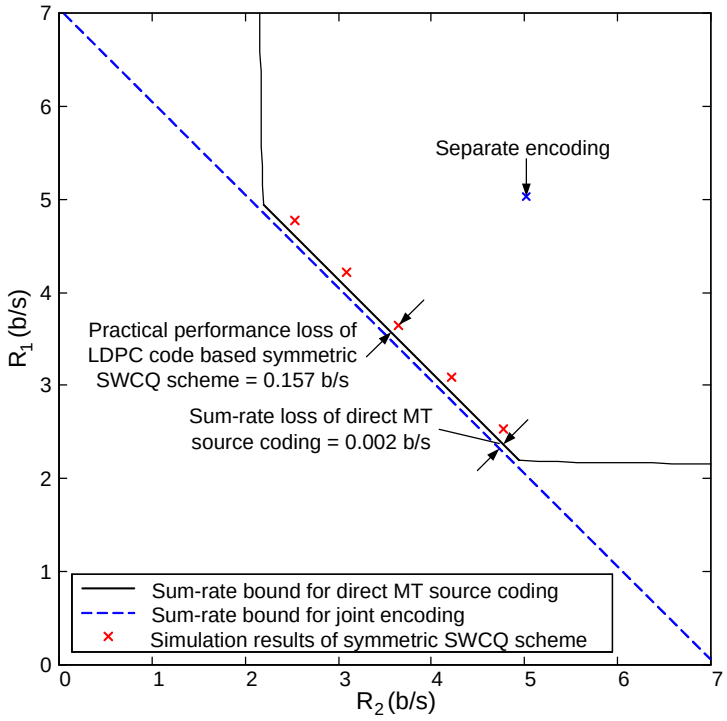

Fig. 2. The BT rate region for the direct Gaussian MT source coding problem with $\sigma_{y_1}^2 = \sigma_{y_2}^2 = \sigma_y^2 = 1, \rho = 0.9, D_1 = D_2 = 0.1$.

$\partial\hat{\mathcal{R}}_{12}^{BT}(D_1, D_2)$ becomes

$$\begin{aligned} \partial\hat{\mathcal{R}}_{12}^{BT}(D) &= \{(R_1, R_2) : R_1, R_2 \geq \frac{1}{2}\log^+[\frac{\sigma_y^2\beta_{max}^*}{2D} - \frac{\rho^2}{1-\rho^2}]; \\ &\quad R_1 + R_2 = \frac{1}{2}\log^+[(1-\rho^2)\frac{\beta_{max}^*\sigma_y^4}{2D^2}]\}, \end{aligned} \tag{2.11}$$

where $\beta_{max}^* = 1 + \sqrt{1 + \frac{4\rho^2 D^2}{(1-\rho^2)^2\sigma_y^4}}$. It is represented by the diagonal line segment in Fig. 2.

B. Indirect MT source coding

The indirect MT source coding setup with two encoders is depicted in Fig. 3. The *remote source* X and two noises N_1 and N_2 are mutually independent i.i.d. random variables drawn from the joint p.d.f. $f_{X,N_1,N_2}(x, n_1, n_2) = f_X(x)f_{N_1}(n_1)f_{N_2}(n_2)$. The block $\{Y_1^n, Y_2^n\}$ is a length-n sequence of noisy observations: $Y_1^n = X^n + N_1^n$, $Y_2^n = X^n + N_2^n$ at the two

encoders. The indirect system shares the form of encoder functions (ϕ_1, ϕ_2) with the direct system (2.1), while having a different decoder function

$$\psi : \{1, 2, ..., 2^{nR_1}\} \times \{1, 2, ..., 2^{nR_2}\} \to \mathcal{X}^n, \tag{2.12}$$

which reconstructs the remote source block as $\hat{X}^n$. Similar to the direct case, we define the achievable rate region $\mathcal{R}^\star(D)$ as the convex hull of the set of all achievable rate pairs (R_1, R_2) such that for any $\epsilon > 0$, there exists a large enough n and a triple (ϕ_1, ϕ_2, ψ) satisfying the distortion constraint

$$\frac{1}{n}\sum_{i=1}^{n} E[d(X_i, \hat{X}_i)] \quad \leq \quad D + \epsilon. \tag{2.13}$$

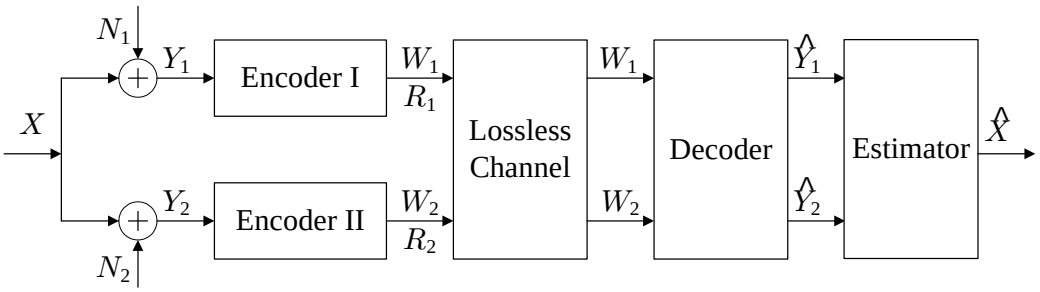

Fig. 3. Two-terminal indirect MT source coding.

The exact achievable rate region for the indirect MT source coding problem is also unknown. For auxiliary random variables Z_1 and Z_2, the inner rate region is given by [4, 55, 64]

$$\begin{aligned} \hat{\mathcal{R}}(D) \quad = \quad & \text{conv}\{\tilde{\mathcal{R}}(Z_1, Z_2) : Z_1 \to Y_1 \to X \to Y_2 \to Z_2, \\ & \exists\, \psi(Z_1^n, Z_2^n) \text{ satisfying } (2.13)\}, \end{aligned} \tag{2.14}$$

while the outer rate region is [4, 55, 64]

$$\begin{aligned}\check{\mathcal{R}}(D) &= \text{conv}\{\tilde{\mathcal{R}}(Z_1, Z_2) : Z_1 \to Y_1 \to X \to Y_2, Z_2 \to Y_2 \to X \to Y_1, \\ &\quad \exists\, \psi(Z_1^n, Z_2^n) \text{ satisfying } (2.13)\}. \end{aligned} \tag{2.15}$$

In the indirect Gaussian MT source coding problem with MSE distortion measure, X is an i.i.d. Gaussian random variable $\sim \mathcal{N}(0, \sigma_x^2)$, and for $i = 1, 2$ the noisy observations at the two encoders are given by $Y_i = X + N_i$, where $N_1 \sim \mathcal{N}(0, \sigma_{n_1}^2)$ and $N_2 \sim \mathcal{N}(0, \sigma_{n_2}^2)$ are i.i.d. Gaussian random variables independent of each other and X. For this special case, Yamamoto and Itoh [64] reported the Yamamoto-Itoh (YI) achievable rate region, which can be expressed in an equivalent form in terms of $(\sigma_x^2, \sigma_{n_1}^2, \sigma_{n_2}^2, D)$ as

$$\hat{\mathcal{R}}^{YI}(D) = \text{conv}\Big(\hat{\mathcal{R}}_1^{YI}(D) \cap \hat{\mathcal{R}}_2^{YI}(D) \cap \hat{\mathcal{R}}_{12}^{YI}(D)\Big), \tag{2.16}$$

where

$$\begin{aligned}\hat{\mathcal{R}}_i^{YI}(D) &= \{(R_1, R_2) : R_i \geq \frac{1}{2}\log^+\big[\frac{\sigma_x^4(2^{-2R_j}\sigma_x^2 + \sigma_{n_j}^2)^2(\sigma_x^2 + \sigma_{n_j}^2)^{-1}}{2^{-2R_j}\sigma_x^4(D - \sigma_{n_i}^2) + \sigma_x^2 D(\sigma_{n_1}^2 + \sigma_{n_2}^2) - \sigma_{n_1}^2\sigma_{n_2}^2(\sigma_x^2 - D)}\big]\}, \\ &\quad i, j = 1, 2, i \neq j, \end{aligned} \tag{2.17}$$

$$\hat{\mathcal{R}}_{12}^{YI}(D) = \{(R_1, R_2) : R_1 + R_2 \geq \frac{1}{2}\log^+\big[\frac{4\sigma_x^2}{\sigma_{n_1}^2\sigma_{n_2}^2 D(\frac{1}{\sigma_x^2} - \frac{1}{D} + \frac{1}{\sigma_{n_1}^2} + \frac{1}{\sigma_{n_2}^2})^2}\big]\}. \tag{2.18}$$

The YI achievable rate region (2.16) is shown to be tight [38, 40], that is, $\hat{\mathcal{R}}^{YI}(D) = \mathcal{R}^\star(D)$. The boundary of $\hat{\mathcal{R}}^{YI}(D)$ consists of a diagonal line segment and two curved portions (see Fig. 4 for an example) *iff*

$$\frac{1}{\sigma_x^2} + \frac{1}{\sigma_{n_1}^2} + \frac{1}{\sigma_{n_2}^2} > \frac{1}{D} > \max\{\frac{1}{\sigma_x^2} - \frac{1}{\sigma_{n_1}^2} + \frac{1}{\sigma_{n_2}^2}, \frac{1}{\sigma_x^2} + \frac{1}{\sigma_{n_1}^2} - \frac{1}{\sigma_{n_2}^2}\}. \tag{2.19}$$

Under this constraint, the *sum-rate bound* $\partial\hat{\mathcal{R}}_{12}^{YI}(D)$ is defined as the set of all achievable rate pairs that minimize the sum-rate $R = R_1 + R_2$.

Note that in the symmetric case with $\sigma_{n_1}^2 = \sigma_{n_2}^2 = \sigma_n^2$, the sum-rate bound $\partial\hat{\mathcal{R}}_{12}^{YI}(D)$

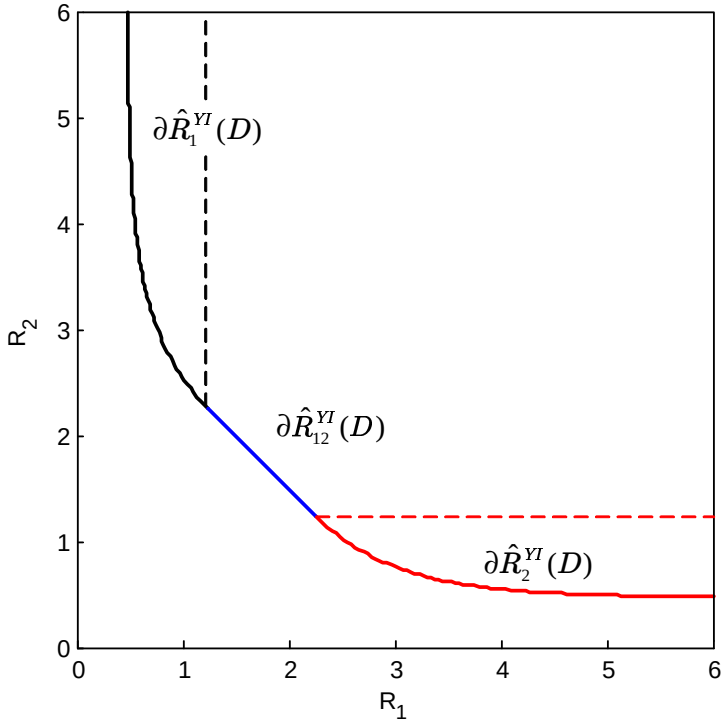

Fig. 4. The YI rate region for the indirect MT problem with $\sigma_x^2 = 1$, $\sigma_{n_1}^2 = \sigma_{n_2}^2 = 0.1$, $D = 0.07$.

becomes

$$\partial\hat{\mathcal{R}}_{12}^{YI}(D) = \{(R_1, R_2) : R_1 + R_2 = \frac{1}{2}\log^+[\frac{\sigma_x^2}{D\theta^2}], R_1, R_2 \geq \frac{1}{2}\log^+[\frac{2\sigma_x^2}{(\sigma_x^2 + D)\theta}]\}, \quad (2.20)$$

where $\theta = 1 - \frac{\sigma_n^2(\sigma_x^2 - D)}{2\sigma_x^2 D}$.

CHAPTER III

THE SUPREMUM SUM-RATE LOSS OF QUADRATIC GAUSSIAN DIRECT MT SOURCE CODING

A. Problem setup and existing knowledge

Let $L \in \mathbb{N} \cap [2, \infty)$, define a length-$L$ Gaussian vector source as $\boldsymbol{Y} = (Y_1, Y_2, ..., Y_L)^T \sim \mathcal{N}(\boldsymbol{\mu_Y}, \boldsymbol{\Sigma_Y})$ with

$$\boldsymbol{\mu_Y} = (\mu_1, \mu_2, \ldots, \mu_L)^T, \quad \boldsymbol{\Sigma_Y} = \begin{bmatrix} \sigma_1^2 & \rho_{12}\sigma_1\sigma_2 & \rho_{13}\sigma_1\sigma_3 & \ldots & \rho_{1L}\sigma_1\sigma_L \\ \rho_{21}\sigma_2\sigma_1 & \sigma_2^2 & \rho_{23}\sigma_2\sigma_3 & \ldots & \rho_{2L}\sigma_2\sigma_L \\ \vdots & \vdots & \vdots & \vdots & \vdots \\ \rho_{L1}\sigma_L\sigma_1 & \rho_{L2}\sigma_L\sigma_2 & \rho_{L3}\sigma_L\sigma_3 & \ldots & \sigma_L^2 \end{bmatrix}. \tag{3.1}$$

Denote $\boldsymbol{Y}^n = (Y_1^n, Y_2^n, ..., Y_L^n)^T = (\boldsymbol{Y}_1, \boldsymbol{Y}_2, \ldots, \boldsymbol{Y}_n)$, where $Y_i^n = (Y_{i,1}, Y_{i,2}, \ldots, Y_{i,n})^T, 1 \leq i \leq L$ is a length-n vector of source samples independently drawn from Y_i.

Define a set of L encoding functions $\boldsymbol{\phi}^{(n)} = \{\phi_1^{(n)}, \phi_2^{(n)}, \ldots, \phi_L^{(n)}\}$ as

$$\phi_i^{(n)}: \ \mathbb{R}^n \ \rightarrow \ \{1, 2, ..., M_i^{(n)}\}, \quad 1 \leq i \leq L, \tag{3.2}$$

and a set of L decoding functions $\boldsymbol{\varphi}^{(n)} = \{\varphi_1^{(n)}, \varphi_2^{(n)}, \ldots, \varphi_L^{(n)}\}$ as

$$\varphi_i^{(n)}: \ \{1, 2, ..., M_1^{(n)}\} \times \{1, 2, ..., M_2^{(n)}\} \times \ldots \times \{1, 2, ..., M_L^{(n)}\} \ \rightarrow \ \mathbb{R}^n, \quad 1 \leq i \leq L. \tag{3.3}$$

Define $R_i = \frac{1}{n} \log_2 M_i^{(n)}$ as the *transmission rate* of the i-th encoder function $\phi_i^{(n)}$, and the total transmission rate $R = \sum_{i=1}^{L} R_i$ of the L encoders is called the *sum-rate* of $\boldsymbol{\phi}^{(n)}$. Notation-wise, for $1 \leq i \leq L$, denote $W_i = \phi_i^{(n)}(Y_i^n)$ as the output of the i-th encoder, and $\hat{Y}_i^n = \varphi_i^{(n)}(W_1, W_2, \ldots, W_L)$ as the reconstructed version of Y_i^n. Also denote $\boldsymbol{W} = (W_1, W_2, ..., W_L)^T$ and $\hat{\boldsymbol{Y}}^n = \boldsymbol{\varphi}^{(n)}(\boldsymbol{\phi}^{(n)}(\boldsymbol{Y}^n)) = (\hat{Y}_1^n, \hat{Y}_2^n, ..., \hat{Y}_L^n)^T$.

Let $\boldsymbol{D} = (D_1, D_2, \ldots, D_L)^T \in (0, \infty)^L$ be an L-tuple target distortion vector, and $d(X, Y) = E\{(X - Y)^2\}$ be the mean squared error (MSE) distortion measure, an L-tuple $\boldsymbol{R} = (R_1, R_2, \ldots, R_L)^T$ is $(\boldsymbol{\Sigma_Y}, \boldsymbol{D})$-*achievable* if for any $\epsilon > 0$, there exists a large enough n and a pair $(\boldsymbol{\phi}^{(n)}, \boldsymbol{\varphi}^{(n)})$ such that for any $i \in \{1, 2, \ldots, L\}$, the following constraints

$$\frac{1}{n} \log_2 M_i^{(n)} \leq R_i + \epsilon, \tag{3.4}$$

$$\frac{1}{n} \sum_{j=1}^{n} E[d(Y_{i,j}, \hat{Y}_{i,j})] \leq D_i + \epsilon, \tag{3.5}$$

are satisfied. Define the $(\boldsymbol{\Sigma_Y}, \boldsymbol{D})$-achievable rate region $\boldsymbol{\mathcal{R}}^{\Updownarrow}_{\boldsymbol{\Sigma_Y}}(\boldsymbol{D})$ as the convex closure of all $(\boldsymbol{\Sigma_Y}, \boldsymbol{D})$-achievable rate tuples, i.e.,

$$\boldsymbol{\mathcal{R}}^{\Updownarrow}_{\boldsymbol{\Sigma_Y}}(\boldsymbol{D}) = \mathrm{cl}\{(R_1, R_2, \ldots, R_L)^T : (R_1, R_2, \ldots, R_L)^T \text{ is } (\boldsymbol{\Sigma_Y}, \boldsymbol{D}) \text{ achievable}\} \tag{3.6}$$

The *minimum sum-rate* with respect to $(\boldsymbol{\Sigma_Y}, \boldsymbol{D})$ is then defined as

$$R^{\Updownarrow}_{\boldsymbol{\Sigma_Y}}(\boldsymbol{D}) = \inf\{ \sum_{i=1}^{L} R_i : (R_1, R_2, \ldots, R_L)^T \in \boldsymbol{\mathcal{R}}^{\Updownarrow}_{\boldsymbol{\Sigma_Y}}(\boldsymbol{D})\}. \tag{3.7}$$

For comparison, we also consider the problem of joint encoding (and joint decoding) of Gaussian vector sources. Let $(\phi^{(n)}_{\Updownarrow}, \varphi^{(n)}_{\Updownarrow})$ be a pair of joint encoding/decoding functions defined as

$$\begin{aligned} \phi^{(n)}_{\Updownarrow} : \ & \underbrace{\mathbb{R}^n \times \mathbb{R}^n \times \ldots \times \mathbb{R}^n}_{L} \ \rightarrow \ \{1, 2, ..., M^{(n)}_{\Updownarrow}\}, \\ \varphi^{(n)}_{\Updownarrow} : \ & \{1, 2, ..., M^{(n)}_{\Updownarrow}\} \ \rightarrow \ \underbrace{\mathbb{R}^n \times \mathbb{R}^n \times \ldots \times \mathbb{R}^n}_{L}. \end{aligned} \tag{3.8}$$

A non-negative rate R is $(\boldsymbol{\Sigma_Y}, \boldsymbol{D})$-*jointly-achievable* if for any $\epsilon > 0$, there exists a large enough n and a pair $(\phi^{(n)}_{\Updownarrow}, \varphi^{(n)}_{\Updownarrow})$ such that the following constraints

$$\frac{1}{n} \log_2 M^{(n)}_{\Updownarrow} \leq R + \epsilon, \tag{3.9}$$

$$\frac{1}{n} \sum_{j=1}^{n} E[d(Y_{i,j}, \hat{Y}_{i,j})] \leq D_i + \epsilon, \qquad \forall i \in \{1, 2, \ldots, L\}, \tag{3.10}$$

are satisfied. The *joint encoding minimum sum-rate* with respect to $(\boldsymbol{\Sigma_Y}, \boldsymbol{D})$ is defined as

$$R^{\Updownarrow}_{\boldsymbol{\Sigma_Y}}(\boldsymbol{D}) \;=\; \inf\{R : R \text{ is } (\boldsymbol{\Sigma_Y}, \boldsymbol{D})\text{−jointly−achievable}\}. \tag{3.11}$$

Then the *sum-rate loss* of distributed over joint encoding is defined as

$$R^{\Delta}_{\boldsymbol{\Sigma_Y}}(\boldsymbol{D}) \;=\; R^{\Updownarrow}_{\boldsymbol{\Sigma_Y}}(\boldsymbol{D}) - R^{\Updownarrow}_{\boldsymbol{\Sigma_Y}}(\boldsymbol{D}). \tag{3.12}$$

1. Existing knowledge

Berger and Tung [4, 55] provide an *inner rate region* inside which all rate tuples are $(\boldsymbol{\Sigma_Y}, \boldsymbol{D})$-achievable: let $\boldsymbol{U} = (U_1, U_2, \ldots, U_L)^T$ be a length-L auxiliary random vector such that

- $U_i = Y_i + Q_i, i = 1, 2, \ldots, L$, where $Q_i \sim \mathcal{N}(0, \sigma^2_{Q_i})$, and all Q_i's are independent of each other and of all Y_i's,
- $\boldsymbol{U}$ satisfies $E\Big\{\big(Y_i - E(Y_i|\boldsymbol{U})\big)^2\Big\} \le D_i$ for all $i = 1, 2, \ldots, L$,

and define $\mathcal{U}(\boldsymbol{\Sigma_Y}, \boldsymbol{D})$ as the set of all auxiliary random vectors $\boldsymbol{U}$ that satisfy the above conditions. Denote the index set $\{1, 2, \ldots, L\}$ as $\mathcal{I}_L$, and for a length-L random vector $\boldsymbol{X} = (X_1, X_2, \ldots, X_L)^T$ and a non-empty subset $\mathcal{A} \subseteq \mathcal{I}_L$, denote $\boldsymbol{X}_{\mathcal{A}}$ as the length-$|\mathcal{A}|$ random vector formed by $\{X_i : i \in \mathcal{A}\}$. Then the following lemma gives the Berger-Tung inner rate region, the proof can be found in [4, 55].

Lemma 1 (Berger-Tung inner rate region) *Define*

$$\boldsymbol{\mathcal{R}}^{BT}_{\boldsymbol{\Sigma_Y}}(\boldsymbol{D}) \;=\; \bigcup_{\boldsymbol{U} \in \mathcal{U}(\boldsymbol{\Sigma_Y}, \boldsymbol{D})} \Big\{(R_1, R_2, \ldots, R_L)^T : \sum_{i \in \mathcal{A}} R_i \ge I(\boldsymbol{Y}_{\mathcal{A}}; \boldsymbol{U}_{\mathcal{A}} | \boldsymbol{U}_{\mathcal{I}_L \setminus \mathcal{A}}) \text{ for all } \mathcal{A} \subseteq \mathcal{I}_L\Big\},$$

then

$$\boldsymbol{\mathcal{R}}^{BT}_{\boldsymbol{\Sigma_Y}}(\boldsymbol{D}) \;\subseteq\; \boldsymbol{\mathcal{R}}^{\Updownarrow}_{\boldsymbol{\Sigma_Y}}(\boldsymbol{D}). \tag{3.13}$$

The *Berger-Tung minimum sum-rate* with respect to $(\boldsymbol{\Sigma_Y}, \boldsymbol{D})$ is

$$R^{BT}_{\boldsymbol{\Sigma_Y}}(\boldsymbol{D}) \;=\; \inf\{\; \sum_{i=1}^{L} R_i : (R_1, R_2, \ldots, R_L)^T \in \boldsymbol{\mathcal{R}}^{BT}_{\boldsymbol{\Sigma_Y}}(\boldsymbol{D})\}. \tag{3.14}$$

$$R^{BT}_{\boldsymbol{\Sigma_Y}}(\boldsymbol{D}) \tag{3.15}$$

$$= \inf \left\{ I(\boldsymbol{Y};\boldsymbol{U}) : \begin{array}{c} \boldsymbol{U} = \boldsymbol{Y} + \boldsymbol{Q} \text{ where } \boldsymbol{Q} \sim \mathcal{N}(\boldsymbol{0}, \boldsymbol{\Lambda_Q}) \text{ is independent of } \boldsymbol{Y} \\ \text{and } E\Big\{\big(Y_i - E(Y_i|\boldsymbol{U})\big)^2\Big\} \le D_i \text{ for all } i = 1, 2, \ldots, L \end{array} \right\} \tag{3.16}$$

If we define

$$\mathscr{D}(\boldsymbol{D}) \;=\; \{\boldsymbol{\mathcal{D}} \in \mathbb{R}^{L\times L} : \boldsymbol{\mathcal{D}} \text{ is positive definite and } \mathrm{diag}(\boldsymbol{\mathcal{D}}) \le \boldsymbol{D}\}, \tag{3.17}$$

$$\mathscr{A}(\boldsymbol{\Sigma_Y}) \;=\; \{\boldsymbol{\mathcal{D}} \in \mathbb{R}^{L\times L} : \boldsymbol{\Lambda} = \boldsymbol{\mathcal{D}}^{-1} - \boldsymbol{\Sigma}_{\boldsymbol{Y}}^{-1} \text{ is diagonal}\} \tag{3.18}$$

where "$\le$" and "$\ge$" represent component-wise inequalities, then the Berger-Tung minimum sum-rate can be rewritten as

$$R^{BT}_{\boldsymbol{\Sigma_Y}}(\boldsymbol{D}) \;=\; \min_{\boldsymbol{\mathcal{D}} \in \mathscr{D}(\boldsymbol{D}) \cap \mathscr{A}(\boldsymbol{\Sigma_Y})} \frac{1}{2} \log_2 \frac{|\boldsymbol{\Sigma_Y}|}{|\boldsymbol{\mathcal{D}}|}. \tag{3.19}$$

Finding the exact rate region $\boldsymbol{\mathcal{R}}^{\Updownarrow}_{\boldsymbol{\Sigma_Y}}(\boldsymbol{D})$ for the general quadratic Gaussian MT source coding problem is very challenging. Hence, researchers have so far focused on several special cases that are easier to handle. One such case is the quadratic Gaussian two-terminal source coding problem, for which Oohama [35] showed partial tightness of the Berger-Tung inner rate region, while Wagner *et al.* [58] finished the story by proving tightness of the Berger-Tung inner sum-rate bound. These results are summarized in the following lemma.

Lemma 2 (Tightness of the Berger-Tung inner rate region for the two-terminal case) *It holds for any positive-definite* $\boldsymbol{\Sigma_Y} \in \mathbb{R}^{2\times 2}$ *and any positive distortion vector* $\boldsymbol{D} \in \mathbb{R}^2$*,*

$$\mathcal{R}^{\Updownarrow}_{\boldsymbol{\Sigma_Y}}(\boldsymbol{D}) = \mathcal{R}^{BT}_{\boldsymbol{\Sigma_Y}}(\boldsymbol{D}). \tag{3.20}$$

Another interesting case of MT source coding is when only one of the L sources is to be reconstructed at the decoder while all others serve as helpers. This is known as the quadratic Gaussian *many-help-one* problem, which still remains open in the general setup. Tavildar *et al.* [53] considered a special case when the source correlation satisfies a "tree-structure" Markov condition and showed that the Berger-Tung inner rate region is tight. Hence we have the following lemma.

Lemma 3 ***(Tightness of the Berger-Tung inner rate region for the tree-structured many-help-one problem)*** *Suppose* $\boldsymbol{\Sigma_Y}$ *satisfies the tree-structure Markov conditions defined in [53], and let* $\boldsymbol{D} = (D, \infty, \infty, \ldots, \infty)^T$*, then*

$$\mathcal{R}^{\Updownarrow}_{\boldsymbol{\Sigma_Y}}(\boldsymbol{D}) = \mathcal{R}^{BT}_{\boldsymbol{\Sigma_Y}}(\boldsymbol{D}). \tag{3.21}$$

For the MT source coding problem with two continuous sources and MSE distortion measure, it is shown that the sum-rate loss is upper-bounded by 1 b/s [72]. Particularly, since jointly Gaussian sources are continuous, we have the following lemma.

Lemma 4 ***(Upper bound on the sum-rate loss of quadratic Gaussian MT source coding with two sources)*** *It holds for any positive-definite* $\boldsymbol{\Sigma_Y} \in \mathbb{R}^{2\times 2}$ *and any positive distortion vector* $\boldsymbol{D} \in \mathbb{R}^2$ *[72],*

$$R^{\Delta}_{\boldsymbol{\Sigma_Y}}(\boldsymbol{D}) \leq 1 \text{ b/s}. \tag{3.22}$$

It is shown in [73] that for two jointly Gaussian sources, as the target distortions D_1 and D_2 go to zero, the sum-rate loss $R^{\Delta}_{\boldsymbol{\Sigma_Y}}(\boldsymbol{D})$ also goes to zero. This result is consistent with the Slepian-Wolf theorem [47]. One can loosely think of MT source coding as the lossy version of Slepian-Wolf coding. For MT source coding with more than two sources, there is still no prior knowledge about the sum-rate loss.

2. The exact sum-rate bound of distributed encoding in the symmetric case

Consider a special case of quadratic Gaussian MT source coding problem, where the sources are *positively symmetric* in the sense that all the sources are zero-mean and interchangeable with positive correlation coefficients between each other, and all the target distortions are equal, i.e.,

$$\boldsymbol{\mu_Y} = \mathbf{0}, \boldsymbol{\Sigma_Y} = \begin{bmatrix} 1 & \rho & \dots & \rho \\ \rho & 1 & \dots & \rho \\ \vdots & \vdots & \vdots & \vdots \\ \rho & \rho & \dots & 1 \end{bmatrix}_{L\times L}, \boldsymbol{D} = \underbrace{(D, D, \dots, D)^T}_{L}, \tag{3.23}$$

for some $L \in \mathbb{N} \cap [2, \infty)$, $\rho \in (0, 1)$ and $D \in (0, 1)$. Then this special case is fully characterized by (L, ρ, D), hence the $(\boldsymbol{\Sigma_Y}, \boldsymbol{D})$-achievable rate region $\boldsymbol{\mathcal{R}}^{\Rsh}_{\boldsymbol{\Sigma_Y}}(\boldsymbol{D})$ can be also denoted as $\boldsymbol{\mathcal{R}}^{\Rsh}_{L,\rho}(D)$. Similarly, the corresponding minimum sum-rate with respect to $(\boldsymbol{\Sigma_Y}, \boldsymbol{D})$ is written as $R^{\Rsh}_{L,\rho}(D)$, and the joint encoding minimum sum-rate as $R^{\Rdsh}_{L,\rho}(D)$; the difference between them, namely,

$$R^{\Delta}_{L,\rho}(D) \triangleq R^{\Rsh}_{L,\rho}(D) - R^{\Rdsh}_{L,\rho}(D), \tag{3.24}$$

is the *sum-rate loss* in the quadratic Gaussian symmetric MT source coding problem defined by (L, ρ, D). For this special case, it is shown in [58] that the Berger-Tung inner

sum-rate bound is tight, i.e., we have the following lemma.

Lemma 5 *For the quadratic Gaussian symmetric MT source coding problem defined by* (L, ρ, D) *such that* $L \in \mathbb{N} \cap [2, \infty)$*,* $\rho \in (0, 1)$ *and* $D \in (0, 1)$*, it holds,*

$$R_{L,\rho}^{\natural}(D) = R_{L,\rho}^{BT}(D). \tag{3.25}$$

Then for any $L \in \mathbb{N} \cap [2, \infty)$, $\rho \in (0, 1)$ and $D \in (0, 1)$, it can be shown that

$$R_{L,\rho}^{BT}(D) = R_{L,\rho}^{\star}(D) \quad = \quad \frac{1}{2} \log_2 \frac{\delta_L(\rho)}{D^L \delta_L(\theta^{\natural})}, \tag{3.26}$$

where $\delta_L(x) \stackrel{\Delta}{=} (1-x)^{L-1}\big(1 + (L-1)x\big)$ for $x \in (\frac{-1}{L-1}, 1)$, and

$$\theta^{\natural} \quad = \quad t^{\natural} + \sqrt{(t^{\natural})^2 + 1/(L-1)}, \tag{3.27}$$

where $t^{\natural} = \frac{L-2}{2(L-1)} - \frac{(1-\rho)\big(1+(L-1)\rho\big)}{2(L-1)D\rho}$.

Before stating our main results, we first gives some notations that are used in sequel. For any $L \in \mathbb{N} \cap [2, \infty)$, $D \in (0, \infty)$, and $\theta \in (-1, 1)$, define $\boldsymbol{\mathcal{S}}_L(D, \theta)$ as a $L \times L$ matrix with equal diagonal elements D and equal off-diagonal elements θD.

B. Sum-rate loss of quadratic Gaussian MT source coding

In this section, we study the minimum sum-rate for joint encoding of Gaussian sources, explicitly evaluate the sum-rate loss due to distributed coding in the symmetric case, and show that the supremum of the sum-rate loss in this symmetric case increases in the order of $\frac{\sqrt{L}}{2} \log_2 e$. It is conjectured that this supremum sum-rate loss in the symmetric case equals to that in general quadratic Gaussian MT source coding.

1. The minimum sum-rate of joint encoding

In this subsection, we give the quadratic Gaussian joint encoding minimum sum-rate $R^{\uparrow\downarrow}_{\boldsymbol{\Sigma_Y}}(\boldsymbol{D})$, which can be computed by solving an optimization problem for general $\boldsymbol{\Sigma_Y}$ and $\boldsymbol{D}$. Particularly, for the symmetric case, the minimum sum-rate $R^{\uparrow\downarrow}_{L,\rho}(D)$ is given explicitly as a function of L, ρ and D.

Let $\boldsymbol{\mathcal{D}}$ be an $L \times L$ positive-definite matrix, then there exists an $L \times L$ non-singular matrix $\boldsymbol{\mathcal{T}}$, such that

$$\boldsymbol{\mathcal{T}}^T \boldsymbol{\mathcal{D}} \boldsymbol{\mathcal{T}} = \boldsymbol{\Lambda}, \tag{3.28}$$

$$\boldsymbol{\mathcal{T}}^T \boldsymbol{\Sigma_Y} \boldsymbol{\mathcal{T}} = \boldsymbol{I}, \tag{3.29}$$

where $\boldsymbol{\Lambda}$ is a diagonal matrix with positive diagonal elements (since both $\boldsymbol{\mathcal{D}}$ and $\boldsymbol{\Sigma_Y}$ are positive-definite). Then $\boldsymbol{\mathcal{T}}$ is called the *simultaneous diagonalization matrix* [18] of $(\boldsymbol{\Sigma_Y}, \boldsymbol{\mathcal{D}})$, and the L column vectors in $\boldsymbol{\mathcal{T}}$ the *generalized eigenvectors*, the L diagonal elements of $\boldsymbol{\Lambda}$ the *generalized eigenvalues*. Write $\mathrm{eig}(\boldsymbol{\Sigma_Y}, \boldsymbol{\mathcal{D}}) = \mathrm{diag}(\boldsymbol{\Lambda})$, and define

$$\mathscr{E}(\boldsymbol{\Sigma_Y}) = \{\boldsymbol{\mathcal{D}} \in \mathbb{R}^{L\times L} : \mathrm{eig}(\boldsymbol{\Sigma_Y}, \boldsymbol{\mathcal{D}}) \le \mathbf{1}\}. \tag{3.30}$$

The following theorem characterizes the minimum sum-rate of joint encoding of Gaussian sources.

Theorem 1 *The quadratic Gaussian joint encoding minimum sum-rate is the solution to the following optimization problem,*

$$R^{\uparrow\downarrow}_{\boldsymbol{\Sigma_Y}}(\boldsymbol{D}) = \min_{\boldsymbol{\mathcal{D}} \in \mathscr{D}(\boldsymbol{D}) \cap \mathscr{E}(\boldsymbol{\Sigma_Y})} \frac{1}{2} \log_2 \frac{|\boldsymbol{\Sigma_Y}|}{|\boldsymbol{\mathcal{D}}|}. \tag{3.31}$$

Proof 1 *The achievability part is straightforward since we can always transform $\boldsymbol{Y}$ into*

$\boldsymbol{Z} = \boldsymbol{\mathcal{T}}^T\boldsymbol{Y}$ at the joint encoder and then employ classical source coding on $\boldsymbol{Z}$ with target distortion vector $\mathrm{diag}(\boldsymbol{\Lambda})$. *At the decoder, $\boldsymbol{Y} = (\boldsymbol{\mathcal{T}}^T)^{-1}\boldsymbol{Z}$ is reconstructed with a distortion matrix $(\boldsymbol{\mathcal{T}}^T)^{-1}\boldsymbol{\Lambda}\boldsymbol{\mathcal{T}}^{-1} = \boldsymbol{\mathcal{D}}$.*

Let $\boldsymbol{Z} = \boldsymbol{\mathcal{T}}^T\boldsymbol{Y}$, then the covariance matrix of $\boldsymbol{Z}$ is the identity matrix $\boldsymbol{I}$ due to definition of $\boldsymbol{\mathcal{T}}$. Then any scheme that achieves a distortion matrix $\boldsymbol{\mathcal{D}}$ for quadratic Gaussian joint encoding of vector source $\boldsymbol{Y}$ must be able to achieve a distortion matrix $\boldsymbol{\Lambda} = \boldsymbol{\mathcal{T}}^T\boldsymbol{\mathcal{D}}\boldsymbol{\mathcal{T}}$ for quadratic Gaussian joint encoding of vector source $\boldsymbol{Z}$. Since $\boldsymbol{Z}$ is a Gaussian vector source with independent unit-variance components, then $\boldsymbol{\Lambda}$ must be a diagonal matrix with all components no larger than 1, i.e., $\boldsymbol{\mathcal{D}} \in \mathscr{E}(\boldsymbol{\Sigma_Y})$. Then the classical rate-distortion theory ensures that

$$
\begin{aligned}
R^{\Updownarrow}_{\boldsymbol{\Sigma_Y}}(\boldsymbol{D}) &\geq \min_{\boldsymbol{\mathcal{D}} \in \mathscr{D}(\boldsymbol{D}) \cap \mathscr{E}(\boldsymbol{\Sigma_Y})} \frac{1}{2}\log_2 \frac{|\boldsymbol{\Lambda}|}{|\boldsymbol{I}|} && (3.32)\\
&= \min_{\boldsymbol{\mathcal{D}} \in \mathscr{D}(\boldsymbol{D}) \cap \mathscr{E}(\boldsymbol{\Sigma_Y})} \frac{1}{2}\log_2 \frac{|\boldsymbol{\mathcal{T}}^T\boldsymbol{\Sigma_Y}\boldsymbol{\mathcal{T}}|}{|\boldsymbol{\mathcal{T}}^T\boldsymbol{\mathcal{D}}\boldsymbol{\mathcal{T}}|} && (3.33)\\
&= \min_{\boldsymbol{\mathcal{D}} \in \mathscr{D}(\boldsymbol{D}) \cap \mathscr{E}(\boldsymbol{\Sigma_Y})} \frac{1}{2}\log_2 \frac{|\boldsymbol{\Sigma_Y}|}{|\boldsymbol{\mathcal{D}}|}. && (3.34)
\end{aligned}
$$

For the special case with positively symmetric sources and equal target distortions, the joint encoding minimum sum-rate $R^{\Updownarrow}_{L,\rho}(D)$ can be written explicitly as a function of L, ρ and D. First, it is sufficient to consider the distortion matrices of the form $\boldsymbol{\mathcal{S}}(D,\theta)$. Hence (3.31) can be simplified as

$$
\begin{aligned}
R^{\Updownarrow}_{L,\rho}(D) &= \min_{\theta \in (-\frac{1}{L-1},1):\boldsymbol{\mathcal{S}}_L(D,\theta) \in \mathscr{E}(\boldsymbol{\Sigma_Y})} \frac{1}{2}\log_2 \frac{\delta_L(\rho)}{D^L\delta_L(\theta)} && (3.35)\\
&= \begin{cases} \frac{1}{2}\log_2 \dfrac{1+(L-1)\rho}{LD-(L-1)(1-\rho)} & D > 1-\rho \\ \frac{1}{2}\log_2 \dfrac{\delta_L(\rho)}{D^L} & D \leq 1-\rho \end{cases}. && (3.36)
\end{aligned}
$$

In another special case of $L = 2$, the joint encoding minimum sum-rate in (3.31) is also computable. In this case, it suffices to consider positively symmetric sources with covariance matrix $\boldsymbol{\Sigma_Y} = \boldsymbol{\mathcal{S}}_2(1,\rho)$, and general target distortion pair $\boldsymbol{D} = (D_1, D_2)^T$ such

that $D_1 \le 1-\rho^2(1-D_2)$ or $D_2 \le 1-\rho^2(1-D_1)$ [58]. Then (3.31) can be simplified as

$$R^{\Updownarrow}_{\boldsymbol{\Sigma_Y}}(\boldsymbol{D}) = \min_{\theta\in(-1,1):\boldsymbol{\mathcal{D}}_2(\theta)\,\in\,\mathscr{E}(\boldsymbol{\Sigma_Y})} \frac{1}{2}\log_2\frac{\delta_L(\rho)}{D^L\delta_L(\theta)}, \tag{3.37}$$

$$= \begin{cases} \dfrac{1}{2}\log_2\dfrac{(1-\rho^2)}{(1-\theta^2_{max})D_1D_2} & \text{if } \rho \ge \rho^\star \\ \dfrac{1}{2}\log_2\dfrac{(1-\rho^2)}{D_1D_2} & \text{if } \rho < \rho^\star \end{cases}, \tag{3.38}$$

where $\rho^\star=\sqrt{(1-D_1)(1-D_2)}$, $\boldsymbol{\mathcal{D}}_2(\theta)=\begin{bmatrix} D_1 & \theta\sqrt{D_1D_2} \\ \theta\sqrt{D_1D_2} & D_2 \end{bmatrix}$.

Remark 1: Denote

$$\boldsymbol{\mathcal{D}}^{\boldsymbol{\Sigma_Y},\boldsymbol{D}}_{min} = \arg\min_{\boldsymbol{\mathcal{D}}\in\mathscr{D}(\boldsymbol{D})\cap\mathscr{E}(\boldsymbol{\Sigma_Y})} \frac{1}{2}\log_2\frac{|\boldsymbol{\Sigma_Y}|}{|\boldsymbol{\mathcal{D}}|}. \tag{3.39}$$

In general, for joint encoding of L sources with a fixed $\boldsymbol{\Sigma_Y}$, there are $L+1$ categories of $\boldsymbol{D}$, each corresponding to a different number of coded transformed sources in the optimal strategy.

0) If all the components in $\boldsymbol{D}$ are no less than 1, there is no need to code. Write this case as $\boldsymbol{D}\in\mathscr{C}_0$.

1) If one or more components in $\boldsymbol{D}$ decrease by a small amount such that exactly one generalized eigenvalue in $\mathrm{eig}(\boldsymbol{\Sigma_Y},\boldsymbol{\mathcal{D}}^{\boldsymbol{\Sigma_Y},\boldsymbol{D}}_{min})$ is less than 1, then only one transformed source need to be coded. Write this case as $\boldsymbol{D}\in\mathscr{C}_1$.

...

L) If all the components in $\boldsymbol{D}$ are small enough such that all the generalized eigenvalues in $\mathrm{eig}(\boldsymbol{\Sigma_Y},\boldsymbol{\mathcal{D}}^{\boldsymbol{\Sigma_Y},\boldsymbol{D}}_{min})$ are less than 1, then all L transformed sources need to be coded. Write this case as $\boldsymbol{D}\in\mathscr{C}_L$.

It follows that if $\boldsymbol{D}\in\mathscr{C}_k$, the joint encoding minimum sum-rate $R^{\Updownarrow}_{\boldsymbol{\Sigma_Y}}(\boldsymbol{D})$ obeys the $\frac{6}{k}$-dB rule in the sense that $R^{\Updownarrow}_{\boldsymbol{\Sigma_Y}}(\boldsymbol{D})$ increases by 1 b/s if (every component of) $\boldsymbol{D}$ decreases by

approximately $\frac{6}{k}$ dB. Although it is not easy to analytically separate the $\mathscr{C}_k$'s, numerical examples of these different cases with $L = 3$ are given in Table I.

Table I. Examples of different cases for joint encoding of $L = 3$ sources.

$\boldsymbol{\Sigma_Y}$	$\boldsymbol{D}^T$	$\mathrm{eig}(\boldsymbol{\Sigma_Y}, \mathcal{D}_{min}^{\boldsymbol{\Sigma_Y},\boldsymbol{D}})$	# coded	$R^{\Updownarrow}_{\boldsymbol{\Sigma_Y}}(\boldsymbol{D})$
$\begin{bmatrix} 1 & 0.9 & 0.8 \\ 0.9 & 1 & 0.7 \\ 0.8 & 0.7 & 1 \end{bmatrix}$	[1.000 1.000 1.000]	[1.000 1.000 1.000]	0	0.000 b/s
	[0.200 0.250 0.300]	[**0.135** 1.000 1.000]	1	1.445 b/s
	[0.100 0.150 0.200]	[**0.064 0.628** 1.000]	2	2.324 b/s
	[0.050 0.100 0.150]	[**0.030 0.417 0.876**]	3	3.251 b/s
	[0.025 0.050 0.075]	[**0.015 0.208 0.438**]	3	4.751 b/s
$\begin{bmatrix} 1 & 0.9 & 0.9 \\ 0.9 & 1 & 0.9 \\ 0.9 & 0.9 & 1 \end{bmatrix}$	[1.000 1.000 1.000]	[1.000 1.000 1.000]	0	0.000 b/s
	[0.200 0.200 0.200]	[**0.143** 1.000 1.000]	1	1.404 b/s
	[0.050 0.050 0.050]	[**0.018 0.500 0.500**]	3	3.904 b/s
	[0.025 0.025 0.025]	[**0.009 0.250 0.250**]	3	5.404 b/s

We say that a target distortion vector $\boldsymbol{D} = (D_1, ..., D_L)^T$ is *saturated* and write $\boldsymbol{D} \in \mathscr{S}_{\boldsymbol{\Sigma_Y}}$ if at least one component of $\mathrm{diag}(\boldsymbol{\mathcal{D}}_{min}^{\boldsymbol{\Sigma_Y},\boldsymbol{D}})$ is strictly less than the corresponding component of $\boldsymbol{D}$. This corresponds to the case when one of the target distortions, say D_1, is too large, such that any scheme that achieves the other target distortions $D_2, ..., D_L$ must be able to achieve a distortion smaller than D_1. For example, if $\boldsymbol{\Sigma_Y} = \boldsymbol{\mathcal{S}}_3(1, 0.9)$ and $\boldsymbol{D} = (1.0\ 0.1\ 0.1)^T$, one can verify that $\mathrm{diag}(\boldsymbol{\mathcal{D}}_{min}^{\boldsymbol{\Sigma_Y},\boldsymbol{D}}) \approx (0.192\ 0.1\ 0.1)^T$. Note that for the quadratic Gaussian MT source coding problem, we can also define a saturation set $\mathscr{S}^{MT}_{\boldsymbol{\Sigma_Y}}$ such that for any $\boldsymbol{D} \in \mathscr{S}^{MT}_{\boldsymbol{\Sigma_Y}}$, at least one component of $\boldsymbol{D}$ is not achieved with equality in the optimal strategy. In general, it is not easy to analytically characterize the sets $\mathscr{S}_{\boldsymbol{\Sigma_Y}}$ and $\mathscr{S}^{MT}_{\boldsymbol{\Sigma_Y}}$, but it is possible to show that $\mathscr{S}_{\boldsymbol{\Sigma_Y}} \supsetneqq \mathscr{S}^{MT}_{\boldsymbol{\Sigma_Y}}$ ("$\supsetneqq$" means strict inclusion, for example, when $\boldsymbol{\Sigma_Y} = \boldsymbol{\mathcal{S}}_3(1, 0.9)$, $\boldsymbol{D} = (0.210\ 0.1\ 0.1)^T \in \mathscr{S}_{\boldsymbol{\Sigma_Y}} \backslash \mathscr{S}^{MT}_{\boldsymbol{\Sigma_Y}}$).

Moreover, it can be shown that

$$\begin{aligned} \boldsymbol{D} = (D_1, D_2, ..., D_L)^T \in \mathscr{C}_L \backslash \mathscr{S}_{\boldsymbol{\Sigma_Y}} \quad &\Rightarrow \quad \boldsymbol{\mathcal{D}}_{min}^{\boldsymbol{\Sigma_Y}, \boldsymbol{D}} \text{ is diagonal, and } \operatorname{diag}(\boldsymbol{\mathcal{D}}_{min}^{\boldsymbol{\Sigma_Y}, \boldsymbol{D}}) = \boldsymbol{D} \\ &\Rightarrow \quad R_{\boldsymbol{\Sigma_Y}}^{\Updownarrow}(\boldsymbol{D}) = \frac{1}{2} \log_2 \frac{|\boldsymbol{\Sigma_Y}|}{\prod_{i=1}^{L} D_i}, \end{aligned} \tag{3.40}$$

this implies that for any unsaturated $\boldsymbol{D} = (D_1, D_2, ..., D_L)^T \in \mathscr{C}_L$, the optimal strategy can exhaust the source correlation in the sense that the resulting estimation errors for different sources are independent Gaussian noises; and the optimal transform is always an equivalent scaled version of the KLT, namely, $\boldsymbol{\mathcal{T}} = \boldsymbol{\mathcal{U}}\boldsymbol{\mathcal{S}}^{-\frac{1}{2}}$, where $\boldsymbol{\Sigma_Y} = \boldsymbol{\mathcal{U}}\boldsymbol{\mathcal{S}}\boldsymbol{\mathcal{U}}^T$ is the SVD decomposition of $\boldsymbol{\Sigma_Y}$.

2. The sum-rate loss of quadratic Gaussian MT source coding

In general, due to Lemma 1, the sum-rate loss for the quadratic Gaussian MT source coding problem can be upper-bounded by the difference between the Berger-Tung inner sum-rate bound and the joint encoding minimum sum-rate, i.e.,

$$R_{\boldsymbol{\Sigma_Y}}^{\Delta}(\boldsymbol{D}) = R_{\boldsymbol{\Sigma_Y}}^{\Updownarrow}(\boldsymbol{D}) - R_{\boldsymbol{\Sigma_Y}}^{\Updownarrow}(\boldsymbol{D}) \tag{3.41}$$

$$\leq R_{\boldsymbol{\Sigma_Y}}^{BT}(\boldsymbol{D}) - R_{\boldsymbol{\Sigma_Y}}^{\Updownarrow}(\boldsymbol{D}) \tag{3.42}$$

$$= \frac{1}{2} \log_2 \frac{\min\limits_{\boldsymbol{\mathcal{D}} \in \mathscr{D}(\boldsymbol{D}) \cap \mathscr{E}(\boldsymbol{\Sigma_Y})} |\boldsymbol{\mathcal{D}}|}{\min\limits_{\boldsymbol{\mathcal{D}} \in \mathscr{D}(\boldsymbol{D}) \cap \mathscr{A}(\boldsymbol{\Sigma_Y})} |\boldsymbol{\mathcal{D}}|}. \tag{3.43}$$

For the special case with positively symmetric sources and equal target distortions, we can combine the joint encoding minimum sum-rate in (3.36) for the quadratic Gaussian source coding problem and the minimum sum-rate in Theorem 5 for the quadratic Gaussian MT source coding problem, and thus evaluate the exact sum-rate loss between the two

problems, i.e., we have

$$R^{\Delta}_{L,\rho}(D) = R^{\Rsh}_{L,\rho}(D) - R^{\Rsh}_{L,\rho}(D) \tag{3.44}$$

$$= \begin{cases} \frac{1}{2}\log_2 \frac{\delta_L(\rho)}{D^L \delta_L(\theta^{\Rsh})} - \frac{1}{2}\log_2 \frac{\delta_L(\rho)}{D^L \delta_L(\theta^{\Rsh})} & D > 1-\rho \\ \frac{1}{2}\log_2 \frac{\delta_L(\rho)}{D^L \delta_L(\theta^{\Rsh})} - \frac{1}{2}\log_2 \frac{\delta_L(\rho)}{D^L \delta_L(0)} & D \le 1-\rho \end{cases}$$

$$= \begin{cases} \frac{1}{2}\log_2 \frac{\delta_L(\theta^{\Rsh})}{\delta_L(\theta^{\Rsh})} & D > 1-\rho \\ \frac{1}{2}\log_2 \frac{1}{\delta_L(\theta^{\Rsh})} & D \le 1-\rho \end{cases}, \tag{3.45}$$

where $\theta^{\Rsh} = 1 - \frac{1-\rho}{D}$ and $\theta^{\Rsh}$ is defined in (3.27).

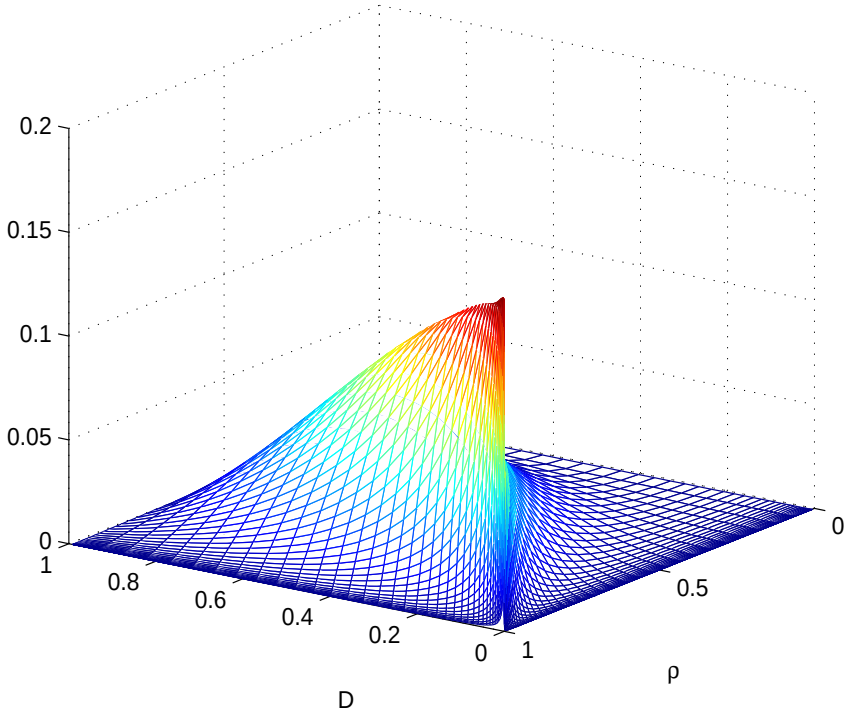

Fig. 5. The sum-rate loss $R^{\Delta}_{2,\rho}(D)$ for the quadratic Gaussian two-terminal source coding problem.

Example of the sum-rate loss $R^{\Delta}_{L,\rho}(D)$ are plotted in Fig. 5 as a function of ρ and D for $L = 2$. When $\rho = 0$, all sources are independent, hence $R^{\Rsh}_{L,\rho}(D) = R^{\Rsh}_{L,\rho}(D) = \frac{L}{2}\log_2 \frac{1}{D}$ and $R^{\Delta}_{L,\rho}(D) = 0$; when $\rho = 1$, all sources are statistically identical, thus coding one of

them suffices, hence $R^{\nleftrightarrow}_{L,\rho}(D) = R^{\nuparrow\downarrow}_{L,\rho}(D) = \frac{1}{2}\log_2\frac{1}{D}$ and $R^{\Delta}_{L,\rho}(D) = 0$; when $D = 0$, we have a Slepian-Wolf coding problem of L sources, hence $R^{\Delta}_{L,\rho}(D) = 0$ due to the no rate loss conclusion of the Slepian-Wolf theorem [47] and its extensions [12, 60]; finally, when $D = 1$, $R^{\nleftrightarrow}_{L,\rho}(D) = R^{\nuparrow\downarrow}_{L,\rho}(D) = 0$ and the rate loss is also zero.

For any fixed $\rho \in (0,1)$, there is a maximum sum-rate loss over all D's, and this maximum sum-rate loss (as a function of ρ) monotonically increases to a supremum value as $\rho \to 1$. Moreover, it is seen from Fig. 5 that the distortion that maximizes the sum-rate loss goes to zero as $\rho \to 1$. This implies that the supremum sum-rate loss is approached from below as both minimum sum-rates $R^{\nuparrow\downarrow}_{L,\rho}(D)$ and $R^{\nleftrightarrow}_{L,\rho}(D)$ go to infinity, while the difference between them remains finite. And the sum-rate loss $R^{\Delta}_{L,\rho}(D)$ has singularity at $(\rho, D) = (1, 0)$.

Lemma 6 *For a given L, the supremum sum-rate loss over all possible ρ's and D's is*

$$\sup_{\rho\in(0,1),D\in(0,1)} R^{\Delta}_{L,\rho}(D) = \frac{1}{2}\log_2\frac{\delta_L\left(\frac{2L+1-\sqrt{1+4L}}{2L^2}\right)}{\delta_L\left(\frac{-1+\sqrt{1+4L}}{2L}\right)} \tag{3.46}$$

$$\overset{L\to\infty}{\rightsquigarrow} \frac{\sqrt{L}}{2}\log_2 e + \frac{1}{2} - \frac{1}{4}\log_2 L, \tag{3.47}$$

where $A \overset{L\to\infty}{\rightsquigarrow} B$ means $\lim_{L\to\infty}(A - B) = 0$.

Proof 2 *See Appendix A.*

Remark: First, (3.46) hold for any integer $L \geq 2$; second, according to (3.46), the exact supremum sum-rate loss is $\frac{1}{2}\log_2\frac{5}{4} = 0.161$ b/s, 0.300 b/s, 1.775 b/s, and 5.260 b/s, for $L = 2, 3, 20$, and 100, respectively; third, the 0.161 b/s supremum sum-rate loss for $L = 2$ is much smaller than the 1 b/s upper bound (see Lemma 4) provided by Zamir in [72]; finally, (3.47) indicates that, as L increases, the supremum sum-rate loss increases in the order of $\frac{\sqrt{L}}{2}\log_2 e$ b/s, since $\lim_{L\to\infty}\frac{1/2-1/4\log_2 L}{\sqrt{L}} = 0$. Fig. 6 plots the supremum sum-rate loss as a function of L, together with its asymptotic limit function (3.47) for comparison.

As $L \to \infty$, we can see that the supremum sum-rate loss asymptotically approaches its limit function (3.47).

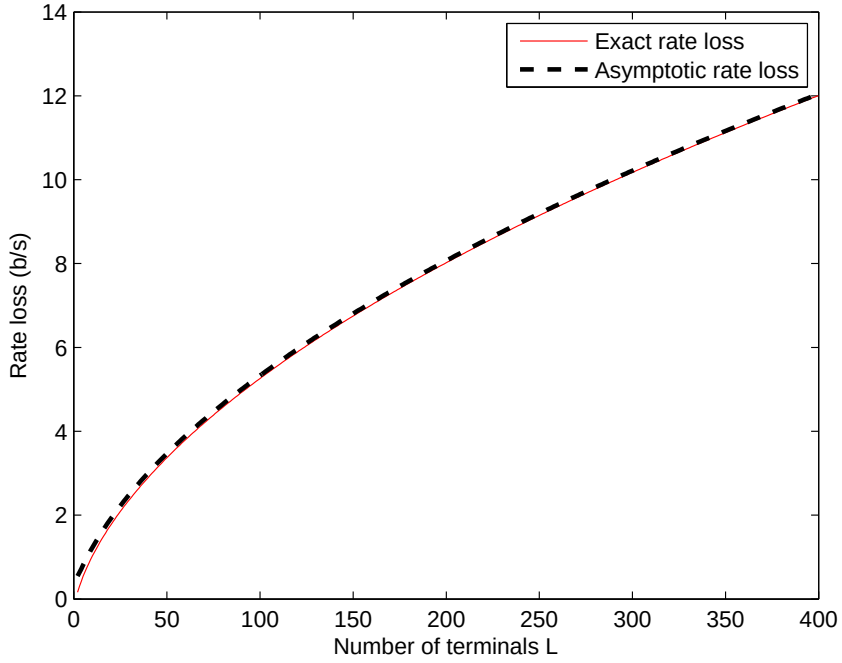

Fig. 6. The supremum sum-rate loss $\sup_{\rho,D} R^{\Delta}_{L,\rho}(D)$ for the quadratic Gaussian MT source coding problem.

Now we compute the exact sum-rate loss for the two-terminal case without the symmetric assumption. The main results in [58] state that

$$R^{\Updownarrow}_{2,\rho}((D_1, D_2)^T) = \frac{1}{2}\log_2 \frac{(1-\rho^2)\beta_{max}}{2D_1 D_2}, \tag{3.48}$$

where $\beta_{max} = 1 + \sqrt{1 + \frac{4\rho^2 D_1 D_2}{(1-\rho^2)^2}}$. For a fixed $\rho \in (0, 1)$, define the maximum rate loss

as

$$R_{2,\rho}^{\Delta_{max}} = \max_{D_1,D_2\in(0,1]} R_{2,\rho}^{\Delta}((D_1,D_2)^T) \tag{3.49}$$

$$= \begin{cases} \frac{1}{2}\log_2 \frac{\beta_{max}}{2}\cdot(1-\theta_{max}^2) & \text{if } \rho \geq \rho^\star \\ \frac{1}{2}\log_2 \frac{\beta_{max}}{2} & \text{if } \rho < \rho^\star \end{cases}, \tag{3.50}$$

where $\theta_{max} = \frac{\rho-\sqrt{(1-D_1)(1-D_2)}}{\sqrt{D_1 D_2}}$. It can be shown that for any $\rho \in (0,1)$, $D_1^{\geq} = D_2^{\geq} = \frac{(1+\rho)^2(1-\rho)}{1+2\rho}$ maximizes $R_{2,\rho}^{\Delta_{max}}$. Then we have

$$\sup_{\rho\in(0,1),D_1,D_2\in(0,1)} R_{2,\rho}^{\Delta}\big((D_1,D_2)^T\big) \tag{3.51}$$

$$= \sup_{\rho\in(0,1)} \frac{1}{2}\log_2\Big(1+\frac{\rho^2}{(1+\rho)^2}\Big) = \frac{1}{2}\log_2\frac{5}{4} = 0.161 \text{ b/s}. \tag{3.52}$$

Fig. 7 plot the sum-rate loss for $\rho = 0.9$ and general D_1 and D_2, we observe that the maximum sum-rate loss for a fixed ρ is achieved at one diagonal point, which is consistent with the analytical results.

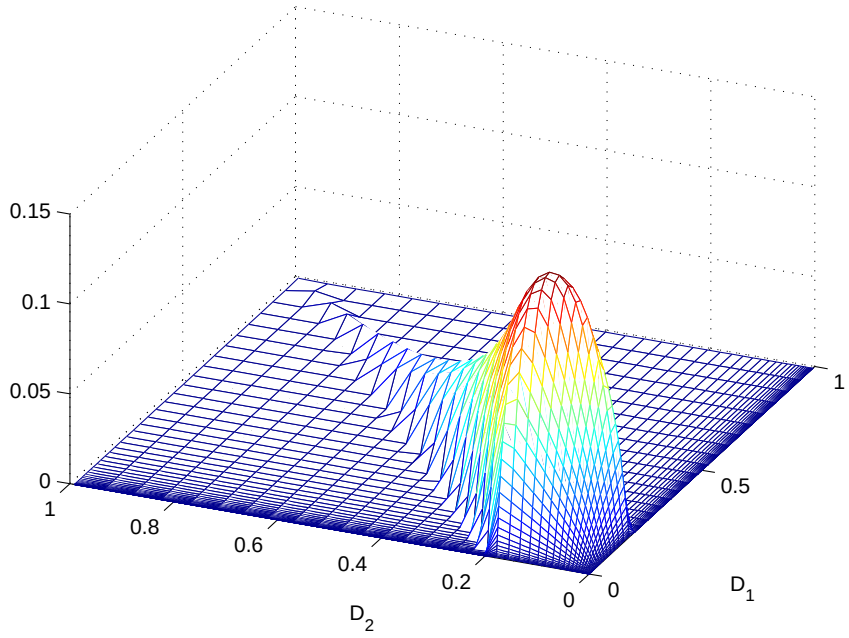

Fig. 7. The sum-rate loss for the quadratic Gaussian MTsource coding problem with two sources $\mathbf{\Sigma_Y} = \mathcal{S}_2(1, 0.9)$ and general D_1 and D_2.

3. A conjecture on the supremum sum-rate loss

In section 2, we show that for the quadratic Gaussian MT source coding problem with two terminals, the supremum sum-rate loss over all symmetric sources and equal distortions is actually the supremum loss over all possible source correlations and distortions.

Moreover, overwhelming numerical evaluations of the upper bound (3.42) have been made for $L = 3$ and $L = 4$ with general source correlations and target distortions, and no exceptions (that exceed the supremum sum-rate loss in (3.46)) have been found. Hence we have the following conjecture.

Conjecture 1 (supremum sum-rate loss for the general quadratic Gaussian MT source coding problem): For any integer $L \geq 2$, it holds,

$$\sup_{\boldsymbol{\Sigma_Y}, \boldsymbol{D}} R^{\Delta}_{\boldsymbol{\Sigma_Y}}(\boldsymbol{D}) = \sup_{\rho \in (0,1), D \in (0,1)} R^{\Delta}_{L,\rho}(D). \tag{3.53}$$

CHAPTER IV

CODE DESIGNS FOR QUADRATIC GAUSSIAN MT SOURCE CODING

A. Proposed code designs for MT source coding

In this section, we propose two code designs for the direct and indirect Gaussian MT coding problems, which are capable of trading off rates between the two encoders. The first is based on *asymmetric SWCQ*, which employs quantization and asymmetric SW coding, and is implemented via source splitting [46]. The second relies on *symmetric SWCQ*, which exploits quantization and symmetric SW coding [49]. We show that using random binning argument [12], both designs can potentially approach any point on the sum-rate bound in either of the two Gaussian MT coding problems.

1. Asymmetric SWCQ

Asymmetric SWCQ is schematically depicted in Fig. 8 in conjunction with source splitting for MT source coding. It consists of a classical source encoder/decoder pair, two WZ encoder/decoder pairs, and a linear combinator.

The *Classical Source Encoder/Decoder pair* is defined by the following four functions

$$\begin{aligned}
\mathcal{Q}_{21} &: \mathcal{Y}_2^n \rightarrow \{1,2,...,2^{nR_{21}^Q}\},\\
\mathcal{E}^{ENT} &: \{1,2,...,2^{nR_{21}^Q}\} \rightarrow \{1,2,...,2^{nR_{21}}\},\\
\mathcal{D}^{ENT} &: \{1,2,...,2^{nR_{21}}\} \rightarrow \{1,2,...,2^{nR_{21}^Q}\},\\
\mathcal{Q}_{21}^{-1} &: \{1,2,...,2^{nR_{21}^Q}\} \rightarrow \boldsymbol{\mathcal{Z}}_{21}^n,
\end{aligned}$$

where R_{21}^Q is the quantization rate of *Quantizer II*, R_{21} is the transmission rate of the Classical Source Encoder, and $\boldsymbol{\mathcal{Z}}_{21}^n$ is an n-dimensional vector codebook of size $2^{nR_{21}^Q}$. Quantizer II first quantizes Y_2^n (which is a block of n source samples in the direct or a block of noisy observations in the indirect setup) using codebook $\boldsymbol{\mathcal{Z}}_{21}^n$ by finding the

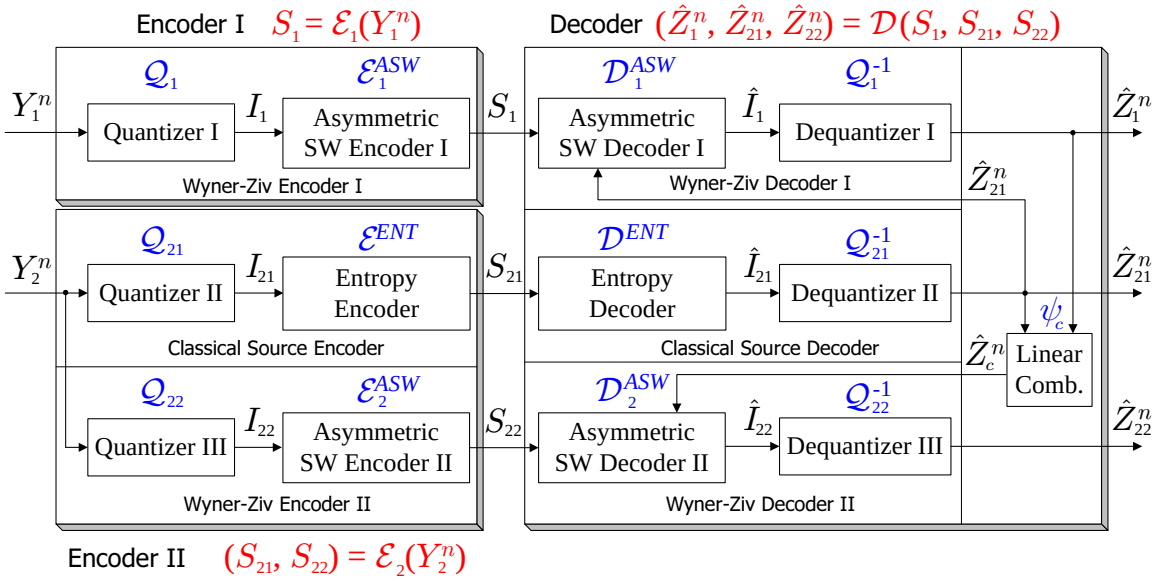

Fig. 8. Block diagram of asymmetric SWCQ for MT source coding.

vector codeword $Z_{21}^n \in \mathcal{Z}_{21}^n$ that is "closest" (e.g., in Euclidean distance) to Y_2^n, and outputs the quantization index $I_{21} = \mathcal{Q}_{21}(Y_2^n) \triangleq \mathbb{i}_{21}(Z_{21}^n)$, where $\mathbb{i}_{21}$ is an *index function* of $\mathcal{Z}_{21}^n$ that bijectively maps each codeword in $\mathcal{Z}_{21}^n$ to an index in $\{1, 2, ..., 2^{nR_{21}^Q}\}$. Then the *Entropy Encoder* compresses I_{21} to $S_{21} = \mathcal{E}^{ENT}(I_{21})$, which is transmitted at rate R_{21} b/s. At the decoder side, the Classical Source Decoder losslessly decompresses S_{21} to $\hat{I}_{21} = \mathcal{D}^{ENT}(S_{21})$ using the *Entropy Decoder*, and then employs *Dequantizer II* to reconstruct Z_{21}^n as $\hat{Z}_{21}^n = \mathcal{Q}_{21}^{-1}(\hat{I}_{21}) \triangleq \mathbb{i}_{21}^{-1}(\hat{I}_{21})$. Operations in the Classical Source Encoder/Decoder pair can be summarized as

$$\begin{aligned} \text{Encoder}: \quad S_{21} &= \mathcal{E}^{ENT}\Big[\mathcal{Q}_{21}(Y_2^n)\Big], \\ \text{Decoder}: \quad \hat{Z}_{21}^n &= \mathcal{Q}_{21}^{-1}\Big[\mathcal{D}^{ENT}(S_{21})\Big]. \end{aligned} \tag{4.1}$$

Wyner-Ziv Encoder/Decoder pair I is defined by the following four functions

$$\begin{aligned}
\mathcal{Q}_1 &: \mathcal{Y}_1^n \rightarrow \{1,2,...,2^{nR_1^Q}\},\\
\mathcal{E}_1^{ASW} &: \{1,2,...,2^{nR_1^Q}\} \rightarrow \{1,2,...,2^{nR_1}\},\\
\mathcal{D}_1^{ASW} &: \{1,2,...,2^{nR_1}\} \times \boldsymbol{\mathcal{Z}}_{21}^n \rightarrow \{1,2,...,2^{nR_1^Q}\},\\
\mathcal{Q}_1^{-1} &: \{1,2,...,2^{nR_1^Q}\} \rightarrow \boldsymbol{\mathcal{Z}}_1^n,
\end{aligned}$$

where R_1^Q is the quantization rate of *Quantizer I*, R_1 the transmission rate of Wyner-Ziv Encoder I, and $\boldsymbol{\mathcal{Z}}_1^n$ a codebook of size $2^{nR_1^Q}$, which is used in Quantizer I to quantize Y_1^n. The resulting quantization index $I_1 = \mathcal{Q}_1(Y_1^n) \triangleq \mathbb{i}_1(Z_1^n)$ is compressed by *Asymmetric SW Encoder I* to $S_1 = \mathcal{E}_1^{ASW}(I_1)$, which is transmitted at rate R_1 b/s. With $\hat{Z}_{21}^n$ as side information, *Wyner-Ziv Decoder I* generates $\hat{I}_1 = \mathcal{D}_1^{ASW}(S_1, \hat{Z}_{21}^n)$ as the reconstruction of I_1, and decodes it to $\hat{Z}_1^n = \mathcal{Q}_1^{-1}(\hat{I}_1) \triangleq \mathbb{i}_1^{-1}(\hat{I}_1)$ with *Dequantizer II*. Operations in the Wyner-Ziv Encoder/Decoder pair I can be summarized as

$$\begin{aligned}
\text{Encoder}: \quad S_1 &= \mathcal{E}_1^{ASW}\Big[\mathcal{Q}_1(Y_1^n)\Big],\\
\text{Decoder}: \quad \hat{Z}_1^n &= \mathcal{Q}_1^{-1}\Big[\mathcal{D}_1^{ASW}(S_1, \hat{Z}_{21}^n)\Big].
\end{aligned} \tag{4.2}$$

To generate the side information for the second Wyner-Ziv encoder/decoder pair, the *Linear Combinator* $\psi_c : \boldsymbol{\mathcal{Z}}_1^n \times \boldsymbol{\mathcal{Z}}_{21}^n \rightarrow \boldsymbol{\mathcal{Z}}_c^n$ implements a linear function $\hat{Z}_c^n = \psi_c(\hat{Z}_1^n, \hat{Z}_{21}^n) = \alpha_c \hat{Z}_1^n + \beta_c \hat{Z}_{21}^n$.

Wyner-Ziv Encoder/Decoder pair II then implements the following four functions

$$\begin{aligned}
\mathcal{Q}_{22} &: \mathcal{Y}_2^n \rightarrow \{1,2,...,2^{nR_{22}^Q}\},\\
\mathcal{E}_2^{ASW} &: \{1,2,...,2^{nR_{22}^Q}\} \rightarrow \{1,2,...,2^{nR_{22}}\},\\
\mathcal{D}_2^{ASW} &: \{1,2,...,2^{nR_{22}}\} \times \boldsymbol{\mathcal{Z}}_c^n \rightarrow \{1,2,...,2^{nR_{22}^Q}\},\\
\mathcal{Q}_1^{-1} &: \{1,2,...,2^{nR_{22}^Q}\} \rightarrow \boldsymbol{\mathcal{Z}}_{22}^n,
\end{aligned}$$

where R_{22}^Q is the quantization rate of *Quantizer III*, R_{22} the transmission rate of the Wyner-

Ziv Encoder II, and $\boldsymbol{\mathcal{Z}}_{22}^n$ a codebook of size $2^{nR_{22}^Q}$, which is used in Quantizer III to quantize Y_2^n. The resulting quantization index $I_{22} = \mathcal{Q}_{22}(Y_2^n) \triangleq \mathbb{i}_{22}(Z_{22}^n)$ is compressed by *Asymmetric SW Encoder II* to $S_{22} = \mathcal{E}_2^{ASW}(I_{22})$, which is transmitted at rate R_{22} b/s. With $\hat{Z}_c^n$ as side information, *Wyner-Ziv Decoder II* generates $\hat{I}_{22} = \mathcal{D}_2^{ASW}(S_{22}, \hat{Z}_c^n)$ as the reconstruction of I_{22}, and decodes it to $\hat{Z}_{22}^n = \mathcal{Q}_{22}^{-1}(\hat{I}_{22}) \triangleq \mathbb{i}_{22}^{-1}(\hat{I}_{22})$ with *Dequantizer III*. Operations in the *Linear Combinator* and the *Wyner-Ziv Encoder/Decoder pair II* can be summarized as

$$\begin{aligned} \text{Encoder}: \quad S_{22} &= \mathcal{E}_2^{ASW}\Big[\mathcal{Q}_{22}(Y_2^n)\Big], \\ \text{Decoder}: \quad \hat{Z}_{22}^n &= \mathcal{Q}_{22}^{-1}\Big[\mathcal{D}_2^{ASW}\big(S_{22}, \psi_c(\hat{Z}_1^n, \hat{Z}_{21}^n)\big)\Big]. \end{aligned} \tag{4.3}$$

Note that, *Encoder I* and *Encoder II* separately encode Y_1^n and Y_2^n using rates R_1 b/s and $R_2 \triangleq R_{21} + R_{22}$ b/s, respectively; *Decoder* then reconstructs the three quantized versions of the sources as $(\hat{Z}_1^n, \hat{Z}_{21}^n, \hat{Z}_{22}^n)$.

Our design for direct MT coding is a combination of asymmetric SWCQ and *Linear Estimator*, which implements the function $\psi_{Direct}^{ASWCQ} : \boldsymbol{\mathcal{Z}_1^n} \times \boldsymbol{\mathcal{Z}_{21}^n} \times \boldsymbol{\mathcal{Z}_{22}^n} \to \mathcal{Y}_1^n \times \mathcal{Y}_2^n$ defined by

$$\begin{pmatrix} \hat{Y}_1^n \\ \hat{Y}_2^n \end{pmatrix} = \begin{bmatrix} \alpha_1^A & \beta_1^A & \gamma_1^A \\ \alpha_2^A & \beta_2^A & \gamma_2^A \end{bmatrix} \begin{pmatrix} \hat{Z}_1^n \\ \hat{Z}_{21}^n \\ \hat{Z}_{22}^n \end{pmatrix}. \tag{4.4}$$

Similarly, our design for indirect MT coding is a combination of asymmetric SWCQ and *Linear Estimator*, which implements the function $\psi_{Indirect}^{ASWCQ} : \boldsymbol{\mathcal{Z}_1^n} \times \boldsymbol{\mathcal{Z}_{21}^n} \times \boldsymbol{\mathcal{Z}_{22}^n} \to \mathcal{X}^n$ defined by

$$\hat{X}^n = (\alpha_X^A \ \beta_X^A \ \gamma_X^A) \cdot (\hat{Z}_1^n \ \hat{Z}_{21}^n \ \hat{Z}_{22}^n)^T. \tag{4.5}$$

The following two theorems state that our asymmetric SWCQ designs can approach any point on the sum-rate bound $\partial\hat{\mathcal{R}}_{12}^{BT}(D_1^*, D_2^*)$ in the direct MT setting and $\partial\hat{\mathcal{R}}_{12}^{YI}(D^*)$ in the indirect setting.

Theorem 2 *Let (R_1^*, R_2^*) be any point on the sum-rate bound $\partial\hat{\mathcal{R}}_{12}^{BT}(D_1^*, D_2^*)$ of (2.9) for the direct MT problem (assume (2.10) is satisfied). For any $\epsilon > 0$, there exists a block length n, two asymmetric SWCQ encoders $\mathcal{E}_1$, $\mathcal{E}_2$, which separately compress sources Y_1 and Y_2 at rates R_1 and R_2, respectively, and an asymmetric decoder $\mathcal{D}$, which jointly reconstructs the sources as $\hat{Y}_1$ and $\hat{Y}_2$, such that*

$$\frac{1}{n}\sum_{i=1}^{n} E[(Y_{j,i} - \hat{Y}_{j,i})^2] < D_j^* + \epsilon, \qquad j = 1, 2, \tag{4.6}$$

$$R_j < R_j^* + \epsilon, \qquad j = 1, 2. \tag{4.7}$$

Proof 3 *See Appendix A.*

Theorem 3 *Let (R_1^*, R_2^*) be any point on the sum-rate bound $\partial\hat{\mathcal{R}}_{12}^{YI}(D^*)$ of (2.18) for the indirect MT problem (assume (2.19) is satisfied). For any $\epsilon > 0$, there exists a block length n, two asymmetric SWCQ encoders $\mathcal{E}_1$, $\mathcal{E}_2$, which separately compress observations Y_1 and Y_2 at rates R_1 and R_2, respectively, and an asymmetric decoder $\mathcal{D}$, which reconstructs source X as $\hat{X}$, such that*

$$\frac{1}{n}\sum_{i=1}^{n} E[(X_i - \hat{X}_i)^2] < D^* + \epsilon, \tag{4.8}$$

$$R_j < R_2^* + \epsilon, \qquad j = 1, 2. \tag{4.9}$$

Proof 4 *See Appendix B.*

2. Symmetric SWCQ

Symmetric SWCQ is schematically depicted in Fig. 9. *Quantizer I* and *Quantizer II* separately quantize Y_1^n and Y_2^n using n-dimensional codebooks $\boldsymbol{\mathcal{Z}}_2^n$ and $\boldsymbol{\mathcal{Z}}_2^n$ of size $2^{nR_1^Q}$ and $2^{nR_2^Q}$, respectively. The resulting quantization indices $I_1 = \mathcal{Q}_1(Y_1^n) \triangleq \mathbb{i}_1(Z_1^n)$ and $I_2 = \mathcal{Q}_2(Y_2^n) \triangleq \mathbb{i}_2(Z_2^n)$ are separately compressed by *Symmetric SW Encoder I* $\mathcal{E}_1^{SSW}$: $\{1, 2, ..., 2^{nR_1^Q}\} \to \{1, 2, ..., 2^{nR_1}\}$ and *Symmetric SW Encoder II* $\mathcal{E}_2^{SSW}$: $\{1, 2, ..., 2^{nR_2^Q}\} \to$

$\{1, 2, ..., 2^{nR_2}\}$ defined by $S_1 = \mathcal{E}_1^{SSW}(I_1)$ and $S_2 = \mathcal{E}_1^{SSW}(I_2)$, respectively. The transmission rates for the two encoders are R_1 b/s and R_2 b/s, respectively.

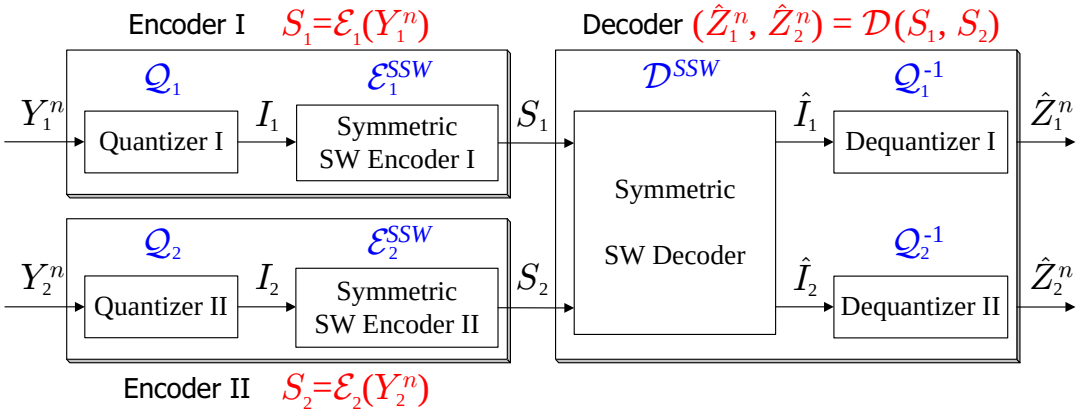

Fig. 9. Block diagram of symmetric SWCQ for MT source coding.

At the decoder side, the *Symmetric SW Decoder* jointly reconstructs the quantization indices I_1 and I_2 based on the received messages S_1 and S_2. Specifically, it implements a function

$$\mathcal{D}^{SSW} : \{1, 2, ..., 2^{nR_1}\} \times \{1, 2, ..., 2^{nR_2}\} \to \{1, 2, ..., 2^{nR_1^Q}\} \times \{1, 2, ..., 2^{nR_2^Q}\} \tag{4.10}$$

defined by $(\hat{I}_1, \hat{I}_2) = \mathcal{D}^{SSW}(S_1, S_2)$. Finally, *Dequantizer I* and *Dequantizer II* reproduce the codewords as $\hat{Z}_1^n = \mathcal{Q}_1^{-1}(\hat{I}_1) \triangleq \mathbb{i}_1^{-1}(\hat{I}_1)$ and $\hat{Z}_2^n = \mathcal{Q}_2^{-1}(\hat{I}_2) \triangleq \mathbb{i}_2^{-1}(\hat{I}_2)$, respectively.

Our direct MT code design is a combination of symmetric SWCQ and *Linear Estimator*, which implements the function $\psi_{Direct}^{SSWCQ} : \boldsymbol{\mathcal{Z}_1^n} \times \boldsymbol{\mathcal{Z}_2^n} \to \mathcal{Y}_1^n \times \mathcal{Y}_2^n$ defined by

$$\begin{pmatrix} \hat{Y}_1^n \\ \hat{Y}_2^n \end{pmatrix} = \begin{bmatrix} \alpha_1^S & \beta_1^S \\ \alpha_2^S & \beta_2^S \end{bmatrix} \begin{pmatrix} \hat{Z}_1^n \\ \hat{Z}_2^n \end{pmatrix}. \tag{4.11}$$

Similarly, our indirect MT code design is a combination of symmetric SWCQ and *Linear Estimator*, which implements the function $\psi_{Indirect}^{SSWCQ} : \boldsymbol{\mathcal{Z}_1^n} \times \boldsymbol{\mathcal{Z}_2^n} \to \mathcal{X}^n$ defined by

$$\hat{X}^n = (\alpha_X^S \ \beta_X^S) \cdot (\hat{Z}_1^n \ \hat{Z}_2^n)^T. \tag{4.12}$$

Similar to the asymmetric SWCQ scheme, the following two theorems assert optimality of our symmetric SWCQ designs in the sense of achieving any point on the sum-rate bounds (2.9) and (2.18). The proofs of both theorems are given in Appendix C.

Theorem 4 *Let (R_1^*, R_2^*) be any point on the sum-rate bound $\partial\hat{\mathcal{R}}_{12}^{BT}(D_1^*, D_2^*)$ of (2.9) for the direct MT problem (assume (2.10) is satisfied). For any $\epsilon > 0$, there exists a block length n, two symmetric SWCQ encoders $(\mathcal{E}_1, \mathcal{E}_2)$, which separately compress sources Y_1 and Y_2 at rates R_1 and R_2, respectively, and a symmetric SWCQ decoder $\mathcal{D}$, which jointly reconstructs the sources as $\hat{Y}_1$ and $\hat{Y}_2$, such that*

$$\frac{1}{n}\sum_{i=1}^{n} E[(Y_{j,i} - \hat{Y}_{j,i})^2] < D_j^* + \epsilon, \qquad j = 1, 2, \tag{4.13}$$

$$R_j < R_j^* + \epsilon, \qquad j = 1, 2. \tag{4.14}$$

Theorem 5 *Let (R_1^*, R_2^*) be any point on the sum-rate bound $\partial\hat{\mathcal{R}}_{12}^{YI}(D^*)$ of (2.18) for the indirect MT problem (assume (2.19) is satisfied). For any $\epsilon > 0$, there exists a block length n, two symmetric SWCQ encoders $(\mathcal{E}_1, \mathcal{E}_2)$, which separately compress observations Y_1 and Y_2 at rates R_1 and R_2, respectively, and a symmetric SWCQ decoder $\mathcal{D}$, which reconstructs source X as $\hat{X}$, such that*

$$\frac{1}{n}\sum_{i=1}^{n} E[(X_i - \hat{X}_i)^2] < D^* + \epsilon, \tag{4.15}$$

$$R_j < R_j^* + \epsilon, \qquad j = 1, 2. \tag{4.16}$$

B. Practical quantizer design and high-rate performance analysis

There are two key components in our SWCQ framework: vector quantization (VQ) and SW coding. Both of them need to be optimal to achieve the sum-rate bounds in (2.11) and (2.20) for the direct and indirect MT problems, respectively; that is, each quantizer must be capable for achieving the rate-distortion limit of its Gaussian input source, and SW coding

capable of compressing the two quantized sources to their joint entropy. Additionally, it also requires the two quantization noises to be independent of the sources (and each other) such that the Markov assumptions in the achievability proofs of [38, 40, 58] are satisfied.

It is shown by Zamir and Berger [73] that at high resolution, high-dimensional dithered lattice quantizer [74, 73, 76] can fulfill the above requirements. When the dimensionality goes to infinity, a dithered lattice quantizer can indeed achieve the rate-distortion limit of the Gaussian source, while producing white Gaussian quantization noise that is independent of the source. The use of independently dithered lattice quantizers for direct MT source coding was suggested in [73] so that the quantization noises are mutually independent. However, it is not practical to implement lattice quantizers in high dimension. Fortunately, TCQ [33] provides a suboptimal yet efficient means of realizing high-dimensional VQ. Although TCQ is not strictly a lattice quantizer, it shares many nice properties (e.g., congruent Voronoi regions) with the latter. Another merit of using TCQ is that its dithering sequence can be generated by a simple i.i.d. uniformly distributed source. This reduces the complexity of TCQ when compared to dithered lattice quantization, which requires the dither sequence to be uniformly distributed over the basic Voronoi region. Moreover, except for the trellis bits, the codeword vectors in the TCQ indices are memoryless, making the design of the succeeding SW coder much easier. Therefore, in our practical code design, we use TCQ for all quantizers described in the previous section.

In the rest of this section, we first review TCQ and show how a dithering sequence can be used in TCQ to produce quantization noise independent of the source, we then perform high-rate performance analysis of our asymmetric and symmetric SWCQ design under practical TCQ and ideal SW coding.

1. Trellis Coded Quantization (TCQ)

TCQ [33] is the source coding counterpart of trellis coded modulation (TCM) [56]. It is the most powerful practical technique for implementing high-dimensional VQ, due to its excellent MSE performance at modest complexity.

A TCQ is defined by a one-dimensional *expanded signal set* (ESS) and trellis of a convolutional code. Suppose we want to quantize a continuous source X using rate R b/s. TCQ first forms an ESS of size 2^{R+1} (denoted as $\mathcal{D}$), and equally partitions it into $N_c = 2^{\tilde{R}+1}$ subsets, $\tilde{R} \leq R$, each having $2^{R-\tilde{R}}$ points. These N_c subsets (also referred to as cosets) are denoted as $\mathcal{D}_0$, $\mathcal{D}_1$, $\mathcal{D}_2$, ..., $\mathcal{D}_{N_c-1}$, and hence $\mathcal{D} = \bigcup_{i=0}^{N_c-1} \mathcal{D}_i$. In general, the partition of the 2^{R+1} signal points in $\mathcal{D}$ proceeds from left to right, labeling consecutive points $\mathcal{D}_0$, $\mathcal{D}_1$, ..., $\mathcal{D}_{N_c-1}$; $\cdots$; $\mathcal{D}_0$, $\mathcal{D}_1$, ..., $\mathcal{D}_{N_c-1}$. This way, each signal point in $\mathcal{D}$ can be denoted as $q_c^w, w = 0, 1, \ldots, 2^{R-\tilde{R}}-1, c = 0, 1, ..., N_c - 1$, where c is the *coset index* such that $q_c^w \in \mathcal{D}_c$, and w the *codeword index*. A *trellis* is defined by a possibly time-dependent state transition diagram of a finite-state machine. More precisely, a length-n rate-$\frac{\tilde{R}}{\tilde{R}+1}$ trellis $\mathbb{T}$ with N_s states is a concatenation of n mappings, where the i-th mapping ($0 \leq i \leq n-1$) is from the i-th state of the machine S_i ($0 \leq S_i \leq N_s - 1$) and the i-th input $\tilde{R}$-bit message m_i to the next state S_{i+1} and the i-th output $(\tilde{R}+1)$-bit message c_i, i.e., $\mathbb{T} = \{\phi_i\}_{i=0}^{n-1}$ with $\phi_i : (S_i, m_i) \mapsto (S_{i+1}, c_i)$. The trellises used in TCQ are usually time-invariant and are based on an underlying convolutional code $\mathcal{C}$ with rate $\frac{\tilde{R}}{\tilde{R}+1}$. Under this constraint, we can define a trellis $\mathbb{T}$ by one of its component mappings $\phi_i \equiv \phi : (S_{current}, m) \mapsto (S_{next}, c)$, where $0 \leq m \leq 2^{\tilde{R}} - 1$ and $0 \leq c \leq 2^{\tilde{R}+1} - 1$. The input-output relation of $\mathbb{T}$ can be written then as $\boldsymbol{c} = \mathbb{T}(\boldsymbol{m})$.

Based on a size-2^{R+1} ESS $\mathcal{D}$ and a length-n trellis $\mathbb{T}$ with N_s-state machine, the source X is quantized using the Viterbi algorithm one block $\mathbf{x}$ at a time. We associate the i-th sample x_i in $\mathbf{x}$ with the coset $\mathcal{D}_{c_i}$ indexed by the output c_i of the trellis, and de-

fine the distortion for x_i as $D_i(c_i) = \min_{w_i} \|x_i - q_{c_i}^{w_i}\|^2$, which is the distortion between x_i and the codeword in $\mathcal{D}_{c_i}$ that is closest to x_i. The Viterbi algorithm then searches for the input vector $\boldsymbol{m} = \{m_0, m_1, \cdots, m_{n-1}\}$ that minimizes the accumulated distortion defined as $D(\boldsymbol{m}) = \sum_{i=0}^{n-1} D_i(\mathbb{T}_i(\boldsymbol{m}))$, where $\mathbb{T}_i(\boldsymbol{m}) = c_i$ is the i-th trellis output corresponding to the input vector $\boldsymbol{m}$. Finally, TCQ stacks the $R - \tilde{R}$ bit-planes of the codeword vector $\mathbf{w} = \{w_0, w_1, \cdots, w_{n-1}\}$ on top of the $\tilde{R}$ bit-planes of trellis vector $\boldsymbol{m}$ to form its output index vector $\mathbf{b} = \{\mathbf{b}_0, \mathbf{b}_1, \cdots, \mathbf{b}_{n-1}\}$, achieving a rate of R b/s, where $\mathbf{b}_i = ((b_i^{R-1}, \cdots, b_i^{\tilde{R}}), (b_i^{\tilde{R}-1}, \cdots, b_i^0))^T$, with $(b_i^{R-1}, \cdots, b_i^{\tilde{R}})$ and $(b_i^{\tilde{R}-1}, \cdots, b_i^0)$ coming from the binary representation of $w_i = (b_i^{R-1} \cdots b_i^{\tilde{R}+1} b_i^{\tilde{R}})_2$ and $m_i = (b_i^{\tilde{R}-1} \cdots b_i^1 b_i^0)_2$, respectively. This way, we can denote a trellis coded quantizer as $\mathbf{b} = \mathcal{Q}_{\mathcal{C},\mathcal{D}}^{TCQ}(\mathbf{x})$. The above defined TCQ is often referred to as *fixed rate* TCQ [33]. Although the ESS of TCQ can be carefully designed according to a specific source distribution, we constrain ourselves to a uniform ESS due to its analytical simplicity and nice properties.

In general, TCQ cannot be classified as a lattice quantizer, because stacking $\tilde{R} + 1$ binary linear code does not necessarily result in a linear code in $GF(2^{\tilde{R}+1})$. However, in the special case of $\tilde{R} = 1$ (number of cosets $N_c = 4$), TCQ shares a nice property with the lattice quantizers: congruent Voronoi regions. Indeed, suppose that $\mathcal{Q}_{\mathcal{C},\mathcal{D}}^{TCQ}$ is a trellis coded quantizer with $\tilde{R} = 1$. Then, for any $\mathbf{b}, \mathbf{b}' \in 2^{R \times n}$, Voronoi region $\mathcal{V}_{\mathbf{b}} = \{\mathbf{x} \in \boldsymbol{\mathcal{X}}^n : \mathcal{Q}_{\mathcal{C},\mathcal{D}}^{TCQ}(\mathbf{x}) = \mathbf{b}\}$ is congruent to Voronoi region $\mathcal{V}_{\mathbf{b}'} = \{\mathbf{x} \in \boldsymbol{\mathcal{X}}^n : \mathcal{Q}_{\mathcal{C},\mathcal{D}}^{TCQ}(\mathbf{x}) = \mathbf{b}'\}$.

Fig. 10 (a) is an example of the Voronoi region $\mathcal{V}_{\mathbf{0}}$ of TCQ with $n = 3$, $\tilde{R} = 1$, $N_s = 4$ and $\mathcal{D} = \{-7, -6, ..., 0, 1, ...7, 8\}$. We can see that $\mathcal{V}_{\mathbf{0}}$ is a non-regular polyhedron with 18 vertices and 12 faces. Fig. 10 (b) illustrates how $\mathcal{V}_{\mathbf{0}}$ and its congruent counterparts fill the three-dimensional space. Clearly, the Voronoi regions of TCQ are not simply translations of each other, while those of lattice quantizers are.

In terms of practical performance, TCQ with a trellis of $N_s = 256$ states performs 0.2 dB away from the distortion-rate bound for *uniform* sources, which is better than any vector

quantizer of dimension less than 69 [52]. With the help of entropy coding, the same 0.2 dB gap can be obtained at all rates by entropy constrained TCQ [32, 52] for any smooth p.d.f. by using carefully designed codebooks. This small performance gap can be further reduce by increasing N_s or $\tilde{R}$, which leads to higher complexity. For example, another 0.1 dB granular gain can be obtained by increasing N_s to 8192 [65].

2. Independently dithered TCQ

TCQ is a powerful and efficient source coding technique; however, there is no guarantee that multiple trellis coded quantizers will produce quantization noises independent of each other (that are also independent of the sources), which is a key requirement in the achievability proofs for the direct and indirect MT source coding [38], [40], [58]. To resolve this issue, we have to consider the possibility of adding a dither to TCQ, just as with the entropy-constraint dithered lattice quantizers. Since TCQ is not a lattice quantizer, classical dithering with uniformly distributed dither over the basic Voronoi region of the lattice no longer produces an independent quantization noise. Thus we have to find an alternative way of generating a dither sequence of TCQ.

In this subsection, we show that under some mild assumptions, a trellis coded quantizer with an i.i.d. dither sequence can produce independent quantization noise. Without loss of generality, we assume that $\tilde{R} = 1$ and the step size of the ESS is one, i.e., the ESS $\mathcal{D} = \{-2^R + 0.5, -2^R + 1.5, ..., 2^R - 0.5\}$ is partitioned into $N_c = 4$ cosets, each with 2^{R-1} points. For a given p.d.f. $f_X(x)$, we define the *accumulated distribution* of $f_X(x)$ with respect to the ESS $\mathcal{D}$ as

$$p_{\mathcal{D}}^{\Sigma}(x) = \begin{cases} f_X(x - 2^R + 4) & x \le 0 \\ \sum_{i=-2^{R-2}+1}^{2^{R-2}-2} f_X(x - 4i) & 0 < x \le 4 \\ f_X(x + 2^R - 8) & x > 4. \end{cases} \tag{4.17}$$

We say that a source distribution $f_X(x)$ is Σ-*uniform* with respect to $\mathcal{D}$ *iff* $p_{\mathcal{D}}^{\Sigma}(x)$ is

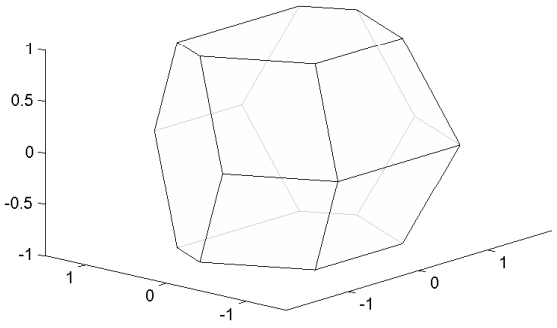

(a)

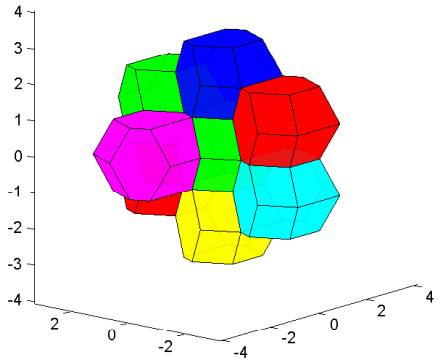

(b)

Fig. 10. Voronoi regions of TCQ when $n = 3$, $\tilde{R} = 1$, $N_s = 4$ and $\mathcal{D} = \{-7, -6, ..., 0, 1, ...7, 8\}$. (a) Voronoi region for the all-zero codeword. (b) Packing of TCQ Voronoi regions.

uniformly distributed in the interval $[0, 4]$. Indeed, all symmetric smooth distributions are very close to Σ-uniform unless the rate R is very low.

The following lemma states that under the Σ-uniform assumption, a trellis coded quantizer with an i.i.d. uniform dither sequence in the range of $[-0.5, 0.5]$ can produce independent quantization noises. The proof is given in Appendix D.

Lemma 7 *Assume $f_{X+V}(x+v)$ is Σ-uniform with respect to $\mathcal{D}$ (with step size 1), where V is a random variable uniformly distributed over $[-0.5, 0.5)$. Define the quantization error*

as

$$Q^n = (X^n + V^n) - [\mathcal{Q}_{\mathcal{D}}^{TCQ}]^{-1}\big[\mathcal{Q}_{\mathcal{D}}^{TCQ}(X^n + V^n)\big], \tag{4.18}$$

where $\mathcal{Q}_{\mathcal{D}}^{TCQ}$ *is a trellis coded quantizer with* $\tilde{R} = 1$*. Then as* n *goes to infinity,* Q_i *becomes independent of* X_i *for* $0 \le i \le n-1$*, i.e.,*

$$\lim_{n\to\infty} p_{X_i,Q_i}(x_i, q_i) = p_{X_i}(x_i) \cdot p_{Q_i}(q_i) \quad \text{or} \quad \lim_{n\to\infty} p_{Q_i|x_i}(q_i|x_i) = p_{Q_i}(q_i). \tag{4.19}$$

An illustrative comparison between dithered and non-dithered trellis coded quantizers is given in Fig. 11, in terms of the joint statistics of the i-th quantization noise Q_i and the i-th source sample X_i. Obviously, dithered TCQ (Fig. 11 (a)) produces independent quantization noise, whereas non-dithered TCQ (Fig. 11 (b)) does not.

Note that for the case with $\tilde{R} > 1$ (i.e., there are more than four cosets), Lemma 7 still holds, since a similar symmetry property (as stated in Proposition 1 of Appendix D) exists among the cosets.

3. High-rate performance analysis

Since a practical MT source coding problem is a source-channel coding problem, where quantization is followed by channel coding for SW coding, the total loss contains quantization loss due to source coding and binning loss due to channel coding [63]. In this subsection, we assume ideal binning (via capacity-achieving channel coding), and restrict ourselves to the high-rate/resolution scenario (i.e., $D^*, D_1^*, D_2^* \to 0$). The asymptotical performance of our TCQ-based asymmetric and symmetric SWCQ schemes for both direct and indirect MT source coding can be characterized by the following two theorems. The proofs are given in Appendix E and F, respectively.

Theorem 6 *Let* (R_1^*, R_2^*) *be any point on the sum-rate bound* $\partial\hat{\mathcal{R}}_{12}^{BT}(D_1^*, D_2^*)$ *of (2.9) for the direct MT source coding problem (assume (2.10) is satisfied), or* $\partial\hat{\mathcal{R}}_{12}^{YI}(D^*)$ *of (2.18)*

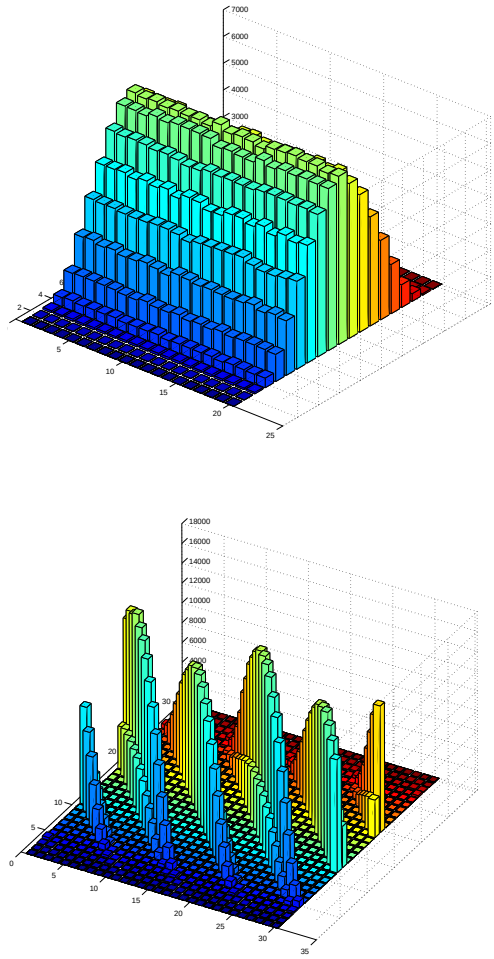

Fig. 11. Joint statistics of quantization noise Q_i and X_i for TCQ (a) with dither and (b) without dither.

for the indirect MT source coding problem (assume (2.19) is satisfied), then under ideal SW coding, the achievable rates R_{21}, R_1, and R_{22} with our asymmetric SWCQ scheme satisfy

$$\begin{aligned} R_1 &= R_1^* + \frac{1}{2}\log(2\pi e G_{\mathcal{Q}_1}) + o(1), \\ R_2 = R_{21} + R_{22} &= R_2^* + \frac{1}{2}\log(2\pi e G_{\mathcal{Q}_{21}}) + \frac{1}{2}\log(2\pi e G_{\mathcal{Q}_{22}}) + o(1), \end{aligned} \tag{4.20}$$

where $G_{\mathcal{Q}_1}, G_{\mathcal{Q}_{21}}$, and $G_{\mathcal{Q}_{22}}$ are the normalized second moments of $\mathcal{V}_0$ for the three employed trellis coded quantizers $\mathcal{Q}_1$, $\mathcal{Q}_{21}$, and $\mathcal{Q}_{22}$, respectively; and $o(1) \to 0$ as $D^*, D_1^*, D_2^* \to$

0.

Theorem 7 *Let (R_1^*, R_2^*) be any point on the sum-rate bound $\partial\hat{\mathcal{R}}_{12}^{BT}(D_1^*, D_2^*)$ of (2.9) for the direct MT source coding problem (assume (2.10) is satisfied), or $\partial\hat{\mathcal{R}}_{12}^{YI}(D^*)$ of (2.18) for the indirect MT source coding problem (assume (2.19) is satisfied), then under ideal SW coding, the achievable sum-rate of our symmetric SWCQ scheme satisfies*

$$R_1 + R_2 \;=\; R_1^* + R_2^* + \frac{1}{2}\log(2\pi e G_{\mathcal{Q}_1}) + \frac{1}{2}\log(2\pi e G_{\mathcal{Q}_2}) + o(1), \tag{4.21}$$

where $G_{\mathcal{Q}_1}$ and $G_{\mathcal{Q}_2}$ are the normalized second moments of $\mathcal{V}_\mathbf{0}$ for the two trellis coded quantizers $\mathcal{Q}_1$ and $\mathcal{Q}_2$, respectively; and $o(1) \to 0$ as $D^*, D_1^*, D_2^* \to 0$.

Before presenting our practical asymmetric and symmetric SW designs, we point out that our results in Theorems 6 and 7 are consistent with those obtained by Zamir and Berger [73] in their theoretical work on MT source coding at high resolution.

C. Practical asymmetric and symmetric SW code designs

The main elements of our practical asymmetric/symmetric SWCQ schemes are dithered TCQ (described in Section 2) and asymmetric/symmetric SW coding based on LDPC and turbo codes. We give details of the latter next.

1. Asymmetric SW code design

The SW theorem [47] was proved using random binning arguments [12]. The main idea is to randomly partition all length-n sequences into disjoint bins, transmit the index of the bin containing the source sequence, and pick from the specified bin a source sequence that is jointly typical with the side information sequence at the decoder. Asymptotically, no rate loss is incurred in SW coding due to the absence of side information at the encoder.

However, there is no efficient decoding algorithm for such a random binning scheme. The first step towards a constructive SW code was given in [61], where the use of a linear

parity-check channel code was suggested for partitioning all the source sequences into bins indexed by *syndromes* of a channel code. The set of all valid codewords (with zero syndrome) of the channel code forms only one bin, while other bins are shifts of this zero-syndrome bin. This approach is detailed below.

Let $\mathcal{C}$ be an (n, k) binary linear block code with generator matrix $\mathbf{G}_{k\times n}$ and parity-check matrix $\mathbf{H}_{(n-k)\times n}$ such that $\mathbf{G}\mathbf{H}^T = \mathbf{0}$. The syndrome of any length-n binary sequence $\mathbf{x}$ with respect to code $\mathcal{C}$ is defined as $\mathbf{s} = \mathbf{x}\mathbf{H}^T$, which is a length-$(n - k)$ binary sequence. Hence there are 2^{n-k} distinct syndromes, each indexing 2^k length-n binary source sequences. A *coset* $\mathcal{C}_\mathbf{s}$ of code $\mathcal{C}$ is defined as the set of all length-n sequences with syndrome $\mathbf{s}$, i.e., $\mathcal{C}_\mathbf{s} = \{\mathbf{x} \in \{0, 1\}^n : \mathbf{x}\mathbf{H}^T = \mathbf{s}\}$.

Consider the problem of SW coding of a binary source X with decoder side information Y (with discrete [47] or continuous [28] alphabet). Syndrome-based SW coding of $\mathbf{x}$ proceeds as follows:

- **Encoding:** The encoder computes the syndrome $\mathbf{s} = \mathbf{x}\mathbf{H}^T$ and sends it to the decoder at rate $R^{SW} = \frac{n-k}{n}$ b/s. By the SW theorem [47],

$$R^{SW} = \frac{n - k}{n} \geq H(X|Y). \tag{4.22}$$

- **Decoding:** Based on the side information $\mathbf{y}$ and received syndrome $\mathbf{s}$, the decoder finds the most probable source sequence $\hat{\mathbf{x}}$ in the coset $\mathcal{C}_\mathbf{s}$, i.e.,

$$\hat{\mathbf{x}} = \arg\max_{\mathbf{x}\in\mathcal{C}_\mathbf{s}} P(\mathbf{x}|\mathbf{y}). \tag{4.23}$$

This syndrome-based approach was first implemented by Pradhan and Ramchandran [41] using block and trellis codes. More advanced channel codes such as turbo codes are later used for asymmetric SW coding [1, 2, 30] to achieve better performance. Following the work in [29], we consider using LDPC codes [19], not only because of their

capacity-approaching performance, but also their flexible code designs using density evolution [45]. Another reason for our choice lies in low-complexity decoding based on the message-passing algorithm, which can be applied in SW coding with only slight modification [29]. Specifically, as in the conventional message-passing algorithm, the input for the i-th variable node is the log-likelihood-ratio (LLR) of x_i defined as

$$\mathrm{L}_{\mathrm{ch}}(x_i) \triangleq \log \frac{P(Y = y_i|X = 1)}{P(Y = y_i|X = 0)}, \quad 0 \le i \le n-1. \tag{4.24}$$

If X is uniform with $P(X = 1) = P(X = 0) = \frac{1}{2}$, we have

$$\mathrm{L}_{\mathrm{ch}}(x_i) = \log \frac{P(X = 1|Y = y_i)}{P(X = 0|Y = y_i)}, \quad 0 \le i \le n-1. \tag{4.25}$$

The j-th syndrome bit s_j, $0 \le j \le n-k-1$, is in fact the binary sum of the source bits corresponding to the ones in the j-th row of the parity-check matrix $\mathbf{H}$. Hence the j-th check node in the Tanner graph is related to s_j. The only difference from conventional LDPC decoding is that one needs to flip the sign of the check-to-bit LLR if the corresponding syndrome bit s_j is one [29]. Moreover, conventional density evolution [45] can be employed to analyze the iterative decoding procedure without any modification [9].

2. Symmetric SW code design

Our symmetric SWCQ design consists of dithered TCQ followed by symmetric SW coding (hence the name *symmetric SWCQ*) based on turbo/LDPC codes. In the remaining part of this section, we describe the employed symmetric SW coding scheme based on the channel partitioning method of [49], elaborate our novel multi-level symmetric SW coding framework for compressing different bit-planes of quantization indices, and compute the loss of the SWCQ design due to practical coding.

a. Symmetric SW coding for uniform binary sources [49]

Let J and K be two memoryless uniform binary sources. They are related by a binary symmetric channel (BSC) with crossover probability $P(J \oplus K = 1) = p$, where $\oplus$ denotes binary addition. Our goal is to separately compress J and K, and to jointly reconstruct them. Due to the SW theorem [47], any rate pair (r_1, r_2) that satisfies

$$\begin{aligned} r_1 &\geq H(J|K) = H(p) \\ r_2 &\geq H(K|J) = H(p) \\ r_1 + r_2 &\geq H(J,K) = H(p) + 1 \end{aligned} \tag{4.26}$$

is achievable. In [49] an efficient algorithm to design good symmetric SW codes by partitioning a single linear parity-check code was proposed. Although this algorithm can be applied to compression of multiple correlated sources, we restrict ourselves to two sources only.

Suppose that we aim at approaching a point (r_1, r_2) (i.e., to compress J at rate r_1 and K at r_2) that satisfies (4.26). Let $\mathcal{C}$ be an (n, k) linear channel block code with $k = (2 - r_1 - r_2)n$. Although both systematic and non-systematic codes can be used for $\mathcal{C}$ [49], for the sake of easy implementation, we assume that $\mathcal{C}$ is a systematic channel code with generator matrix $\boldsymbol{G} = \begin{bmatrix} \boldsymbol{I}_k & \boldsymbol{P}_{k\times(n-k)} \end{bmatrix}$. We partition $\mathcal{C}$ into two subcodes, $\mathcal{C}_1$ and $\mathcal{C}_2$, defined by generator matrices

$$\boldsymbol{G}_1 = [\boldsymbol{I}_{m_1} \quad \boldsymbol{O}_{m_1\times m_2} \quad \boldsymbol{P}_1] \text{ and } \boldsymbol{G}_2 = [\boldsymbol{O}_{m_2\times m_1} \quad \boldsymbol{I}_{m_2} \quad \boldsymbol{P}_2],$$

which consist of the top m_1 and bottom m_2 rows of $\boldsymbol{G}$, respectively, where $m_1 \triangleq (1 - r_1)n$, $m_2 \triangleq (1 - r_2)n$ (thus $m_1 + m_2 = k$). Then the parity-check matrices for $\mathcal{C}_1$ and $\mathcal{C}_2$ can be written as

$$\boldsymbol{H}_1 = \begin{bmatrix} \boldsymbol{O}_{m_2\times m_1} & \boldsymbol{I}_{m_2} & \boldsymbol{O}_{m_2\times(n-k)} \\ \boldsymbol{P}_1^T & \boldsymbol{O}_{(n-k)\times m_2} & \boldsymbol{I}_{n-k} \end{bmatrix}, \tag{4.27}$$

$$\boldsymbol{H}_2 = \begin{bmatrix} \boldsymbol{I}_{m_1} & \boldsymbol{O}_{m_1\times m_2} & \boldsymbol{O}_{m_1\times(n-k)} \\ \boldsymbol{O}_{(n-k)\times m_1} & \boldsymbol{P}_2^T & \boldsymbol{I}_{n-k} \end{bmatrix}, \tag{4.28}$$

respectively.

Encoding: It is done by multiplying u^n and v^n, the realization of J^n and K^n, respectively, by the corresponding parity check matrix $\boldsymbol{H}_1$ and $\boldsymbol{H}_2$, respectively. We partition the length-n vectors u^n and v^n into three parts (which are of lengths m_1, m_2, and $n-k$)

$$u^n = \left[u_1^{m_1} \quad u_2^{m_2} \quad u_3^{n-k}\right], \qquad v^n = \left[v_1^{m_1} \quad v_2^{m_2} \quad v_3^{n-k}\right]. \tag{4.29}$$

Then, the resulting syndrome vectors are

$$s_1^{n-m_1} = u^n\boldsymbol{H}_1^T = \left[u_2^{m_2} \quad u_3^{n-k} \oplus u_1^{m_1}\boldsymbol{P}_1\right], s_2^{n-m_2} = v^n\boldsymbol{H}_2^T = \left[v_1^{m_1} \quad v_3^{n-k} \oplus v_2^{m_2}\boldsymbol{P}_2\right], \tag{4.30}$$

which are directly send to the decoder. It is easy to see that the total number of transmitted bits for u^n and v^n is $m_2 + (n-k) = nr_1$ and $m_1 + (n-k) = nr_2$, respectively, with the desirable sum-rate of $r_1 + r_2$ b/s.

Decoding: Upon receiving the syndrome vectors $s_1^{n-m_1}$ and $s_2^{n-m_2}$, the decoder forms an auxiliary length-n row vector as

$$\begin{aligned} s^n &= \left[v_1^{m_1} \; u_2^{m_2} \; (u_3^{n-k} \oplus v_3^{n-k}) \oplus u_1^{m_1}\boldsymbol{P}_1 \oplus v_2^{m_2}\boldsymbol{P}_2\right] \\ &= \left[v_1^{m_1} \; u_2^{m_2} \; (u_3^{n-k} \oplus v_3^{n-k}) \oplus [u_1^{m_1} \; v_2^{m_2}]\boldsymbol{P}\right]. \end{aligned} \tag{4.31}$$

Then it finds a codeword c^n of the main code $\mathcal{C}$ closest (in Hamming distance) to s^n. Let

the vector $[\hat{u}_1^{m_1} \quad \hat{v}_2^{m_2}]$ be the systematic part of c^n, then u^n and v^n are recovered as

$$\hat{u}^n = \hat{u}_1^{m_1}\boldsymbol{G}_1 \oplus \left[\boldsymbol{O}_{1\times m_1} \quad u_2^{m_2} \quad u_3^{n-k} \oplus u_1^{m_1}\boldsymbol{P}_1\right] \tag{4.32}$$

$$\hat{v}^n = \hat{v}_2^{m_2}\boldsymbol{G}_2 \oplus \left[v_1^{m_1} \quad \boldsymbol{O}_{1\times m_2} \quad v_3^{n-k} \oplus v_2^{m_2}\boldsymbol{P}_2\right]. \tag{4.33}$$

It is shown in [49] that if the (n, k) main code $\mathcal{C}$ approaches the capacity of a BSC with crossover probability p, then the above designed symmetric SW code approaches the SW limit for the same binary symmetric correlation channel model.

b. Correlation model between B_1 and B_2

To apply the above symmetric SW coding scheme, first, we have to model the correlation between outputs of the two dithered quantizers B_1^n and B_2^n. Clearly, this correlation is uniquely determined by the pair of dither sequences (V_1^n, V_2^n) used in the two quantizers. Now fix a pair of (V_1^n, V_2^n), and expand the trellis bit-plane (J_1^n, K_1^n) to the corresponding coset index sequences $(C_{\mathcal{Q}_1}^n = \mathbb{T}_{\mathcal{Q}_1}(J_1^n), C_{\mathcal{Q}_2}^n = \mathbb{T}_{\mathcal{Q}_2}(K_1^n))$, then correlation modeling is done on the sample level by computing the joint p.m.f. $P(\bar{B}_1, \bar{B}_2)$, where $\bar{B}_1$ and $\bar{B}_2$ are the indices of the signal points $q_{C_{\mathcal{Q}_1}}^{W_{\mathcal{Q}_1}}$ and $q_{C_{\mathcal{Q}_2}}^{W_{\mathcal{Q}_2}}$ (the ESS $\mathcal{D}$ are the same for both quantizers), respectively, to which the sources are quantized, namely,

$$\begin{aligned} \bar{B}_1 &= W_{\mathcal{Q}_1} \times 4 + C_{\mathcal{Q}_1} = (J_m J_{m-1} \ldots J_2)_2 \times 4 + C_{\mathcal{Q}_1}, \\ \bar{B}_2 &= W_{\mathcal{Q}_2} \times 4 + C_{\mathcal{Q}_2} = (K_m K_{m-1} \ldots K_2)_2 \times 4 + C_{\mathcal{Q}_2}. \end{aligned} \tag{4.34}$$

One possible solution to compute $P(\bar{B}_1, \bar{B}_2)$ is to collect empirical statistics of $(\bar{B}_1, \bar{B}_2)$ by counting the number of occurrences of each quantization index pair $(\bar{B}_1, \bar{B}_2)$ based on the quantization output of training data generated according to the joint p.d.f. of (Y_1, Y_2). This method is similar to that used in [65]. However, to get a good approximate of two-dimensional p.m.f. $P(\bar{B}_1, \bar{B}_2)$ using empirical statistics, we need a large number of Monte

Carlo simulations, which is time-consuming, especially when the number of quantization levels is large, which is the case in the high-rate regime we consider.

A simpler solution can be obtained by assuming a Markov chain $\bar{B}_1 \to \bar{Y}_1 \to \bar{Y}_2 \to \bar{B}_2$, where $\bar{Y}_1 = Y_1 + V_1$ and $\bar{Y}_2 = Y_2 + V_2$ are the actual inputs to the two TCQ quantizers. That is,

$$P_{\bar{B}_1,\bar{B}_2|\bar{Y}_1,\bar{Y}_2}(\bar{b}_1,\bar{b}_2|\bar{y}_1,\bar{y}_2) \;=\; P_{\bar{B}_1|\bar{Y}_1}(\bar{b}_1|\bar{y}_1)\cdot P_{\bar{B}_2|\bar{Y}_2}(\bar{b}_2|\bar{y}_2). \tag{4.35}$$

Note that both $P_{\bar{B}_1|\bar{Y}_1}(\bar{b}_1|\bar{y}_1)$ and $P_{\bar{B}_2|\bar{Y}_2}(\bar{b}_2|\bar{y}_2)$ are the one-dimensional output-input relationship of non-dithered TCQ, which can be approximated using the method described in [65]. Specifically, we write

$$\begin{aligned}
& P_{\bar{B}_1,\bar{B}_2}(\bar{b}_1,\bar{b}_2) \\
= \;& \int_{-\infty}^{\infty}\int_{-\infty}^{\infty} P_{\bar{B}_1,\bar{B}_2|\bar{Y}_1,\bar{Y}_2}(\bar{b}_1,\bar{b}_2|\bar{y}_1,\bar{y}_2)\cdot p_{\bar{Y}_1,\bar{Y}_2}(\bar{y}_1,\bar{y}_2)\; d\bar{y}_1 d\bar{y}_2 \\
= \;& \int_{-\infty}^{\infty}\int_{-\infty}^{\infty} P_{\bar{B}_1|\bar{Y}_1}(\bar{b}_1|\bar{y}_1)\cdot P_{\bar{B}_2|\bar{Y}_2}(\bar{b}_2|\bar{y}_2)\cdot p_{\bar{Y}_1,\bar{Y}_2}(\bar{y}_1,\bar{y}_2)\; d\bar{y}_1 d\bar{y}_2 \\
\approx \;& \sum_{i=-T}^{T}\sum_{j=-T}^{T} P_{\bar{B}_1|\bar{Y}_1}(\bar{b}_1|\eta_i)\cdot P_{\bar{B}_2|\bar{Y}_2}(\bar{b}_2|\eta_j)\cdot \int_{\Theta_i}\int_{\Theta_j} p_{\bar{Y}_1,\bar{Y}_2}(\bar{y}_1,\bar{y}_2)\; d\bar{y}_1 d\bar{y}_2 \qquad (4.36) \\
\approx \;& \theta^2\cdot \sum_{i=-T}^{T}\sum_{j=-T}^{T} P_{\bar{B}_1|\bar{Y}_1}(\bar{b}_1|\eta_i)\cdot P_{\bar{B}_2|\bar{Y}_2}(\bar{b}_2|\eta_j)\cdot p_{\bar{Y}_1,\bar{Y}_2}(\eta_i,\eta_j), \qquad (4.37)
\end{aligned}$$

where the real line $\mathbb{R}$ is partitioned into $2T + 1$ length-θ intervals (except two boundary ones): $\Theta_{-T}, \Theta_{-T+1}, ..., \Theta_T$, with $\eta_i, i = -T, ..., T$, being the middle point of the i-th interval Θ_i. Note that the last approximation in (4.37) may be inaccurate if θ is not small enough or the correlation coefficient ρ is very close to 1. Under these circumstances, we can resort to the numerical method described in [13] to compute the bivariate Gaussian probability $\int_{\Theta_i}\int_{\Theta_j} p_{\bar{Y}_1,\bar{Y}_2}(\bar{y}_1,\bar{y}_2)\; d\bar{y}_1 d\bar{y}_2$.

An example of the resulting joint p.m.f. $p(\bar{B}_1, \bar{B}_2)$ computed using (4.36) with $V_1 = V_2 = 0$ and the number of bit planes $m = 3$ is plotted in Fig. 12. Note that, because of the symmetry assumptions on the sources (recall that we assume $\sigma^2_{y_1} = \sigma^2_{y_2}$ in the direct case

and $\sigma_{n_1}^2 = \sigma_{n_2}^2$ in the indirect case) and the quantizers (the same quantization step size q), $p(\bar{B}_1, \bar{B}_2)$ is symmetric with respect to the diagonal line on the $(\bar{B}_1, \bar{B}_2)$ plane. We also observe that most of the probability mass is concentrated near the diagonal line, because the quantization outputs of the two correlated sources/noisy observations, Y_1 and Y_2, are still correlated. Based on $p(\bar{B}_1, \bar{B}_2)$, we develop a multi-level coding framework for SW coding of the bit-planes of B_1 and B_2.

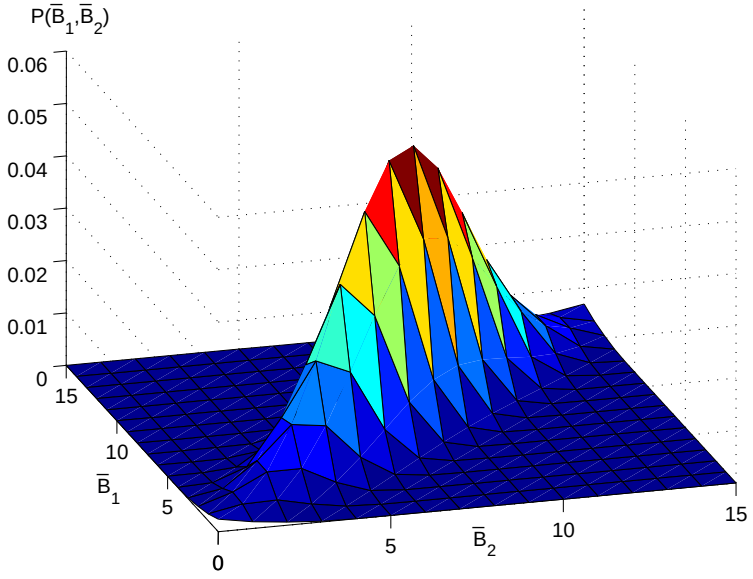

Fig. 12. Joint p.m.f. of quantization outputs $p(\bar{B}_1, \bar{B}_2)$.

c. Multi-level symmetric SW coding framework

Let $(J_1, \ldots, J_m)$ and $(K_1, \ldots, K_m)$ be binary representations of B_1 and B_2, respectively. J_1 and K_1 are the trellis bit-planes, used to specify one of the four cosets for each sample. The rest are codeword bit-planes, which are the output of the scalar quantizer with the specified coset as its codebook. Hence, given a trellis bit-plane, all codeword bit-planes are memoryless. Then, from the chain rule, we have

$$H(B_1, B_2) = H(J_1, \ldots, J_m, K_1, \ldots, K_m) = H(J_1, K_1) + \sum_{j=2}^{m} H(J_j, K_j | \mathcal{M}_{j-1}), \quad (4.38)$$

where $\mathcal{M}_{j-1} \triangleq (J_{j-1}, K_{j-1}, \ldots, J_1, K_1)$. To introduce flexibility in the rate allocation between the two encoders, we employ the symmetric SW code design based on channel code partitioning [49] for each bit-plane of B_1 and B_2. Note that if we assume ideal source coding (with independent dithering) and ideal SW coding, $Y_1, Y_2, \hat{Z}_1, \hat{Z}_2$ are jointly Gaussian. In this case, $H(B_1, B_2) = I(Y_1 Y_2; \hat{Z}_1 \hat{Z}_2)$ is the sum-rate bound defined in (2.9) and (2.18); hence we have the following lemma. The proof is straightforward (hence skipped) by considering two extreme cases of multi-level symmetric SW coding when we attempt to allocate the minimum rate to B_1 or B_2.

Lemma 8 *For fixed dithered quantizers $\mathcal{Q}_1$ and $\mathcal{Q}_2$ with outputs $B_1 = \{J_1, ..., J_m\}$ and $B_2 = \{K_1, ..., K_m\}$, any rate pair (R_1, R_2) that satisfies $R^s_{min} \le R_1, R_2 \le R^s_{max}$, where*

$$R^s_{max} = H(J_1) + \sum_{j=2}^{m} H(J_j|\mathcal{M}_{j-1}), \quad R^s_{min} = H(K_1|J_1) + \sum_{j=2}^{m} H(K_j|\mathcal{M}_{j-1}, J_j), \tag{4.39}$$

is potentially achievable with our multi-level symmetric SW codes.

If we compute the difference between (R^s_{max}, R^s_{min}) and one of the corner points on the inner sum-rate bound, which is $(R^a_{max}, R^a_{min}) = (H(B_1), H(B_2|B_1))$, we have a gap of

$$\Delta_R = R^a_{max} - R^s_{max} = R^s_{min} - R^a_{min} = \sum_{j=2}^{m} I(J_j; K_{j-1} \ldots K_1 | J_{j-1} \ldots J_1) \ge 0. \tag{4.40}$$

This gap comes from the different coding order between multi-level symmetric and asymmetric SW coding in the extreme cases. Our experiments show that this gap is very small in practice (e.g., 0.03 b/s). One possible improvement of this pure symmetric design is to use asymmetric SW coding for some of the bit-planes. If we carefully design the order of SW coding, the resulting SWCQ design not only can approach more points on the inner sum-rate bounds than the symmetric SWCQ design, but also has better practical performance.

d. Practical implementation

In practice, there is a rate loss due to the suboptimality of TCQ. In addition, compressing trellis bit-planes J_1, K_1 to $H(J_1, K_1)$ b/s is very difficult because of the lack of a mechanism for exploiting the memory in these trellis bits in practical SW coding. We thus send J_1 and K_1 to the decoder using one b/s for each and incur some loss in rate (note that for the two-bit variables J_1 and K_1, the second bit is a function of the first bit).

For SW coding of J_j and K_j, $2 \leq j \leq m$, the symmetric SW code design in [49] cannot be directly applied because the correlation between J_j and K_j conditioned on $\mathcal{M}_{j-1}$ is more complex than the BSC correlation model exploited in [49]. Our proposed multi-level coding framework generalizes the approach of [49] in terms of handling more general correlation models, while still enjoying the desirable property of arbitrarily allocating the total number of output syndrome bits between the two encoders. The key novelties lie in the construction of look-up tables for the probabilities $\{P(J_j = 1|K_j = 0, \mathcal{M}_{j-1})$, $P(J_j = 0|K_j = 1, \mathcal{M}_{j-1})$, $P(K_j = 1|J_j = 0, \mathcal{M}_{j-1})$, $P(K_j = 0|J_j = 1, \mathcal{M}_{j-1})$, $P(J_j \oplus K_j = 0|\mathcal{M}_{j-1})\}$, which are used for computing the LLR's at the multi-level channel decoder. An example of the look-up table for $P(J_2 \oplus K_2 = 0|\mathcal{M}_1)$ (recall that $\mathcal{M}_1 = \{J_1, K_1\}$) is given in Table II.

Table II. Look-up table for $P(J_2 \oplus K_2 = 0|\mathcal{M}_1)$.

$J_1 \setminus K_1$	0	1	2	3
0	0.9959	0.9558	0.5019	0.0451
1	0.9558	0.9958	0.9553	0.5045
2	0.5028	0.9561	0.9958	0.9567
3	0.0456	0.5037	0.9562	0.9959

According to [49], part of the SW-coded syndrome bits for J_j and K_j consists of a portion of the uncompressed J_j and K_j (see (4.30)). To exploit cross-bit-plane correlation

among the codeword bits $\{J_2, \ldots, J_m\}$ (and likewise among codeword bits $\{K_2, \ldots, K_m\}$), we employ *adaptive arithmetic coding* separately at each encoder to compress this part of the syndrome bits from 1 b/s to $H(J_i|J_{i-1} \ldots J_1)$ (or $H(K_i|K_{i-1} \ldots K_1)$) b/s. The remaining syndrome bits are sent to the decoder without further compression. Note that the j-th bit-plane J_j (or K_j), $2 \leq j \leq m$, is compressed with rate r_{j1} (or r_{j2}) using the symmetric SW coding scheme of [49] outlined in Section a while assuming all previously reconstructed bit-planes as decoder side information. Thus we design an (n, k_j) linear block code $\mathcal{C}_j$ with $k_j = \frac{2-r_{j1}-r_{j2}}{(2-h_j)}n$, where $h_j \triangleq \frac{1}{n}H(J_j^n|J_{j-1}^n, \ldots, J_1^n) = \frac{1}{n}H(K_j^n|K_{j-1}^n, \ldots, K_1^n)$; we set $r_{j1} + r_{j2} > h_j$ to ensure $k_j < n$.

D. Simulation results

1. Asymmetric SWCQ

For the direct MT source coding problem, sources Y_1 and Y_2 are zero mean, jointly Gaussian with variances $\sigma_{y_1}^2 = \sigma_{y_2}^2 = 1$ and correlation coefficient $\rho = 0.99$. The target distortions D_1^* and D_2^* are both set to be 0.001, then the sum-rate bound $\partial\hat{\mathcal{R}}_{12}^{BT}(D_1^*, D_2^*)$ for the direct MT problem can be computed using (2.9) as

$$R_1 + R_2 \geq \frac{1}{2}\log^+[(1-\rho^2)\frac{\beta_{max}\sigma_{y_1}^2\sigma_{y_2}^2}{2D_1^*D_2^*}] = 7.142 \text{ b/s}. \tag{4.41}$$

Suppose we are attempting to approach the middle point of sum-rate bound $\partial\hat{\mathcal{R}}_{12}^{BT}(D_1^*,D_2^*)$, i.e., $R_1^* = R_2^* = 7.142/2 = 3.571$ b/s. Then using equations (B.6) - (B.8) and (B.11), we can compute the three quantization distortions (d_{21}, d_1, d_{22}) (assuming ideal quantization) and the minimum MSE coefficients $(\alpha_1^A, \beta_1^A, \gamma_1^A)$, $(\alpha_2^A, \beta_2^A, \gamma_2^A)$, and (α_c, β_c), yielding

$$d_{21} = 0.14937908, \quad d_1 = 0.00105018, \quad d_{22} = 0.00105762;$$
$$\alpha_1^A = 0.95239893, \quad \beta_1^A = 0.00032965, \quad \gamma_1^A = 0.04674618;$$
$$\alpha_2^A = 0.04707583, \quad \beta_2^A = 0.00666912, \quad \gamma_2^A = 0.94572981;$$
$$\alpha_c = 0.86743434, \quad \beta_c = 0.12288739. \tag{4.42}$$

For the indirect MT source coding problem, source X and noises N_1 and N_2 are zero mean, jointly Gaussian, and mutually independent with variances $\sigma_x^2 = 1$, $\sigma_{n_1}^2 = \sigma_n^2 = \frac{1}{99}$, and $\sigma_{n_2}^2 = \sigma_n^2 = \frac{1}{99}$, respectively. Noisy observations are given by $Y_1 = X + N_1$ and $Y_2 = X + N_2$. We refer to the ratio $\sigma_x^2/\sigma_n^2 = 99 = 19.96$ dB as *correlation signal to noise ratio* (CSNR). The target distortion is set to $D^* = 0.00555 = -22.58$ dB. Then the sum-rate bound $\partial\hat{\mathcal{R}}_{12}^{YI}(D^*)$ for the indirect MT problem can be computed using (2.18) as

$$R_1 + R_2 \geq \frac{1}{2}\log^+\Big[\frac{4\sigma_x^2}{\sigma_{n_1}^2\sigma_{n_2}^2 D(\frac{1}{\sigma_x^2} - \frac{1}{D^*} + \frac{1}{\sigma_{n_1}^2} + \frac{1}{\sigma_{n_2}^2})^2}\Big] = 7.142 \text{ b/s}. \tag{4.43}$$

Due to equations (C.1)-(C.4), one can verify that (d_{21}, d_1, d_{22}) and (α_c, β_c) are the same as those in (4.42), while $(\alpha_X^A, \beta_X^A, \gamma_X^A)$ are computed using (C.4) as

$$\alpha_X^A = 0.49722766, \quad \beta_X^A = 0.00349566, \quad \gamma_X^A = 0.49372983. \tag{4.44}$$

In our implementation, to get the quantization distortions (d_{21}, d_1, d_{22}) in (4.42), we employ three dithered TCQ quantizers with parameters

1. $\mathcal{Q}_{21}$: $R_{TCQ} = 5$ b/s, step size $\Delta_{21} = 0.7850$;

2. $\mathcal{Q}_1$: $R_{TCQ} = 7$ b/s, step size $\Delta_1 = 0.06570$;

3. $\mathcal{Q}_{22}$: $R_{TCQ} = 7$ b/s, step size $\Delta_{22} = 0.06594$.

The transmission rates with ideal SW coding, i.e., $R_{21} = \frac{1}{n}H(B_{21}^n)$, $R_1 = \frac{1}{n}H(B_1^n|\hat{Z}_{21}^n)$, and $R_{22} = \frac{1}{n}H(B_{22}^n|\hat{Z}_c^n)$ are computed using Monte Carlo simulations. Practical SW encoders

are based on turbo and irregular LDPC codes, which are designed such that the decoding bit error rate is less than 10^{-6}. In our simulations, the block length (BL) for both turbo and LDPC codes equals to 10^6, and the maximum number of iterations is set to 100 for turbo decoding and 500 for LDPC decoding. Table III shows the resulting bit-plane-level conditional entropies and the practical SW coding rates. With turbo based asymmetric SW coding, the total transmission rate $R_{21} + R_1 + R_{22} = 1.506 + 3.650 + 2.180 = 7.336$ b/s. Practical distortions are $(D_1, D_2) = (-30.05 \text{ dB}, -30.01 \text{ dB})$ for the direct setting and $D = -22.60$ dB for the indirect setting, satisfying the target distortion constraints. Hence our asymmetric SWCQ design based on turbo codes performs $7.336 - 7.142 = 0.194$ b/s away from both sum-rate bounds $\partial\hat{\mathcal{R}}_{12}^{BT}(D_1^*, D_2^*)$ for the direct setting and $\partial\hat{\mathcal{R}}_{12}^{YI}(D^*)$ for the indirect setting. With LDPC based asymmetric SW coding, the total transmission rate is $R_{21} + R_1 + R_{22} = 1.506 + 3.623 + 2.152 = 7.281$ b/s, which is $7.281 - 7.142 = 0.139$ b/s away from both sum-rate bounds. These results together with the sum-rate bounds for both the direct and indirect MT settings are depicted in Fig. 13.

The loss of 0.139 b/s for the best results with LDPC based asymmetric SW coding consists of three 0.03 b/s losses (corresponding to the 1.34 dB granular gain of 256-state TCQ, or roughly 0.19 dB loss in distortion) from the suboptimality of TCQ, a total of 0.04 b/s loss (see Table III) from practical arithmetic/SW coding, and a very small loss from the jointly Gaussian assumption of the two quantized versions at the two encoders.

2. Symmetric SWCQ

In the implementation of symmetric SWCQ scheme, we use the same set of source distributions and target distortions as in Section 1, namely,

$$\begin{aligned} \text{Direct setting}: &\quad \sigma_{y_1}^2 = \sigma_{y_2}^2 = 1, \rho = 0.99, \quad D_1^* = D_2^* = 0.001; \\ \text{Indirect setting}: &\quad \sigma_x^2 = 1, \sigma_{n_1}^2 = \sigma_{n_2}^2 = \tfrac{1}{99}, \quad D^* = 0.00555. \end{aligned} \tag{4.45}$$

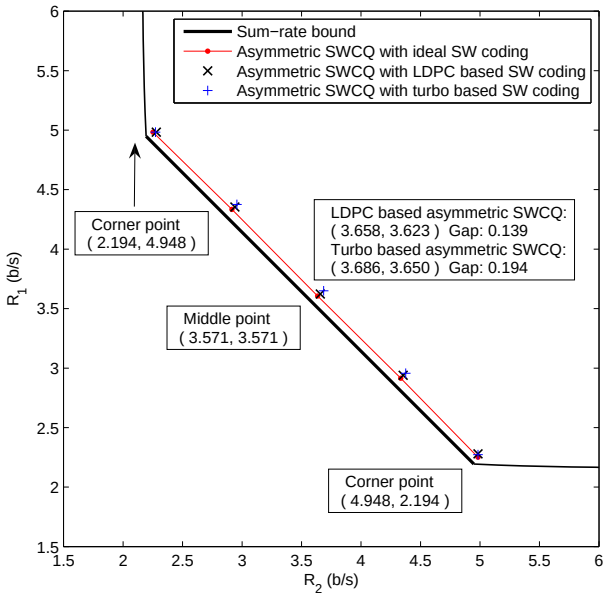

(a)

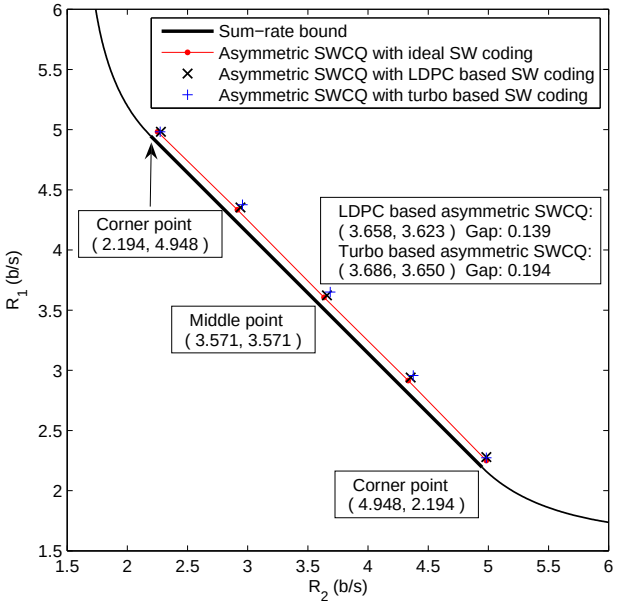

(b)

(a) Direct MT: $D_1^* = D_2^* = -30.00$ dB, $\rho = 0.99$; (b) Indirect MT: $D^* = -22.58$ dB, $\sigma_{n_1}^2 = \sigma_{n_2}^2 = \frac{1}{99}$.

Fig. 13. Results of asymmetric SWCQ with TCQ and turbo/LDPC-based SW coding for the direct and indirect MT problems. The corner point with LDPC based SW coding is (2.262,4.983) b/s, total sum-rate loss is 0.103 b/s. The corner point with turbo based SW coding is (2.273,4.983) b/s, total sum-rate loss is 0.114 b/s.

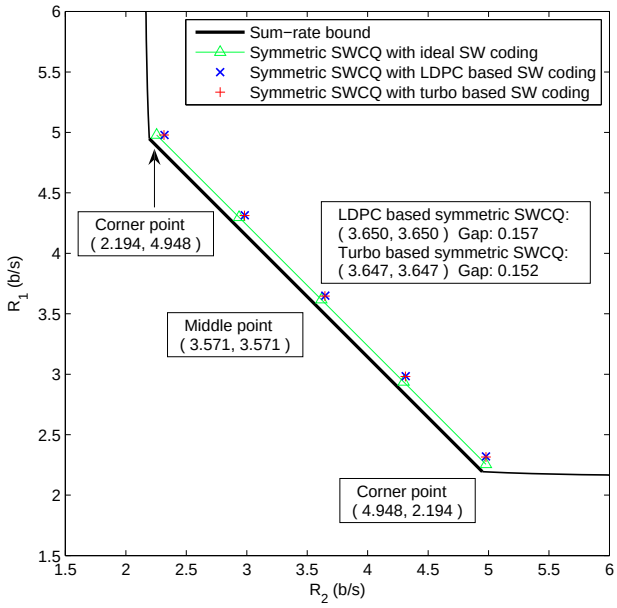

(a)

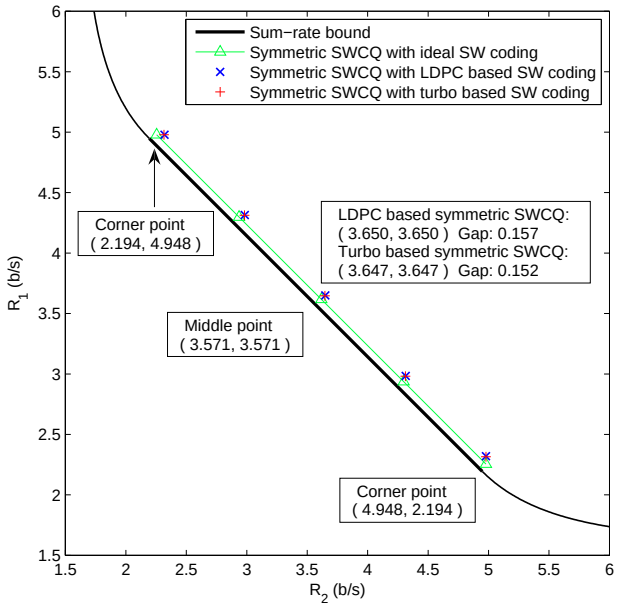

(b)

(a) Direct MT: $D_1^* = D_2^* = -30.00$ dB, $\rho = 0.99$; (b) Indirect MT: $D^* = -22.58$ dB, $\sigma_{n_1}^2 = \sigma_{n_2}^2 = \frac{1}{99}$.

Fig. 14. Results of symmetric SWCQ with TCQ and turbo/LDPC-based SW coding for the direct and indirect MT problems. The corner point with LDPC based SW coding is (2.320,4.979) b/s, total sum-rate loss is 0.157 b/s. The corner point with turbo based SW coding is (2.315,4.979) b/s, total sum-rate loss is 0.152 b/s.

Table III. Entropies vs practical rates at high rate for direct and indirect MT coding using asymmetric SWCQ.

Quantizer	Bit Plane #	Entropy (b/s)	Practical Rate (b/s)		Irregular LDPC Code Profile
			Turbo (BL=10^6)	LDPC (BL=10^6)	
$\mathcal{Q}_{21}$	All	1.504	1.506	1.506	–
$\mathcal{Q}_1$	1	1.000	1.000	1.000	–
	2	1.000	1.000	1.000	–
	3	0.998	1.000	1.000	–
	4	0.588	0.625	0.600	$\lambda(x) = 0.1536x + 0.2398x^2 + 0.0747x^6 + 0.0888x^7 + 0.0174x^9 + 0.0105x^{10} + 0.0215x^{14} + 0.0063x^{15} + 0.0336x^{16} + 0.0074^{17} + 0.0025x^{21} + 0.0061x^{24} + 0.0348x^{25} + 0.0777x^{28} + 0.0524x^{29} + 0.0015x^{98} + 0.1714x^{99}; \rho(x) = 0.35x^7 + 0.65x^8$.
	5	0.020	0.025	0.023	$\lambda(x) = 0.0818x + 0.2207x^2 + 0.0397x^4 + 0.1374x^6 + 0.0774x^7 + 0.0106x^{14} + 0.0640x^{15} + 0.0143x^{17} + 0.0121x^{20} + 0.0616x^{21} + 0.0141x^{30} + 0.0781x^{39} + 0.0661x^{40} + 0.0081x^{48} + 0.0269x^{49} + 0.0449x^{64} + 0.0086x^{65} + 0.0289x^{66} + 0.0047x^{67}; \rho(x) = x^{259}$.
	6	0.000	0.000	0.000	–
	7	0.000	0.000	0.000	–
	All	3.606	3.650	3.623	–
$\mathcal{Q}_{22}$	1	1.000	1.000	1.000	–
	2	0.908	0.925	0.920	$\lambda(x) = 0.3315x + 0.2869x^2 + 0.0079x^4 + 0.0447x^6 + 0.1068x^8 + 0.0016x^9 + 0.0030x^{10} + 0.0038x^{11} + 0.0032x^{14} + 0.0028x^{15} + 0.1091x^{19} + 0.0188x^{20} + 0.0014x^{60} + 0.0064x^{61} + 0.0328x^{65} + 0.0188x^{66} + 0.0040x^{98} + 0.0164x^{99}; \rho(x) = 0.2x^2 + 0.8x^3$.
	3	0.223	0.250	0.230	$\lambda(x) = 0.0937x + 0.2225x^2 + 0.0375x^6 + 0.1605x^7 + 0.0014x^9 + 0.0117x^{16} + 0.1529x^{17} + 0.0010x^{28} + 0.0808x^{36} + 0.0289x^{37} + 0.0209x^{56} + 0.0028x^{57} + 0.1854x^{98}; \rho(x) = x^{26}$.
	4	0.0004	0.005	0.002	$\lambda(x) = 0.0002x + 0.3390x^2 + 0.0108x^3 + 0.0158x^4 + 0.3057x^5 + 0.0064x^{19} + 0.0173x^{20} + 0.0718x^{21} + 0.0592x^{22} + 0.1221x^{34} + 0.0446x^{35} + 0.0069x^{42}; \rho(x) = x^{2749}$.
	5	0.000	0.000	0.000	–
	6	0.000	0.000	0.000	–
	7	0.000	0.000	0.000	–
	All	2.131	2.180	2.152	–
Total	-	7.241	7.336	7.281	–

Then the sum-rate bounds $\partial\hat{\mathcal{R}}_{12}^{BT}(D_1^*, D_2^*)$ for the direct setting and $\partial\hat{\mathcal{R}}_{12}^{YI}(D^*)$ for the indirect setting are both $R_1 + R_2 \geq 7.142$ b/s, and the two quantization distortions are $d_1 = d_2 = 0.0010502$. We employ two identical dithered TCQ quantizers with parameters

1. $\mathcal{Q}_1$: R_{TCQ} = 7 b/s, step size $\Delta_1 = 0.06570$;

2. $\mathcal{Q}_2$: R_{TCQ} = 7 b/s, step size $\Delta_2 = 0.06570$.

The conditional entropies for the seven bit-planes of B_1 and B_2 are shown in Table IV (due to the symmetry between the sources and encoders, J_i's and K_i's are interchangeable).

Table IV. Conditional entropies for the seven bit-planes of B_1 and B_2 for direct and indirect MT source coding with symmetric SWCQ at high rate.

Bit Plane	$H(J_iK_i\|\mathcal{M}_{i-1})$ (b/s)	$H(J_i\|\mathcal{M}_{i-1})$ (b/s)	$H(J_i\|J_{i-1}...J_1)$ (b/s)	Practical Rate (b/s)			Rate loss (b/s)		
				Turbo		LDPC	Turbo		LDPC
				BL=10^6	BL=10^5	BL=10^5	BL=10^6	BL=10^5	BL=10^5
1	2.000	1.000	1.000	2.000	2.000	2.000	0.000	0.000	0.000
2	1.945	1.000	1.000	1.965	1.970	1.970	0.020	0.025	0.025
3	1.307	1.000	1.000	1.340	1.360	1.340	0.033	0.053	0.033
4	1.002	1.000	1.000	1.005	1.010	1.005	0.003	0.008	0.003
5	0.840	0.840	0.842	0.842	0.842	0.842	0.002	0.002	0.002
6	0.139	0.139	0.141	0.141	0.141	0.141	0.002	0.002	0.002
7	0.0001	0.0001	0.0001	0.001	0.001	0.001	0.001	0.001	0.001
Total	7.234	-	-	7.294	7.324	7.299	0.060	0.090	0.065

In our practical SW code implementation based on turbo codes, the code length n equals 10^6, and we control the transmission rates such that the decoding probability of error is less than 10^{-6} after 100 iterations. In the bottom-up order, the seven bit planes of B_1 and B_2 are coded in the following way:

1. The first bit plane (J_1, K_1) is directly transmitted using 2 b/s.

2. The second, third, and fourth bit-plane are coded using symmetric SW coding [49], wherein the turbo code rates are 0.035 b/s, 0.64 b/s, and 0.995 b/s, respectively. Since $H(J_2|J_1) = H(J_3|J_2, J_1) = H(J_4|J_3, J_2, J_1) = 1.000$ b/s, then the practical transmission rates are $1 + (1 - 0.035) = 1.965$ b/s, $1 + (1 - 0.66) = 1.34$ b/s, and $1 + (1 - 0.995) = 1.005$ b/s, respectively.

3. The fifth, sixth, and seventh bit-plane are all compressed to their conditional entropy $H(J_i|J_{i-1},...,J_1)$ for $i = 5,6,7$. We can do this since $H(K_i|J_i,\mathcal{M}_{i-1}) \approx 0$ for $i = 5,6,7$.

The subtotal in rate loss due to practical SW coding is $0.020 + 0.033 + 0.003 + 0.005 \approx 0.060$ b/s. Using linear estimators with minimum MSE coefficients, the resulting distortions are $(D_1, D_2) = (-30.07\ \mathrm{dB}, -30.00\ \mathrm{dB})$ for the direct setting and $D = -22.63$ dB for the indirect setting. Compared to the sum-rate bound $R_1 + R_2 \geq 7.142$ b/s, the total rate loss with turbo code for SW coding is thus $7.294 - 7.142 = 0.152$ b/s in the specific direct and indirect MT coding problems we consider.

We also implement the practical SW code based on LDPC codes using the method described in [49]. Since LDPC code is often nonsystematic, matrix inverse operation is needed offline [49], *hence the code length n is set to 10^5 due to memory limitations*. Optimized by density evolution and differential evolution as in [45], LDPC codes are generated for the second, third, and fourth bit planes. Simulation results with a maximum of 200 iterations are also shown in Table IV. The total rate loss of symmetric SWCQ with LDPC codes for both direct and indirect MT coding problems is $7.299 - 7.142 = 0.157$ b/s. Detailed results together with the theoretical bounds are shown in Fig. 14. We see that practical SW codes based on LDPC codes (of length 10^5 bits) perform slightly worse than that based on turbo codes (of length 10^6 bits), with a SW rate loss of 0.065 b/s compared to 0.060 b/s, this is due to the shorter block length with LDPC codes. Indeed, at the same block length of 10^5, LDPC code based scheme performs $0.090 - 0.065 = 0.025$ b/s better than the turbo based scheme, as shown in Table IV.

3. Low rate performance and complexity analysis

We next evaluate the performance of our asymmetric and symmetric SWCQ schemes at low transmission rate, and compare the results to those in [42] for the indirect MT problem at a practical sum-rate of 4.0 b/s.

In our simulations for symmetric SWCQ, CSNR is set to $\sigma_x^2/\sigma_n^2 = 99 = 19.96$ dB, and the target distortion is $D^* = -18.58$ dB. Then the sum-rate bound $\partial\hat{\mathcal{R}}_{12}^{YI}(D^*) = 3.728$ b/s. Practical results with LDPC code based symmetric SW coding are shown in Table V, where block length $n = 10^5$. The total transmission rate is 3.999 b/s, which is 0.27 b/s away from the sum-rate bound $\partial\hat{\mathcal{R}}_{12}^{YI}(D^*)$. At the same sum-rate and CSNR, the scheme in [42] can achieve distortion of -16.3 dB, which corresponds to a theoretical sum-rate of 3.048 b/s, and is more than 2 dB worse than our results.

Table V. Conditional entropies for direct and indirect MT coding at low rate.

Bit Plane #	$H(J_iK_i\|\mathcal{M}_{i-1})$ (b/s)	$H(J_i\|\mathcal{M}_{i-1})$ (b/s)	$H(J_i\|J_{i-1}...J_1)$ (b/s)	Practical Rate (b/s)	Rate loss (b/s)
1	1.923	1.000	0.999	1.950	0.027
2	1.086	1.000	1.000	1.100	0.014
3	0.818	0.818	0.824	0.824	0.006
4	0.119	0.119	0.125	0.125	0.006
Total	3.946	-	-	3.999	0.053

In our simulations for asymmetric SWCQ, CSNR is set to $\sigma_x^2/\sigma_n^2 = 99 = 19.96$ dB, and the target distortion is $D^* = -18.30$ dB. Then the sum-rate bound $\partial\hat{\mathcal{R}}_{12}^{YI}(D^*) = 3.631$ b/s. Practical results with LDPC code based asymmetric SW coding are shown in Table VI, where block length $n = 10^6$. The total transmission rate is 4.00 b/s, which is 0.37 b/s away from the sum-rate bound $\partial\hat{\mathcal{R}}_{12}^{YI}(D^*)$. This performance gap is larger than that with the symmetric SWCQ, which is due to the inefficiency in compressing the trellis bit planes using asymmetric SW coding [65]. However, the overall distortion $D^* = -18.30$ dB with asymmetric SWCQ is still much better than the -16.3 dB performance in [42] at the same sum-rate and CSNR.

Complexity-wise, the best results of [42] for a sum-rate of 4 b/s are obtained with 8-level Lloyd-Max fixed-length scalar quantizer and 32-state trellis codes, while our asymmetric SWCQ scheme employs 256-state TCQ and LDPC codes. The running time on an Intel Core 2 Duo 1.8GHz machine and peak memory usage are shown in Table VII.

Table VI. Entropies vs practical rates at low rate for direct and indirect MT coding using asymmetric SWCQ.

Quantizer	Bit Plane #	Conditional Entropy (b/s)	Practical Rate (b/s)
$\mathcal{Q}_{21}$	All	1.231	1.231
$\mathcal{Q}_1$	1	1.000	1.000
	2	0.822	0.840
	3	0.077	0.090
	4	0.000	0.000
	All	1.799	1.830
$\mathcal{Q}_{22}$	1	0.861	0.880
	2	0.053	0.060
	3	0.000	0.000
	4	0.000	0.000
	All	0.914	0.940
Total	-	3.934	4.001

Table VII. Computational complexity and peak memory usage for asymmetric SWCQ and symmetric SWCQ.

SWCQ scheme		Encoding		Decoding	
		Time (sec)	Memory (MByte)	Time (sec)	Memory (MByte)
Asymmetric (BL=10^6)	LDPC based	366	75.1	981	372
	Turbo based	365	21.5	2291	966
Symmetric (BL=10^5)	LDPC based	25.3	2.1	11.8	15.1
	Turbo based	25.0	2.1	75.6	95.5

CHAPTER V

MT VIDEO CODING

A. Problem setup and notations

Let $\mathcal{L} = \{L_1, L_2, ..., L_n\}$ and $\mathcal{R} = \{R_1, R_2, ..., R_n\}$ be the left and right n-frame stereo video sequences, respectively, and the frame size is fixed at $W \times H$ for both sequences. Denote $(\mathscr{E}_L^*, \mathscr{D}_L^*)$ and $(\mathscr{E}_R^*, \mathscr{D}_R^*)$ as the H.264/AVC encoder/decoder pairs for the left and right sequences, respectively, where only the first frames L_1 and R_1 of the two sequences are intra-coded (I-frames), and all the remaining frames are inter-coded (P-frames). The bit rate in bits per second (bps) is $\mathscr{R}_L^*$ for the left sequence, and $\mathscr{R}_R^*$ for the right sequence. The reconstructed version of the left and right sequences are $\widehat{\mathcal{L}}^{D(q)} = \{\widehat{L}_1^{D(q)}, ..., \widehat{L}_n^{D(q)}\}$ and $\widehat{\mathcal{R}}^{D(q)} = \{\widehat{R}_1^{D(q)}, ..., \widehat{R}_n^{D(q)}\}$, respectively, where q is the *quantization parameter* used in the H.264/AVC coders. The average peak signal-to-noise ratio (PSNR) of both sequences is defined as

$$\mathscr{P}^* = \frac{1}{2n}\sum_{k=1}^{n} 10\log_{10}\frac{255^2}{\frac{1}{WH}\|L_k - \widehat{L}_k^{D(q)}\|^2} + \frac{1}{2n}\sum_{k=1}^{n} 10\log_{10}\frac{255^2}{\frac{1}{WH}\|R_k - \widehat{R}_k^{D(q)}\|^2}\text{dB}, \quad (5.1)$$

where $\frac{1}{WH}\|A - B\|^2$ is the average squared difference between images A and B.

We consider the problem of MT source coding of stereo video sequences such that, at the same video quality, the resulting total bit rate (or sum rate) is smaller than that of individual H.264/AVC coding. Thus, our goal is to design an MT video coder $(\mathscr{E}_L, \mathscr{E}_R, \mathscr{D}_{LR})$ that is capable of achieving a smaller sum rate compared to that of separate H.264/AVC encoding on the stereo video sequences $(\mathcal{L}, \mathcal{R})$ at the same average PSNR $\mathscr{P}^*$, i.e., $\mathscr{R}_L + \mathscr{R}_R < \mathscr{R}_L^* + \mathscr{R}_R^*$ while $\mathscr{P} = \mathscr{P}^*$, where $\mathscr{R}_L$ and $\mathscr{R}_R$ are the bit rate of the left and right sequences, respectively, and $\mathscr{P}$ is the average PSNR, obtained with MT video coding.

Our main idea of MT video coding of $(\mathcal{L}, \mathcal{R})$ is to employ the DCT to explore spatial

correlation among neighboring pixels, motion compensation to remove temporal redundancies between consecutive video frames, and stereo matching and motion fusion *at the decoder* to generate side information for SW and WZ coding.

Before describing the details of our proposed MT video coding schemes, we need to introduce some notations. Let $L_1(i,j)$ be the 4×4 macroblock whose top-left corner is at the $(4i+1)$-th row and $(4j+1)$-th column of frame L_1, with $0 \le i < H/4$, $0 \le j < W/4$. Write the intra-predicted version of $L_1(i,j)$ and the corresponding intra-prediction mode $\mathcal{K}_1^{I(q)}(i,j)$ as (for simplicity, we assume that only 4×4 luma intra-prediction is used)

$$\left(L_1^{I(q)}(i,j), \mathcal{K}_1^{I(q)}(i,j)\right) = \mathbb{P}^I\left(\widehat{L}_1^{D(q)}(i,j-1), \widehat{L}_1^{D(q)}(i-1,j), \widehat{L}_1^{D(q)}(i-1,j+1)\right), \quad (5.2)$$

where q is the quantization parameter, $\mathbb{P}^I(\cdot,\cdot,\cdot)$ represents the intra prediction operation, whose arguments are the previously decoded macroblocks (if available) $\widehat{L}_1^{D(q)}(i,j-1)$, $\widehat{L}_1^{D(q)}(i-1,j)$ and $\widehat{L}_1^{D(q)}(i-1,j+1)$. Then the corresponding residual block and its H.264/AVC integer-transformed version are expressed as

$$L_1^{R(q)}(i,j) = L_1(i,j) - L_1^{I(q)}(i,j) \quad \text{and} \quad L_1^{T(q)}(i,j) = \mathbb{T}(L_1^{R(q)}(i,j)), \quad (5.3)$$

respectively, where $\mathbb{T}(\cdot)$ represents the integer DCT.

Define a dead-zone quantizer as

$$\mathcal{C}(d,d^0): W \xrightarrow{\text{quantized to}} \begin{cases} \left\lceil (W + \frac{d^0}{2})/d \right\rceil \cdot d & W < -\frac{d^0}{2} \\ 0 & -\frac{d^0}{2} \le W \le \frac{d^0}{2} \\ \left\lfloor (W - \frac{d^0}{2})/d \right\rfloor \cdot d & W > \frac{d^0}{2} \end{cases} \quad (5.4)$$

where d is the quantization step size, d^0 is the size of the dead-zone, W is the input, and $\lceil x \rceil$ (resp. $\lfloor x \rfloor$) is the closest integer to x that is larger (resp. smaller) than x. Then the equivalent H.264/AVC dead-zone quantizer [59] with quantization parameter $QP = q$ can be denoted as $C_q^I = \mathcal{C}(d_q, \frac{4}{3}d_q)$ for intra-frames and $C_q^P = \mathcal{C}(d_q, \frac{5}{3}d_q)$ for inter-frames, where

d_q is the quantization step size with $q = 1, 2, ..., 52$.

Write the quantization levels of the (i, j)-th block as

$$L_1^{K(q)}(i,j) \;=\; \mathbb{Q}\Big(L_1^{T(q)}(i,j), C_q^I\Big), \tag{5.5}$$

and the corresponding de-quantized version of the residual block as

$$\widehat{L}_1^{T(q)}(i,j) \;=\; \mathbb{Q}^{-1}\Big(L_1^{K(q)}(i,j), C_q^I\Big) = L_1^{K(q)}(i,j) \cdot d_q. \tag{5.6}$$

The reconstructed (i, j)-th block (before deblocking filtering) is denoted as

$$\widehat{L}_1^{D(q)}(i,j) \;=\; \mathbb{T}^{-1}\Big(\widehat{L}_1^{T(q)}(i,j)\Big) + L_1^{I(q)}(i,j), \tag{5.7}$$

which will be used in intra-predicting the neighboring macroblocks. Moreover, we will drop the index (i, j) to denote the corresponding $W \times H$ frame, for example, the $W \times H$ intra-predicted frame is written as $L_1^{I(q)} = \bigcup_{0 \le i < H/4, 0 \le j < W/4} \{L_1^{I(q)}(i,j)\}$.

Similarly, for the P-frame L_k, write $L_k(i, j)$ as the original macroblock at the (i, j)-th position, and

$$\Big(L_k^{P(q)}(i,j), \mathcal{M}_{L_k}^{P(q)}(i,j)\Big) \;=\; \mathbb{P}^P\Big(\widehat{L}_{k-1}^{D(q)}, \mathcal{M}_{max}\Big) \tag{5.8}$$

as the inter-predicted residual block and the (i, j)-th motion vector, respectively, where $\mathbb{P}^P$ represents the inter prediction operation, whose arguments are the previously decoded $(k - 1)$-frame and the maximum motion search range $\mathcal{M}_{max}$, then we must have

$$-\mathcal{M}_{max} \le \mathcal{M}_{L_k}^{P(q)}(i,j) - \widehat{\mathcal{M}}_{L_k}^{P(q)}(i,j) \le \mathcal{M}_{max}, \tag{5.9}$$

where $\widehat{\mathcal{M}}_{L_k}^{P(q)}(i,j)$ is the predicted motion vector for the (i, j)-th macroblock. Table VIII lists important notations used in this chapter. All other notations follow the same naming rule unless otherwise noted.

Table VIII. Notations for H.264/AVC.

Category	Notation	Explanation	Defined in
H.264/AVC intra	L_1	First frame of the left sequence	
	$L_1^{I(q)}$	H.264/AVC **intra-predicted** frame for L_1 with $QP = q$	(5.2)
	$L_1^{R(q)}$	H.264/AVC **residual** frame for L_1 with $QP = q$	(5.3)
	$L_1^{T(q)}$	H.264/AVC **transformed** residual frame for L_1 with $QP = q$	(5.3)
	$L_1^{K(q)}$	H.264/AVC **residual quantization levels** for L_1 with $QP = q$	(5.5)
	$\widehat{L}_1^{T(q)}$	H.264/AVC **de-quantized** residual frame for L_1 with $QP = q$	(5.6)
	$\widehat{L}_1^{D(q)}$	H.264/AVC **reconstruction** of L_1 with $QP = q$	(5.7)
H.264/AVC inter	$\widehat{L}_k^{P(q)}$	H.264/AVC **inter-predicted** frame for L_k with $QP = q$	(5.8)
	$\mathcal{M}_{L_k}^{P(q)}$	H.264/AVC **motion vectors** for L_k with $QP = q$	(5.8)
	$\widehat{\mathcal{M}}_{L_k}^{P(q)}$	H.264/AVC **predicted motion vectors** for L_k with $QP = q$	

B. Proposed MT video coding scheme 1

In our first proposed MT video coder, the left sequence $\mathcal{L}$ is first compressed by H.264/AVC using a group of picture (GOP) structure IP...PI and transmitted to the joint decoder. The right sequence $\mathcal{R}$ is then WZ coded with the decoded left sequence as decoder side information. The right I-frame and P-frames are compressed using different algorithms, because there is no *a priori* knowledge about the stereo correlation between the two sequences when compressing the right I-frame, while for the right P-frames, previous decoded pairs of frames provide information about the stereo correlation (via a motion fusion algorithm that uses previous disparity map and incorporates the 3D camera geometry information), whose reliability depends on the quality of previous decoded frames. Another reason is because the I-frame uses intra-prediction with different prediction modes, whereas the P-frames use inter-prediction with different motion vectors. The motion vectors of the left and right sequences are highly correlated, thus exploring this correlation will help reduce the transmission rate of the motion vectors, which is important at low rates when the motion vectors occupy a large portion of the compressed bitstream.

1. MT video coding of I-frames

Our proposed MT video coding scheme for the right I-frame R_1 is depicted in Fig. 15. First, the left sequence $\mathcal{L}$ is compressed at Encoder 1 using H.264/AVC and transmitted to the joint decoder, using quantizers $C^I_{q_1} = \mathcal{C}(d_{q_1}, \frac{4}{3}d_{q_1}), C^P_{q_1} = \mathcal{C}(d_{q_1}, \frac{5}{3}d_{q_1})$ and a transmission rate of $\mathscr{R}_L$ bps. Then the first frame R_1 of right sequence is intra-coded using a quantizer $C^I_{q_2} = \mathcal{C}(d_{q_2}, \frac{4}{3}d_{q_2})$ with a larger $QP = q_2$ rather than $QP = q_1$ to produce a low-quality reconstruction $\widehat{R}_1^{D(q_2)}$ at the decoder. A rough disparity map $\widetilde{\mathcal{D}}_1$ between $\widehat{R}_1^{D(q_2)}$ and the H.264/AVC-decoded left I-frame $\widehat{L}_1^{D(q_1)}$ is generated, i.e.,

$$\widetilde{\mathcal{D}}_1 \;=\; \mathbb{D}(\widehat{L}_1^{D(q_1)}, \widehat{R}_1^{D(q_2)}), \tag{5.10}$$

where $\mathbb{D}(A, B)$ is the disparity map between frame A and frame B generated by the BP based stereo matching algorithm [15], which is detailed in Section D. $\widetilde{\mathcal{D}}_1$ is then used to produce a side information $R_1^{W(q_1)}$ by warping $\widehat{L}_1^{D(q_1)}$, i.e.,

$$R_1^{W(q_1)} \;=\; \mathbb{W}(\widehat{L}_1^{D(q_1)}, \widetilde{\mathcal{D}}_1), \tag{5.11}$$

where $\mathbb{W}(\mathcal{A}, \mathcal{D})$ denote the warped version of frame $\mathcal{A}$ according to disparity map $\mathcal{D}$, i.e., the intensity of (i, j)-th pixel of $\mathbb{W}(\mathcal{A}, \mathcal{D})$ equals to that of the $(i + \delta^V_{i,j}, j + \delta^H_{i,j})$-th pixel of $\mathcal{A}$, where $\delta^V_{i,j}$ and $\delta^H_{i,j}$ denote the vertical and horizontal disparity values of the disparity map $\mathcal{D}$, respectively.

Now the encoder re-quantizes the residual DCT coefficients $R_1^{T(q_2)} = \mathbb{T}(R_1^{R(q_2)})$ using the same quantizer $C^I_{q_1} = \mathcal{C}(d_{q_1}, \frac{4}{3}d_{q_1})$ as that for the left I-frame, without doing another intra-prediction step, i.e.,

$$\widetilde{R}_1^{K(q_1)} \;=\; \mathbb{Q}(R_1^{T(q_2)}, C^I_{q_1}). \tag{5.12}$$

We choose proper q_1 and q_2 such that $q_1 = q_2 - 12k$ where $k \in \mathbb{N}$, which ensures that the two quantizers $C^I_{q_1}$ and $C^I_{q_2}$ are *embedded* in the sense that every quantization threshold

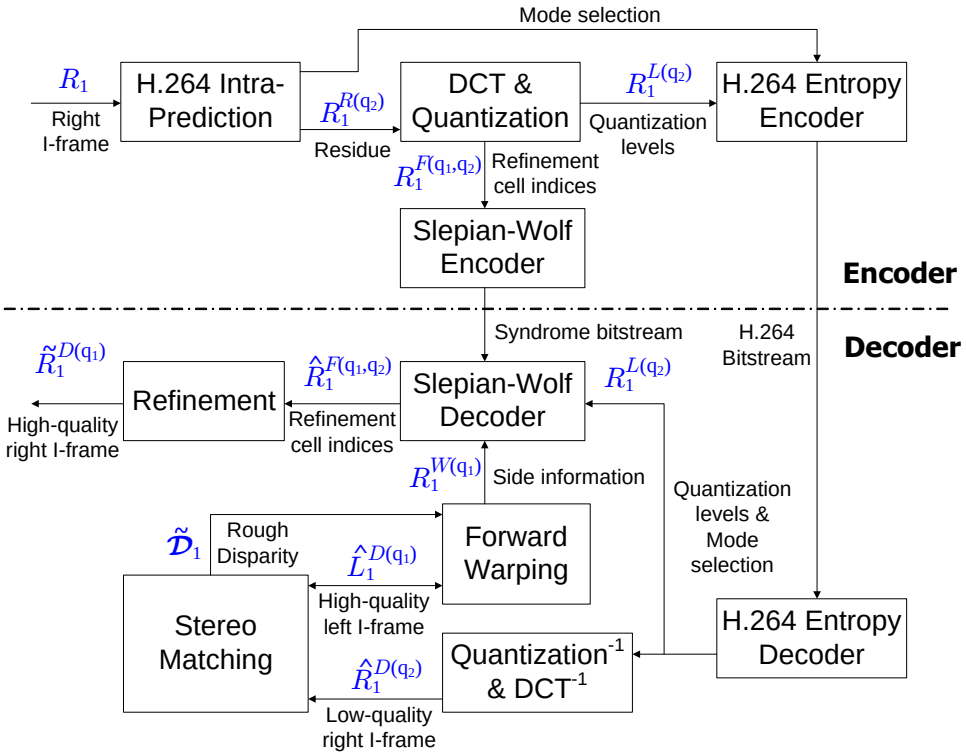

Fig. 15. The codec for the right I-frame R_1 in our first proposed MT video coder.

in $C_{q_1}^I$ must also be a threshold in $C_{q_2}^I$. Moreover, we write

$$C_{q_2}^I = (n, n_0) \times C_{q_1}^I \tag{5.13}$$

if the zeroth quantization cell of $C_{q_2}^I$ contains n_0 cells of $C_{q_1}^I$ while each non-zero cell of $C_{q_2}^I$ contains n cells of $C_{q_1}^I$ (we only consider the case when n_0 is an odd integer). For example, when $q_1 = 22, q_2 = 34$, we have $C_{34}^I = (4, 5) \times C_{22}^I$, as shown in Fig. 16.

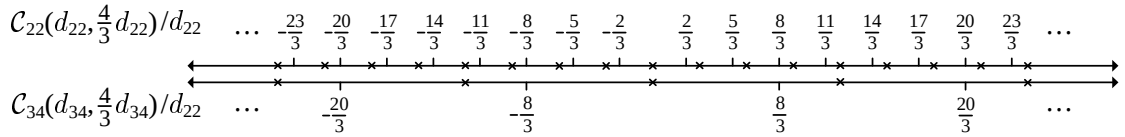

Fig. 16. Quantizers used in the codec for the right I-frame in our first proposed MT video coder.

Now let $R_1^{F(q_1,q_2)}$ be the refining cell indices that distinguish among the n or n_0 finer

quantization cells of $C_{q_1}^I$ in a given coarse quantization cell of $C_{q_2}^I$, i.e.,

$$R_1^{F(q_1,q_2)} = \begin{cases} \widetilde{R}_1^{K(q_1)} - nR_1^{K(q_2)} + \frac{n_0-1}{2}, & \text{if} \quad R_1^{K(q_2)} < 0 \\ \widetilde{R}_1^{K(q_1)} - nR_1^{K(q_2)} + \frac{2n-n_0-1}{2}, & \text{if} \quad R_1^{K(q_2)} \geq 0 \end{cases}. \tag{5.14}$$

Then we compress $R_1^{F(q_1,q_2)}$ with $\widetilde{R}_1^{K(q_2)}$ and $R_1^{W(q_1)}$ as decoder side informations **using SW coding**. To model the correlation between the I-frame quantization levels $\widetilde{R}_1^{K(q_1)}$ and the side information $R_1^{W(q_1)}$, we collect the joint statistics over all n frames to build an empirical model. Specifically, define

$$\widetilde{R}_1^{K(q^\star)} = \mathbb{Q}\Big(\mathbb{T}(R_1^{W(q_1)} - R_1^{I(q_2)}), C_{q^\star}^I\Big), \tag{5.15}$$

where $q^\star \ll q_1, q_2$ (that is, $C_{q^\star}^I$ is a much finer quantizer than $C_{q_1}^I$ and $C_{q_2}^I$). Then for each of the 16 position in a 4×4 macroblock, we count the occurrences of all possible pair $(l_2, l^\star)$ in $(\widetilde{R}_k^{K(q_1)}(i,j)_c, \widetilde{R}_k^{K(q^\star)}(i,j)_c)$ for all $0 \leq i < H/4, 0 \leq j < W/4$, $c = 0, 1, ..., 15$, and $k = 1, 2, ..., n$, where $A(i,j)_c$ is the c-th coefficient of the 4×4 macroblock $A(i,j)$. Now we have the joint statistics

$$\mathcal{N}_{I_c}(l_2, l^\star) = \sum_{k=1}^{n} \sum_{i=0}^{H/4-1} \sum_{j=0}^{W/4-1} \mathcal{I}(\widetilde{R}_k^{K(q_1)}(i,j)_c = l_2 \text{ and } \widetilde{R}_k^{K(q^\star)}(i,j)_c = l^\star), c = 0, 1, ..., 15, \tag{5.16}$$

where $\mathcal{I}(\cdot)$ is the binary indicator function. An example of the resulting statistics $\mathcal{N}_{I_c}(\cdot,\cdot)$ with $c = 0$ (i.e., the DC coefficients) for I-frame residual coefficients is shown in Fig. 17.

Clearly, given the knowledge of $\widetilde{R}_1^{K(q_2)}$, $R_1^{F(q_1,q_2)}$ is uniquely determined by $\widetilde{R}_1^{K(q_1)}$, thus the decoder can always generate conditional probabilities

$$Pr\Big\{R_1^{F(q_1,q_2)}(i,j)_c = f \Big| \widetilde{R}_1^{K(q_2)}(i,j)_c = l_2, \widetilde{R}_1^{K(q^\star)}(i,j)_c = l^\star\Big\} = \frac{\mathcal{N}_{I_c}(l_{2,min} + f, l^\star)}{\sum_{l=l_{2,min}}^{l_{2,max}} \mathcal{N}_{I_c}(l, l^\star)}, \tag{5.17}$$

where $l_{2,min} = nl_2 - \frac{n_0-1}{2} + \mathcal{I}(l_2 > 0)\frac{n_0+1-n}{2}$, $l_{2,max} = nl_2 + \frac{n_0-1}{2} - \mathcal{I}(l_2 < 0)\frac{n_0+1-n}{2}$. With these conditional probabilities at the decoder, $R_1^{F(q_1,q_2)}$ is compressed by multi-level SW coding (described in Section F), and the resulting syndromes are sent to the decoder. Then

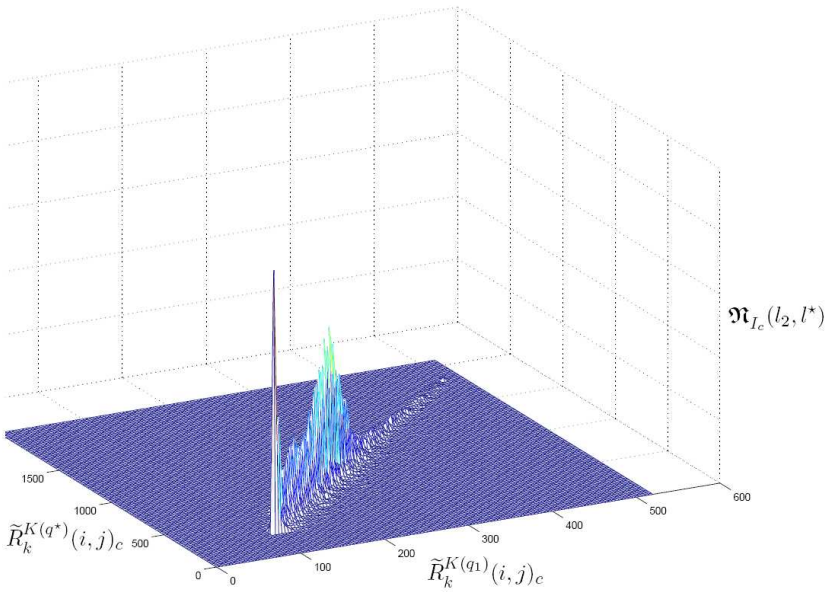

Fig. 17. Example of the correlation model for I-frame coefficients.

the final decoded I-frame $\widetilde{R}_1^{D(q_1)}$ is generated. Note that $\widetilde{R}_1^{D(q_1)}$ is not necessarily the same as the H.264/AVC decoded version $\widehat{R}_1^{D(q_1)}$, since the intra-predicted versions $R_1^{I(q_1)}$ and $R_1^{I(q_2)}$ are different.

2. MT video coding of P-frames

Our proposed MT video coding scheme for the right P-frames is depicted in Fig. 18. The coded bitstream for the k-th inter-coded frame R_k ($k = 2, 3, ..., n$) with $QP = q_1$ consists of three parts, namely, the overhead information $\mathcal{O}_{R_k}^{P(q_1)}$ (which is directly compressed by H.264/AVC), the motion vectors $\mathcal{M}_{R_k}^{P(q_1)}$, and texture bits $\mathcal{U}_{R_k}^{P(q_1)}$ for the DCT coefficients. Denote the compressed bits of $\mathcal{O}_{R_k}^{P(q_1)}$ and $\mathcal{M}_{R_k}^{P(q_1)}$ as $B_k^{M,O}$, and the compressed bits of $\mathcal{U}_{R_k}^{P(q_1)}$ as B_l^X.

Before compressing R_k for $k = 2, ..., n$ at Encoder 2, we assume that the joint decoder has access to the reconstructions $\{\widehat{L}_1^{D(q_1)}, ..., \widehat{L}_{k-1}^{D(q_1)}, \widehat{L}_k^{D(q_1)}\}$ and $\{\widetilde{R}_1^{D(q_1)}, ..., \widetilde{R}_{k-1}^{D(q_1)}\}$. At the decoder, we first employ stereo matching algorithm to generate a disparity map $\mathcal{D}_{k-1} = \mathbb{D}(\widehat{L}_{k-1}^{D(q_1)}, \widetilde{R}_{k-1}^{D(q_1)})$ between $\widehat{L}_{k-1}^{D(q_1)}$ and $\widetilde{R}_{k-1}^{D(q_1)}$. Using a slightly modified stereo matching

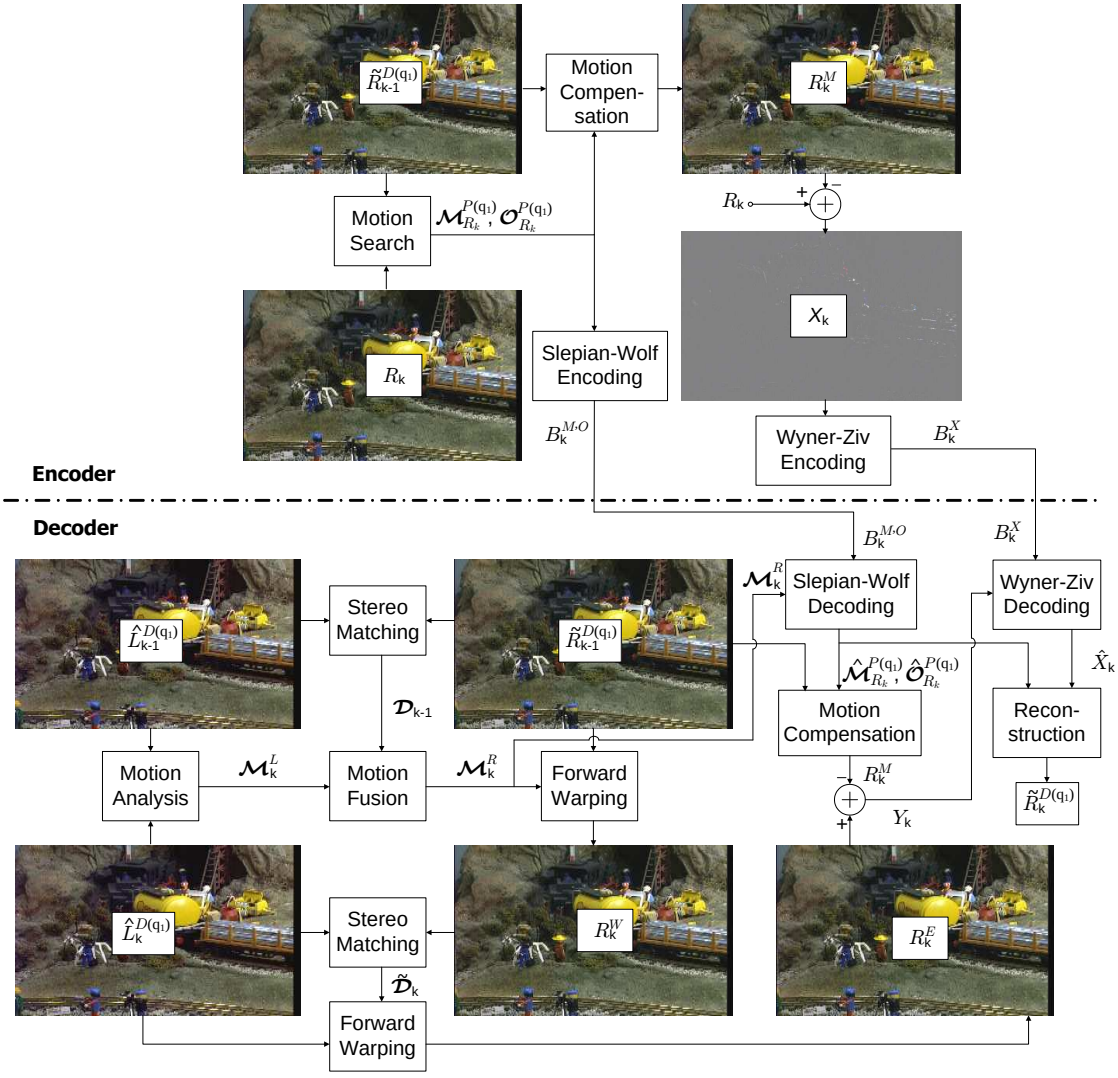

Fig. 18. The codec for the right P-frames in our first proposed MT video coder.

algorithm (by allowing vertical disparities), we also obtain a forward motion field $\mathcal{M}_k^L$ from $\widehat{L}_{k-1}^{D(q_1)}$ to $\widehat{L}_k^{D(q_1)}$, and write

$$\mathcal{M}_k^L \;=\; \mathbb{M}\Big(\widehat{L}_{k-1}^{D(q_1)}, \widehat{L}_k^{D(q_1)}\Big). \tag{5.18}$$

Then, use knowledge about the 3D stereo camera settings and follow the "identical motion constraint", we apply a novel motion fusing algorithm to produce the right forward motion

field $\mathcal{M}_k^R$ based on the known information $\mathcal{D}_{k-1}$ and $\mathcal{M}_k^L$, i.e.,

$$\mathcal{M}_k^R \;=\; \mathbb{F}\Big(\mathcal{M}_k^L, \mathcal{D}_{k-1}\Big). \tag{5.19}$$

The detailed motion fusion algorithm will be described in Section E. It is obvious that the motion vectors $\mathcal{M}_{R_k}^{P(q_1)}$ in the H.264/AVC bitstream are correlated to the motion field $\mathcal{M}_k^R$. Hence **SW coding** is employed to compress $\mathcal{M}_{R_k}^{P(q_1)}$ with $\mathcal{M}_k^R$ as decoder side information. Specifically, define

$$\widetilde{M}_{R_k}^{P(q_1)}(\boldsymbol{i},\boldsymbol{j}) \;=\; \text{median}\Big(\mathcal{M}_k^R(\boldsymbol{i},\boldsymbol{j})\Big), \tag{5.20}$$

as the side information for the motion vector of the $(\boldsymbol{i},\boldsymbol{j})$-th block, where we use bold indices $\boldsymbol{i}$ and $\boldsymbol{j}$ to allow various inter-search mode, including 16×16, 16×8, and 8×16, etc. Instead of directly doing SW coding on the motion vectors $M_{R_k}^{P(q_1)}(\boldsymbol{i},\boldsymbol{j})$, which are with memory, the encoder generates the motion vector difference (MVD) defined as the difference between the motion vectors $M_{R_k}^{P(q_1)}(\boldsymbol{i},\boldsymbol{j})$ and their predicted versions $\widehat{M}_{R_k}^{P(q_1)}(\boldsymbol{i},\boldsymbol{j})$ (using the same prediction method as in H.264/AVC), i.e., $\Delta M_{R_k}^{P(q_1)}(\boldsymbol{i},\boldsymbol{j}) = M_{R_k}^{P(q_1)}(\boldsymbol{i},\boldsymbol{j}) - \widehat{M}_{R_k}^{P(q_1)}(\boldsymbol{i},\boldsymbol{j})$, and compresses $\Delta M_{R_k}^{P(q_1)}$ using SW coding. The side information for the MVDs are generated as

$$\widetilde{\Delta M}_{R_k}^{P(q_1)}(\boldsymbol{i},\boldsymbol{j}) \;=\; \widetilde{M}_{R_k}^{P(q_1)}(\boldsymbol{i},\boldsymbol{j}) - \widehat{\widetilde{M}}_{R_k}^{P(q_1)}(\boldsymbol{i},\boldsymbol{j}), \tag{5.21}$$

where $\widehat{\widetilde{M}}_{R_k}^{P(q_1)}(\boldsymbol{i},\boldsymbol{j})$ is the $(\boldsymbol{i},\boldsymbol{j})$-th H.264/AVC-predicted motion vector using the neighboring $\widetilde{M}_{R_k}^{P(q_1)}(\boldsymbol{i},\boldsymbol{j})$'s as references. Now we assume that the MVDs are memoryless sources, collect joint statistics between the MVDs $\Delta M_{R_k}^{P(q_1)}(\boldsymbol{i},\boldsymbol{j})$ and estimated MVDs $\widetilde{\Delta M}_{R_k}^{P(q_1)}(\boldsymbol{i},\boldsymbol{j})$ for all $n-1$ P-frames to build an empirical model, and compute the condi-

tional probabilities for the MVDs, we have

$$\mathcal{N}_{MVD}(m,m') = \sum_{k=2}^{n} \sum_{(\boldsymbol{i},\boldsymbol{j})} \mathcal{I}(\Delta M_{R_k}^{P(q_1)}(\boldsymbol{i},\boldsymbol{j}) = m, \widetilde{\Delta M}_{R_k}^{P(q_1)}(\boldsymbol{i},\boldsymbol{j}) = m'); \tag{5.22}$$

$$Pr\Big\{\Delta M_{R_k}^{P(q_1)}(\boldsymbol{i},\boldsymbol{j}) = m \Big| \widetilde{\Delta M}_{R_k}^{P(q_1)}(\boldsymbol{i},\boldsymbol{j}) = m'\Big\} = \frac{\mathcal{N}_{MVD}(m,m')}{\sum_{\bar{m}=-\mathcal{M}_{max}}^{\mathcal{M}_{max}} \mathcal{N}_{MVD}(\bar{m},m')}. \tag{5.23}$$

An example of the correlation model for motion vectors is shown in Fig. 19 (a).

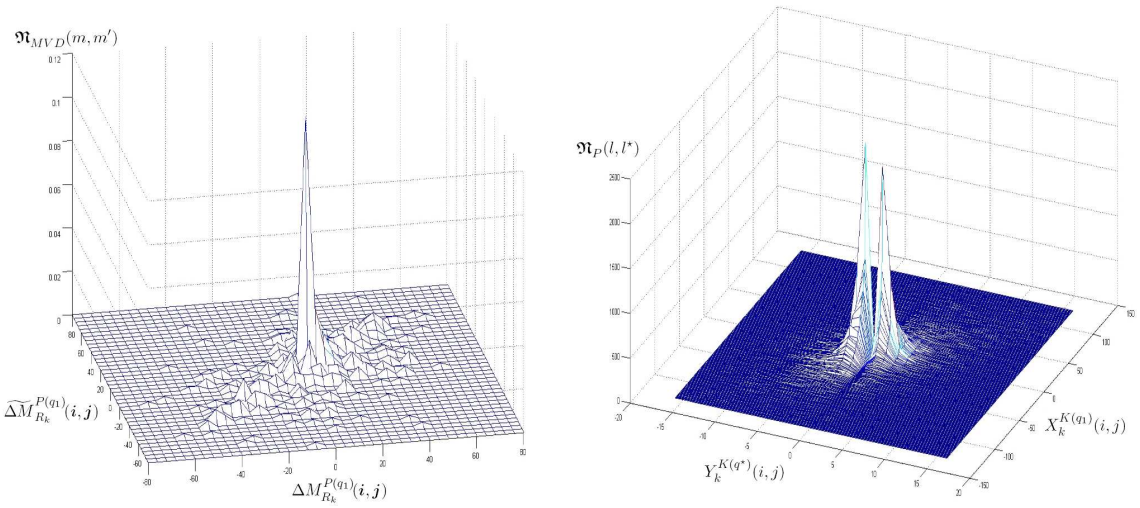

(a) (b)

Fig. 19. An example of the correlation model for (a) P-frame motion vectors and (b) P-frame residual coefficients.

Next, $\widetilde{R}_{k-1}^{D(q_1)}$ is warped according to the right motion field $\mathcal{M}_k^R$, generating an estimate R_k^W of the k-th frame R_k, i.e.,

$$R_k^W = \mathbb{W}\Big(\widetilde{R}_{k-1}^{D(q_1)}, \mathcal{M}_k^R\Big). \tag{5.24}$$

Now an estimation of the k-th disparity map can be obtained from $\widehat{L}_k^{D(q_1)}$ and R_k^W, then we have

$$\widetilde{\mathcal{D}}_k = \mathbb{D}\Big(\widehat{L}_k^{D(q_1)}, R_k^W\Big). \tag{5.25}$$

Assume ideal SW decoding, such that $\mathcal{M}_{R_k}^{P(q_1)}$ is perfectly reconstructed at the decoder,

then exactly the same motion compensated frame R_k^M at the encoder can be formed by warping $\widetilde{R}_{k-1}^{D(q_1)}$ according to $\mathcal{M}_{R_k}^{P(q_1)}$, i.e.,

$$R_k^M = \mathbb{W}\Big(\widetilde{R}_{k-1}^{D(q_1)}, \mathcal{M}_{R_k}^{P(q_1)}\Big). \tag{5.26}$$

Consequently, the source and side information for **WZ coding** are computed as

$$X_k = R_k - \mathbb{W}(\widetilde{R}_{k-1}^{D(q_1)}, \mathcal{M}_{R_k}^{P(q_1)}) = R_k - R_k^M; \tag{5.27}$$

$$Y_k = \mathbb{W}(\widehat{L}_k^{D(q_1)}, \widetilde{\mathcal{D}}_k) - \mathbb{W}\big(\widetilde{R}_{k-1}^{D(q_1)}, \mathcal{M}_{R_k}^{P(q_1)}\big), \tag{5.28}$$

respectively, for $k = 2, ..., n$, where $R_k^E = \mathbb{W}(\widehat{L}_k^{D(q_1)}, \widetilde{\mathcal{D}}_k)$ is the warped version of $\widehat{L}_k^{D(q_1)}$ using disparity map $\widetilde{\mathcal{D}}_k$. Finally, WZ coding is employed to explore the remaining correlation between X_k and Y_k and joint decoder reconstructs $\widetilde{\mathcal{R}}^{D(q_1)} = \{\widetilde{R}_1^{D(q_1)}, ..., \widetilde{R}_n^{D(q_1)}\}$ using a total transmission rate of $\mathscr{R}_R = \sum_{i=1}^{n} \mathscr{R}_R^i$ bps. To do this, the WZ encoder and decoder quantizes the transformed source $\mathbb{T}\Big(X_k(i,j)\Big)$ and transformed side information $\mathbb{T}\Big(Y_k(i,j)\Big)$, using dead-zone quantizers $C_{q_1}^P = \mathcal{C}(d_{q_1}, \frac{5}{3}d_{q_1})$ and $C_{q^\star}^P = \mathcal{C}(d_{q^\star}, \frac{5}{3}d_{q^\star})$, respectively. The resulting quantization levels $X_k^{K(q_1)}(i,j) = \mathbb{Q}\Big(\mathbb{T}\Big(X_k(i,j)\Big), C_{q_1}^P\Big)$ are then coded by a multi-level SW encoder with $Y_k^{K(q^\star)}(i,j) = \mathbb{Q}\Big(\mathbb{T}\Big(Y_k(i,j)\Big), C_{q^\star}^P\Big)$ as decoder side information. Similar to the SW coding of MVDs, we collect joint statistics for all $n-1$ P-frames to build an empirical correlation model,

$$\mathscr{N}_P(l, l^\star) = \sum_{k=2}^{n} \sum_{i=0}^{H/4-1} \sum_{j=0}^{W/4-1} \mathcal{I}\Big(X_k^{K(q_1)}(i,j) = l, Y_k^{K(q^\star)}(i,j) = l^\star\Big), \tag{5.29}$$

and compute

$$Pr\Big\{X_k^{K(q_1)}(i,j) = l \Big| Y_k^{K(q^\star)}(i,j) = l^\star\Big\} = \frac{\mathscr{N}_P(l, l^\star)}{\sum_{\bar{l}=l_{min}}^{l_{max}} \mathscr{N}_P(\bar{l}, l^\star)}. \tag{5.30}$$

Finally, the joint decoder uses the syndrome bits and the log-likelihood ratios computed using the correlation model and the side information to reconstruct $X_k^{K(q_1)}(i,j)$ and hence

$\hat{X}_k$. An example of the correlation model for P-frame residual coefficients is shown in Fig. 19 (b). Detailed encoding/decoding algorithms for MT source coding can be found in [69].

C. Proposed MT video coding scheme 2 with source splitting of the I-frames

Theoretically, the first MT video coding scheme proposed in Section B can only achieve the corner points of the MT sum rate bound, meaning the encoder for the left sequence always uses the same rate (resulted from H.264/AVC coding). To build a MT video coder that is capable of trading of rates between the two encoders, one solution is to employ the source splitting method of [46], which is first introduced for SW coding, and then applied for quadratic Gaussian MT source coding in [69]. The main idea of source splitting is to "split" one of the sources into two parts, then transmit the first part using classical source coding, the second part using **WZ coding** given the decoded first source, and the third part using **another WZ coder** with the decoded versions of the two sources as side information. Such a scheme can potentially achieve any point on the MT sum rate bound if the sources are jointly Gaussian under the assumption of ideal quantization and SW coding [69]. However, for practical sources including stereo video sequences, since source-splitting includes an extra WZ coding step, we should expect a slightly larger sum rate loss (compared to our first proposed MT video coding scheme) – the price to pay for arbitrary rate allocation.

The block diagram for our second proposed MT video codec (for I-frames) is shown in Fig. 20. The left I-frame is first coded by H.264/AVC using a dead-zone quantizer with quantizer $C^I_{q_2^L}$, then the residual frame $L_1^{R(q_2^L)}$ is quantized using another quantizer $C^I_{q_1}$; similarly, the right I-frame is coded by H.264/AVC using a dead-zone quantizer with quantizer $C^I_{q_2^R}$, and the residual frame $R_1^{R(q_2^R)}$ is quantized using $C^I_{q_1}$. The quantization thresholds are selected such that the resulting two quantizers for the same sequence are

embedded, i.e.,

$$C^I_{q_2^L} = (n^L, n_0^L) \times C^I_{q_1} \quad \text{and} \quad C^I_{q_2^R} = (n^R, n_0^R) \times C^I_{q_1}, \tag{5.31}$$

which implies that the finer quantization levels $\widetilde{L}_1^{K(q_1)}$ and $\widetilde{R}_1^{K(q_1)}$ are uniquely determined by the coarse quantization levels $\widehat{L}_1^{K(q_2^L)}$ and $\widehat{R}_1^{K(q_2^R)}$ and the refining cell indices $L_1^{F(q_1,q_2^L)}$ and $R_1^{F(q_1,q_2^R)}$ defined as

$$L_1^{F(q_1,q_2^L)} = \begin{cases} \widetilde{L}_1^{K(q_1)} - n^L L_1^{K(q_2^L)} + \frac{n_0^L-1}{2}, & \text{if} \quad L_1^{K(q_2^L)} < 0 \\ \widetilde{L}_1^{K(q_1)} - n^L L_1^{K(q_2^L)} + \frac{2n^L-n_0^L-1}{2}, & \text{if} \quad L_1^{K(q_2^L)} \geq 0 \end{cases}, \tag{5.32}$$

$$R_1^{F(q_1,q_2^R)} = \begin{cases} \widetilde{R}_1^{K(q_1)} - n^R R_1^{K(q_2^R)} + \frac{n_0^R-1}{2}, & \text{if} \quad R_1^{K(q_2^R)} < 0 \\ \widetilde{R}_1^{K(q_1)} - n^R R_1^{K(q_2^R)} + \frac{2n^R-n_0^R-1}{2}, & \text{if} \quad R_1^{K(q_2^R)} \geq 0 \end{cases}. \tag{5.33}$$

This property significantly reduces the decoder's computational complexity.

The two coarse versions $\widehat{L}_1^{D(q_2^L)}$ and $\widehat{R}_1^{D(q_2^R)}$ are first transmitted to the decoder, where a disparity map $\widetilde{\mathcal{D}}_1 = \mathbb{D}\Big(\widehat{L}_1^{D(q_2^L)}, \widehat{R}_1^{D(q_2^R)}\Big)$ is generated between these two decoded I-frames. With $\widetilde{\mathcal{D}}_1$ at the decoder, the decoded right I-frame $\widehat{R}_1^{D(q_2^R)}$ is warped to generate a side information for SW coding of the lower two bit-planes (that are used to distinguish among n^L or n_0^L quantization cells) of the left I-frame, i.e., $\widehat{L}_1^{W(q_2^R)} = \mathbb{W}\Big(\widehat{R}_1^{D(q_2^R)}, \widetilde{\mathcal{D}}_1\Big)$.

Next, as in our first proposed scheme, we compute

$$\widetilde{L}_1^{K(q_1)} = \mathbb{Q}(L_1^{T(q_2^L)}, C^I_{q_1}), \quad \text{and} \quad \widetilde{L}_1^{K(q^\star)} = \mathbb{Q}\Big(\mathbb{T}(\widehat{L}_1^{W(q_2^R)} - L_1^{I(q_2^L)}), C^I_{q^\star}\Big); \tag{5.34}$$

and for each $c = 0, 1, ..., 15$, define

$$\mathscr{N}^{SP}_{I1_c}(l_2, l^\star) = \sum_{k=1}^{n} \sum_{i=0}^{H/4-1} \sum_{j=0}^{W/4-1} \mathcal{I}(\widetilde{L}_k^{K(q_1)}(i,j)_c = l_2, \widetilde{L}_k^{K(q^\star)}(i,j)_c = l^\star) \tag{5.35}$$

$$Pr\Big\{L_1^{F(q_1,q_2^L)}(i,j)_c = f \Big| \widetilde{L}_1^{K(q_2^L)}(i,j)_c = l_2, \widetilde{L}_1^{K(q^\star)}(i,j)_c = l^\star\Big\} = \frac{\mathscr{N}^{SP}_{I1_c}(l_{2,min} + f, l^\star)}{\sum_{l=l_{2,min}}^{l_{2,max}} \mathscr{N}^{SP}_{I1_c}(l, l^\star)} \tag{5.36}$$

An example of the correlation model $\mathscr{N}^{SP}_{I1}$ for the first SW coding step is shown in

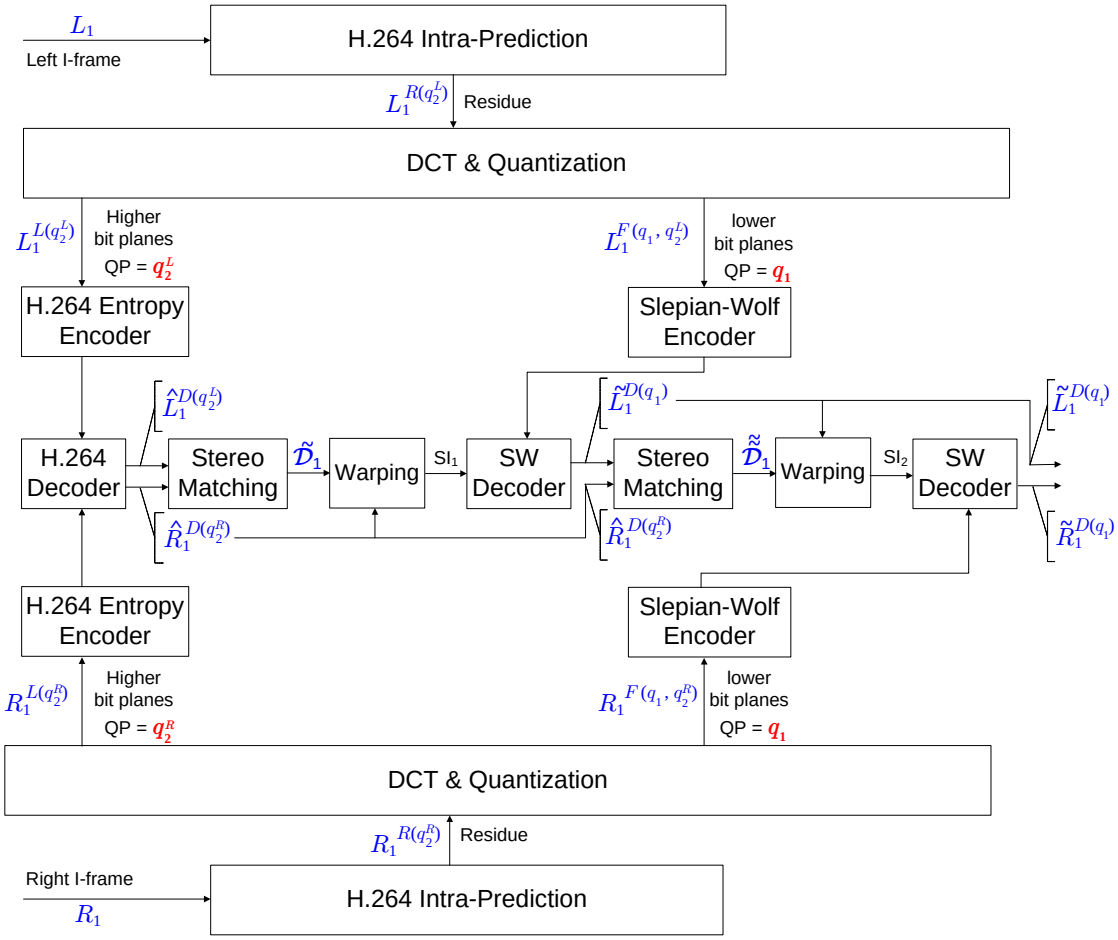

Fig. 20. MT video coding of I-frames using source splitting.

Fig. 21. Then the refinement cell indices $L_1^{F(q_1,q_2^L)}$ of the left I-frame $\widehat{L}_1^{D(q_1)}$ can be compressed and reconstructed at the decoder. Hence a new disparity map $\widetilde{\widetilde{\mathcal{D}}}_1 = \mathbb{D}\left(\widehat{L}_1^{D(q_1)}, \widehat{R}_1^{D(q_2^R)}\right)$ is generated, and another SW coding step is done to compress the cell indices of the right I-frame $R_1^{F(q_1,q_2^R)}$. Finally, the decoded version of the left I-frame $\widehat{L}_1^{D(q_1)}$ and the right I-frame $\widetilde{R}_1^{D(q_1)}$ are reconstructed at the decoder.

Before moving on, we point out that conceptually source splitting can also be applied to the P-frames. However, our practical implementation does not improve the sum rate performance than that without source splitting of the P-frames. Explanations are given in Section 5.2.2.

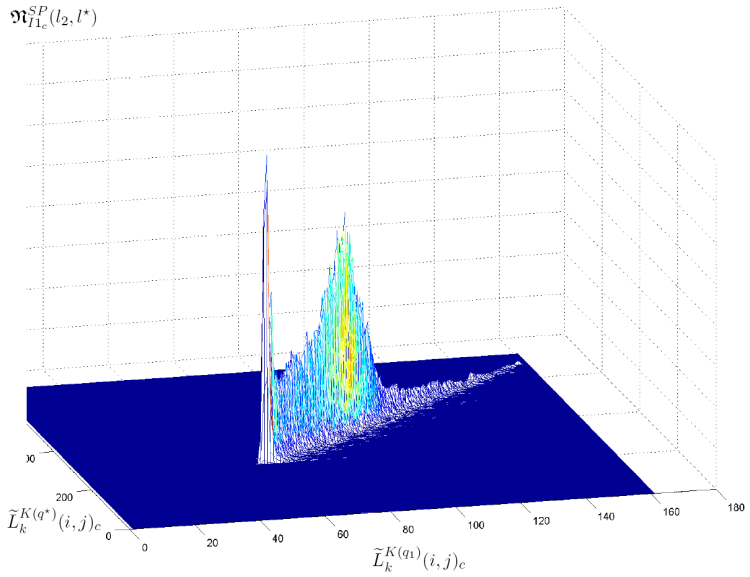

Fig. 21. An example of the correlation model for I-frame residual coefficients our second proposed MT video coder.

D. BP based stereo matching algorithm

In this subsection, we provide some details of the BP based stereo matching algorithm, which is the key to explore the binocular correlation between the left and right sequences. Suppose $\mathcal{P}$ is the set of all pixels in the reference frame, and $\mathcal{L}$ is the set of possible discrete disparity values. The disparity of a pixel $p \in \mathcal{P}$ is denoted as f_p. Then the stereo matching problem is formalized as an energy minimization problem with total energy [15]

$$E(f) = \sum_{p \in \mathcal{P}} D_p(f_p) + \sum_{p,q \in \mathcal{N}} V(f_p - f_q), \tag{5.37}$$

where $D_p(f_p)$ is the cost of assigning disparity value f_p to pixel p, $\mathcal{N}$ is the set of neighboring pixel pairs, and $V(f_p - f_q)$ is the cost function of assigning disparity values f_p and f_q to neighboring pixels p and q. To solve this minimization problem, Felzenszwalb *et al.* [15] implemented the standard "max-product" algorithm, where messages are passed between each pair of neighboring pixels (p, q) in an iterative manner. More specifically, at

t-th iteration, a message $m^t_{p\to q}$, a length-$|\mathcal{L}|$ vector, is updated in the following way,

$$m^t_{p\to q}(f_q) = \min_{f_p}\Big(V(f_p - f_q) + D_p(f_p) + \sum_{s\in\mathcal{N}(p)\setminus q} m^{t-1}_{s\to p}(f_p)\Big), \tag{5.38}$$

where $m^{t-1}_{s\to p}(f_p)$ is the component in message $m^{t-1}_{s\to p}$ (sent from s to p at $(t-1)$-th iteration) that corresponds to the disparity value f_p. After T iterations (where T is a fixed number), a final disparity value f^*_q is assigned for each pixel q, such that

$$f^*_q = \arg\min_{f_q} b_q(f_q), \quad \text{where} \quad b_q(f_q) = D_q(f_q) + \sum_{p\in\mathcal{N}(q)} m^T_{p\to q}(f_q). \tag{5.39}$$

In general, updating messages $m^t_{p\to q}$ will take $O(|\mathcal{L}|^2)$ time where $|\mathcal{L}|$ is the number of possible disparities. However, if the cost function $V(f_p - f_q)$ in (5.37) is in the following form,

$$V(f_p - f_q) \;=\; \min(c|f_p - f_q|, d), \quad \text{where} \quad c, d \in \mathbb{R}^+, \tag{5.40}$$

it is possible to compute new messages in $O(|\mathcal{L}|)$ time. Detailed message update algorithm can be found in [15]. Finally, a disparity map is generated in $O(|\mathcal{P}|\cdot|\mathcal{L}|)$ time, where $|\mathcal{P}|$ is the number of pixels.

E. Motion fusion

In this subsection, we give details on the motion fusion algorithm for estimating the right forward motion field. The 3D camera geometry is depicted again in Fig. 22 (a). Although originally designed for stereo matching, the BP based algorithm [50, 15] can also be applied for motion field estimation. Since most stereo cameras are aligned such that no vertical disparity exists between corresponding pixels, the algorithm in [50] only allows horizontal disparities, which are clearly not enough for motion field. Hence we slightly modify the above algorithm by allowing vertical disparities: $\boldsymbol{d}_s$, all scalar disparities d_s become vector disparities $\boldsymbol{d}_s$; the Birchfield and Tomasi's pixel dissimilarity $|F(s, \boldsymbol{d}_s, I)|$ [50] is changed

to

$$F(s, \boldsymbol{d}_s, I) = \min\{\bar{d}(s, s', I)/\sigma_f, \bar{d}(s', s, I)/\sigma_f\}, \tag{5.41}$$

where $\bar{d}(s, s', I)$=$\min\{|I_K(s) - I_R(s')|, |I_K(s) - I_R^{\leftarrow}(s')|, |I_K(s) - I_R^{\rightarrow}(s')|, |I_K(s) - I_R^{\uparrow}(s')|, |I_K(s) - I_R^{\downarrow}(s')|\}$, s' is the matching pixel of s with disparity $\boldsymbol{d}_s$, and $\{I_R^{\leftarrow}(s'), I_R^{\rightarrow}(s'), I_R^{\uparrow}(s'), I_R^{\downarrow}(s')\}$ are the linearly interpolated intensity halfway between s' and its neighboring pixel to the left, right, top and bottom, respectively, and σ_f is the image noise variance that depends on the quality of input pictures.

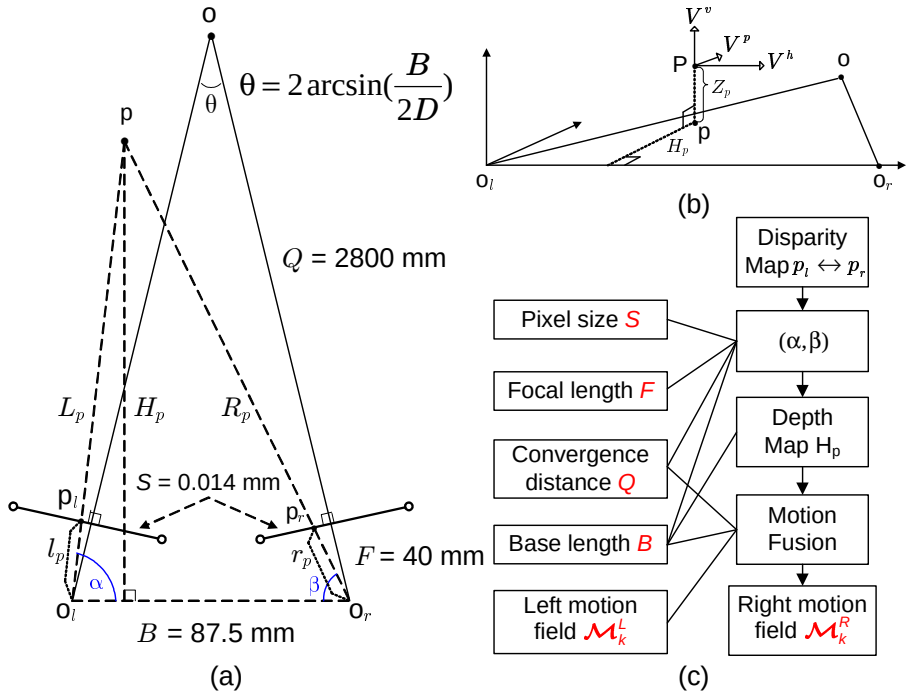

Fig. 22. Stereo motion fusion (a) 3D camera geometry (b) motion decomposition; (c) block diagram.

The next step is to fuse the disparity map $\mathcal{D}$ and the left motion field $\mathcal{M}^L$ to estimate the right motion field $\mathcal{M}^R$. As shown in Fig. 22 (b), the 3D motion vector can be decomposed into three components: horizontal motion V_h that is parallel to $o_l o_r$, vertical motion V_v that is perpendicular to the $oo_l o_r$ plane, and parallel motion V_p that is perpendicular to both V_h and V_v (which is ignored in the motion fusion algorithm). Recall from Section A

that F is the focal length of both cameras, B the base line distance $o_l o_r$ between the two cameras, S the pixel size in the imaging plane, and Q the convergence distance. The stereo motion fusion algorithm has the following steps (see block diagram in Fig. 22 (c)).

1. Estimating the depth. Calculate angles α and β using the horizontal coordinate of the pixel s. Then the depth of s is $H_p = B/[(\tan(\alpha))^{-1} + (\tan(\beta))^{-1}]$.
2. Estimating the right horizontal motion vector $v_h^r = V_h^r r_p/R_p$ based on the depth H_p and the left horizontal motion vector $v_h^l = V_h^l l_p/L_p$ using (note that $V_h^l = V_h^r$)

$$\frac{v_h^r}{v_h^l} = \frac{r_p L_p}{l_p R_p} = \frac{\sin(\alpha + \frac{\theta}{2})\sin(\beta)}{\sin(\beta + \frac{\theta}{2})\sin(\alpha)}. \tag{5.42}$$

3. Estimating the right vertical motion vector using

$$\frac{v_v^r}{v_v^l} = \frac{v_h^r}{v_h^l} = \frac{\sin(\alpha + \frac{\theta}{2})\sin(\beta)}{\sin(\beta + \frac{\theta}{2})\sin(\alpha)}. \tag{5.43}$$

F. Multi-level SW coding of motion vectors and quantization levels

In this subsection, we describe the multi-level SW encoding and decoding algorithms, which are used to compress the motion vectors and the quantization levels of the residual coefficients. We first break the m-ary motion vectors or quantized residual coefficients into $\log_2 m$ bit planes, and then use binary SW coding to compress the bit planes. For the motion vectors, which is often a 2^n-array source, a regular labeling suffices. However, the refining cell indices $R_1^{F(q_1,q_2^L)}$ and $R_1^{F(q_1,q_2^R)}$ in our first and second proposed schemes are not necessarily 2^k-ary sources. For example, when $(n^L, n_0^L) = (4, 5)$ and $(n^R, n_0^R) = (2, 3)$, $L_1^{F(q_1,q_2^L)}$ and $R_1^{F(q_1,q_2^R)}$ are 5-ary and ternary sources, respectively. This necessitates irregular labeling as shown in Fig. 23.

Specifically, for the 5-ary source $R_1^{F(q_1,q_2^R)}$, the first two bit planes are used to distinguish between index sets $\Big\{\{0,4\},\{1\},\{2\},\{3\}\Big\}$, and the third bit plane is used to distinguish between $\{0\}$ and $\{4\}$. Similarly, for the ternary source $R_1^{F(q_1,q_2^R)}$, the first bit plane

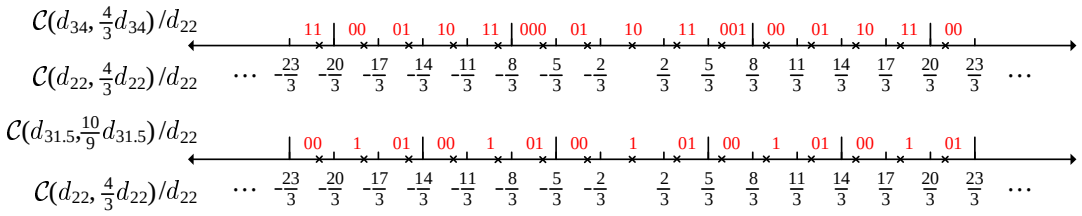

Fig. 23. Labeling of cell indices, the top figure is the labeling of $R_1^{F(q_1,q_2^L)}$ for our first proposed scheme and the bottom figure depicts the labeling of $R_1^{F(q_1,q_2^R)}$ for our second proposed scheme.

is used to distinguish between index sets $\{0, 2\}$ and $\{1\}$, and the second bit plane is used to distinguish between $\{0\}$ and $\{2\}$. Detailed encoding/decoding algorithms again can be found in [69].

G. Experimental results

In our experiments, the stereo video sequences are captured by two closely located cameras in the setting depicted in Fig. 24. Each camera has a focal length of $F = 40$mm and pixel size $s = 0.014$mm. The two cameras are separated by a baseline distance of $B = o_l o_r = 87.5$mm to observe the same scene from two different angles. The convergence distance of the cameras is $Q = oo_l = oo_r = 2.80$m, and the convergence angle is defined as $\theta = 2\arcsin\left(\frac{B}{2D}\right) \approx 2.13^\circ$. Both test sequences "tunnel" and "aqua" can be downloaded at "http://lena.tamu.edu/sequences.zip", and the first pair of frames of the "tunnel" sequences are also shown in Fig. 24.

We use the Y-component of the 720 × 288 "tunnel" and "aqua" as test stereo video sequences, each with 20 left frames and 20 right frames. Since the efficiency of MT video coding hinges upon the video quality at the decoder (for accurate correlation modeling), we target at both low-rate and high-rate regimes and expect the latter to be more favorable for MT video coding.

Since MT video coding is expected to perform better than separate encoding (and decoding), but worse than joint encoding (and decoding), as one benchmark, we use H.264/AVC

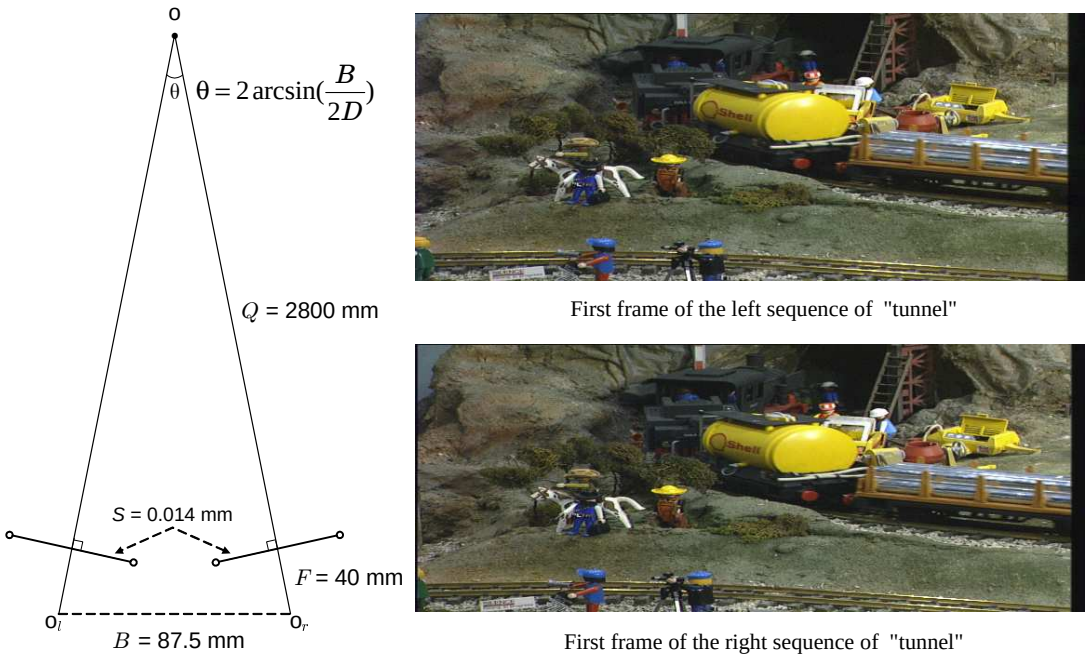

Fig. 24. 3D camera settings (left) and first pair of frames (right) from "tunnel": top-right is the left first frame, and bottom-right is the right first frame.

for separate encoding (and decoding) of the left and right sequences using the IP...P structure. For "tunnel", we code the left and right sequences using the H.264/AVC reference software JM73 [26], and list the coding parameters and statistics of the resulting bitstream for both the low-rate and high-rate cases in Table IX.

For joint encoding, we interleave the left and right stereo video sequences and use H.264/AVC (with the same parameters) to code the interleaved sequence with two reference frames in motion estimation. We note that this is but one way of generating the benchmark for joint coding[1]. Better benchmarks can be obtained by using more reference frames in motion estimation.

In MT video coding, the disparity maps and motion fields are generated in half-pel

[1]We also ran the Joint Scalable Video Model software [44] to compress "tunnel". However, the total bit rate is 6.461 Mbps, which is only slightly smaller than the 6.501 Mbps obtained with our simple H.264/AVC-based joint encoding scheme (with two reference frames) at the same visual quality. Similar result was also obtained for "aqua".

Table IX. H.264/AVC compression parameters and statistics for "tunnel".

Parameters	Low-rate regime	High-rate regime
QP I frame	35	22
QP P frame	33	20
Total frames	20	20
Inter-search mode	16×16,16×8,8×16	16×16,16×8,8×16
Motion precision	quarter-pel	quarter-pel
Statistics	Low-rate regime	High-rate regime
I-frame bits (%)	32.8	17.3
Overhead bits (%)	5.8	1.6
Motion vector bits (%)	13.6	3.5
Coefficients bits (%)	47.8	77.6
Total	287,248 bits	286,584 bits
Bit rate	866.3 kbps	6.630 Mbps
Average PSNR	31.15 dB	40.59 dB

precision by the modified stereo matching algorithm described in Section E. The parameter values are consistent with those in [50]: $e_d = 0.01, \sigma_d = 8, e_p = 0.05, \sigma_p = 0.6$. We also incorporate segmentation results produced by the mean-shift algorithm [10].

In our implementation, the SW rate is determined by simulation: if the conditional entropy is much smaller (e.g., > 0.05 b/s) than the self entropy, SW coding is used, and the SW rate is set to be the smallest value such that decoding is successful (determined by simulation); if the conditional entropy is very close (e.g., < 0.05 b/s difference) to the self entropy, arithmetic coding is used instead.

1. Low-rate regime

In the low-rate regime, the sum rate is relatively low (866.28 kbps at a frame rate of 30 f/s), leading to poor reconstruction quality. Consequently, the disparity map and the motion field generated from the decoded frames are not very reliable compared to those from the originals. Hence in the implemented MT video coding scheme 1, only the motion vectors (generated from the originals and independent of the coding rate) for the inter-coded blocks are SW coded with side information generated at the decoder, while the I-frames and P-

frame residual coefficients are directly coded by H.264/AVC. Using the joint statistics collected from all 20 frames of "tunnel" for an empirical correlation model, and a multi-level SW code implemented by LDPC codes with 7 bit planes each for the vertical and horizontal component of motion vectors, we are able to save 3,747 bits from the 38,970 motion vector bits in the right bitstream (all the other components are entropy coded as in H.264/AVC). The SW coding block length varies from frame to frame, and ranges in $(800, 1100)$. Fig. 25 compares the performance of separate encoding, MT video coding, and joint encoding of "tunnel".

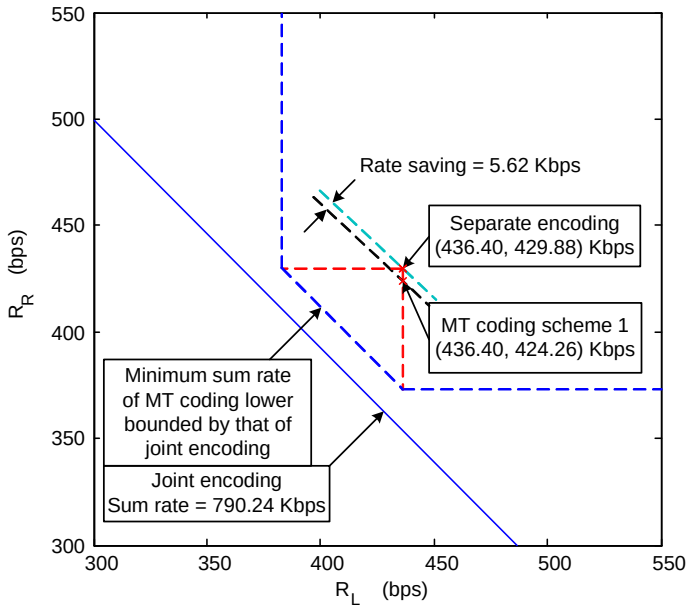

Fig. 25. Comparison between separate H.264/AVC coding, MT video coding, and joint encoding at the same average PSNR of $\mathscr{P} = 31.15$ dB over all 40 frames for "tunnel".

2. High-rate regime

a. MT video coding without source splitting of the I-frames

In the high-rate case, since most of the bits are spent on coding the residual frame (77.2% of the bit stream as indicated in Table 1) in our first proposed MT video coding scheme (without source-splitting of the I-frames), we implement the algorithms described in Section 1

for I-frame coding (with P_l = 34 and P_h = 22) and in Section 2 for the residual coefficients of the P-frames. Generic correlation models between the sources and the side informations are generated based on the joint statistics collected from all 20 frames of "tunnel". Nested scalar quantization [76, 28] followed by multi-level SW coding (using LDPC codes) are employed for WZ coding. In our implementations, the WZ coding block length for the I-frame coefficients is 12,096, while that for the P-frame coefficients ranges in $(4000, 6000)$. Table X lists the SW code rate used for each of the 4×4 residual coefficients (for each of the two bit planes).

Table X. Practical SW coding rates (in b/s) for the I-frame 4x4 residual coefficients of "tunnel".

	Bit plane #1				Bit plane #2			
	0	1	2	3	0	1	2	3
0	0.83	0.78	0.67	0.39	0.84	0.77	0.64	0.40
1	0.80	0.74	0.61	0.32	0.82	0.72	0.61	0.35
2	0.77	0.71	0.51	0.26	0.82	0.71	0.52	0.23
3	0.76	0.66	0.45	0.19	0.78	0.66	0.42	0.17

For "tunnel", the total saving is 32,548 bits, which is equivalent to 48.8 kbps, or 0.75% of the total sum rate. Similar experiments on the "aqua" stereo video sequences give a total sum rate savings of 37.0 kbps, or 0.53% of the total sum rate. Performance comparisons among separate encoding, MT video coding, and joint encoding for the "tunnel" and "aqua" sequences are shown in Fig. 26.

We additionally run experiments on "tunnel" with both separate and joint encoding at the same sum rate of 6.581 Mbps (by slightly adjusting the H.264/AVC encoding parameters in Table IX) as with MT video coding. This allows us to compare the PSNR vs. frame number performance of these three different schemes at the same sum rate in Fig. 27.

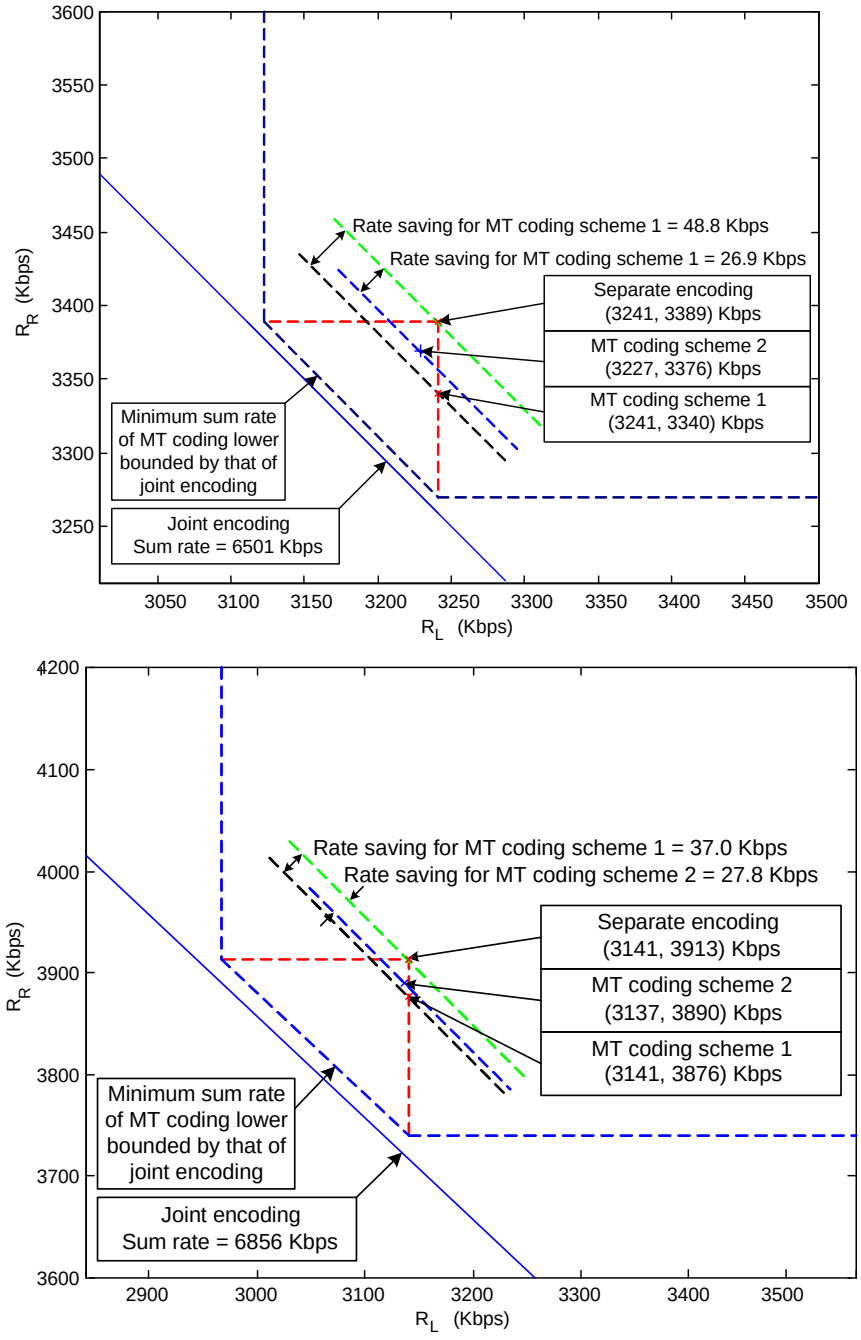

Fig. 26. Comparison between separate H.264/AVC coding, MT video coding, and joint encoding of "tunnel" (left) with the same average PSNR of $\mathscr{P} = 40.59$ dB and "aqua" (right) with the same average PSNR of $\mathscr{P} = 40.66$ dB.

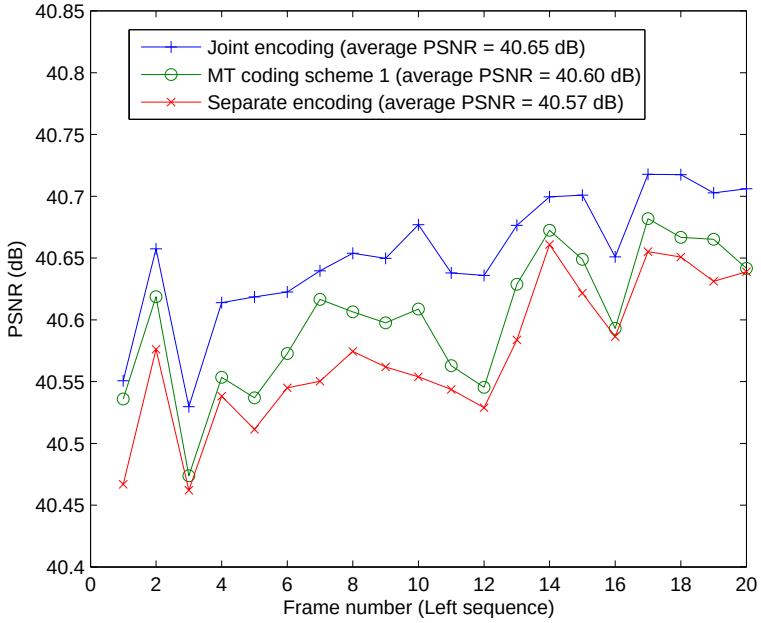

(a) Left sequence

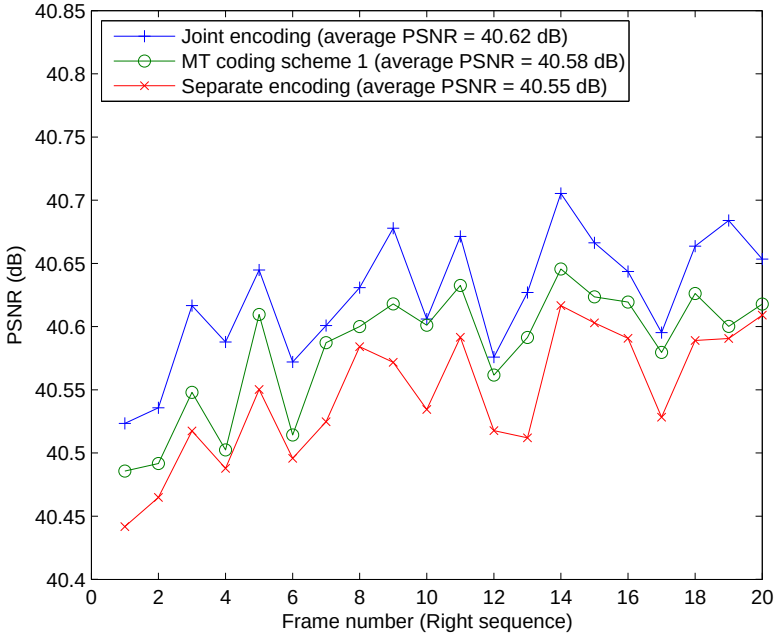

(b) Right sequence

Fig. 27. Comparison (in terms of PSNR vs. frame number) between separate H.264/AVC coding, MT video coding, and joint encoding at the same sum rate of 6.581 Mbps for "tunnel".

Remarks:

- From Fig. 26, we see that R_L by design is the same for both separate H.264/AVC coding and MT video coding. Thus our first proposed scheme (without source splitting) is "asymmetric" in nature, meaning that it can only approach the corner points of the rate region at best. Note that, although the minimum sum rate of MT video coding is not known, it is lower bounded by the sum rate of joint encoding.
- It is seen from Figs. 25 and 26 that, compared to separate H.264/AVC coding, MT video coding achieves some savings at low sum rate and a bit more at high sum rate. However, the rate saving is 48.4 Kbps (or 0.75%) for "tunnel" and 15.8 Kbps (or 0.53%) for "aqua" – less less than one percent in this case. In addition, we used the true joint statistics in our experiments, leading to best scenario performance. Thus, it is in general **not** easy to beat separate H.264/AVC coding with MT video coding, especially at low sum rate. This underscores one of the challenging issues with practical MT video coding that is correlation modeling. A true generic correlation model should be built off-line by collecting joint statistics from many stereo video sequences – much like codebook training (e.g., for Huffman coding and for vector quantization) in classic source coding. Towards this end, we run simulations using a slightly more general correlation model computed from both "tunnel" and "aqua" (after mixing them together). At the same average PSNR of 40.59 dB for "tunnel", the sum-rate saving of MT video coding over separate H.264/AVC coding is now 17.6 (instead of 48.4) Kbps. For "aqua", the new sum-rate saving is 15.8 (instead of 37.0) Kbps at the same average PSNR of 40.66 dB.
- We believe that our marginal 0.75% sum rate savings with MT video coding for "tunnel" in the high-rate regime are partially due to the small 1.94% rate savings with joint coding (both over separate H.264/AVC coding). We expect improvements with both MT video coding and joint encoding when multiple reference frames are

used in motion estimation and fusion.

- In this work, we do not emphasize low-complexity encoding (as advocated in [43, 71]). Instead, our only premise is distributed coding, i.e., no collaboration between the encoders. The complexity of our MT video encoders is essentially the same as that of H.264/AVC encoding. The complexity of the joint MT video decoder is high due to stereo matching, which takes around 40 minutes per frame on our Pentium IV 2.0GHz PC.

b. MT video coding with source splitting of the I-frames

We also implement our second proposed scheme based on source splitting (described in Section C) of the I-frames. The quantizers are set to

$$C^I_{q_1} = \mathcal{C}\{d_{22}, \frac{4}{3}d_{22}\},\ C^I_{q_2^L} = \mathcal{C}\{d_{34}, \frac{4}{3}d_{34}\} = \mathcal{C}\{4d_{22}, \frac{16}{3}d_{22}\},\ C^I_{q_2^R} = \mathcal{C}\{3d_{22}, \frac{10}{3}d_{22}\}, \quad (5.44)$$

as shown in Fig. 28. Then we have $(n^L, n_0^L) = (4, 5)$ and $(n^R, n_0^R) = (4, 5)$. These quantizers are carefully chosen such that rate savings can be achieved for both the left and right sequences.

Generic correlation models between the sources and the side informations are generated based on the joint statistics collected from all 20 frames of "tunnel" sequence. The rate saving is 8,470 bits for the right sequence and 9,468 bits for the left sequence. The total saving is equivalent to 26.9 kbps, or 0.41% of the total bit rate. Again, the WZ coding block length for the I-frame coefficients is fixed at 12,096. Experiments are also run on the Y-component of "aqua" sequences. The total saving is equivalent to 27.8 kbps, or 0.39% of the total bit rate. Performance comparisons between separate encoding, MT video coding, and joint encoding for both "tunnel" and "aqua" are also included in Fig. 26.

Remarks:

- We see from Fig. 26 that source splitting on top of SWCQ does lead to flexible

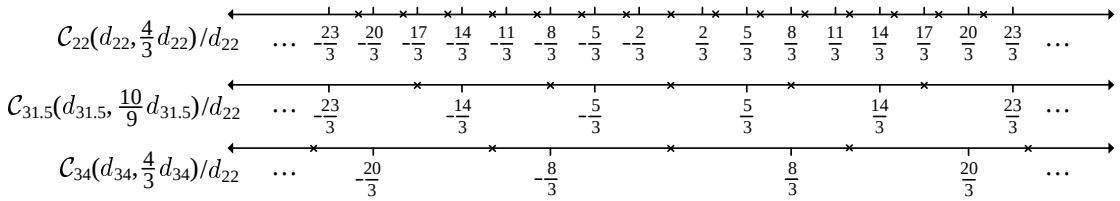

Fig. 28. Quantizers used in our second proposed MT video coder based on source splitting of the I-frames.

rate allocation between the two encoders, while achieving savings in the sum rate. However, with source splitting, we obtain less sum rate savings than without source splitting in our first proposed scheme. This is mainly due to the fact that one more WZ coding step (with attendant performance loss in practice) is needed with source splitting. Additionally, splitting the left I-frame also introduces rate loss since a coarser intra-predicted version $\widehat{L}^{D(q_2^L)}$ is used instead of $\widehat{L}^{D(q_1)}$.

- In order to outperform separate H.264/AVC Intra coding, choices of the quantizers $C^I_{q_1}$, $C^I_{q_2^L}$ and $C^I_{q_2^R}$ are crucial. Note that $C^I_{q_1}$ determines the final reconstruction quality of the left and right I-frames, while $C^I_{q_2^L}$ and $C^I_{q_2^R}$ control the amount of rate savings. Clearly, $C^I_{q_2^L}$ and $C^I_{q_2^R}$ cannot be too coarse since otherwise the quality of the coarse disparity map $\widetilde{\mathcal{D}}_1$ will be very poor. Moreover, from our experiments, we find that to achieve positive rate savings for both the left and right I-frames, it is necessary for $C^I_{q_2^R}$ to be a much finer quantizer than $C^I_{q_2^L}$. This can be explained as follows. The first reconstructed version of the right I-frame $\widehat{R}_1^{D(q_2^R)}$ is used to generate decoder side information for WZ coding of the refinement cell indices $L_1^{F(q_1,q_2^L)}$ of the left I-frame; if $C^I_{q_2^R}$ is too coarse, the obtained decoder side information will contain little information about $L_1^{F(q_1,q_2^L)}$, which makes the first WZ coding step ineffective (in terms of beating H.264/AVC Intra coding). In fact, we may consider the extreme case when the left and right I-frames are exactly the same, i.e., $L_1 = R_1$, then $\widehat{R}_1^{D(q_2^R)} = \widehat{L}_1^{D(q_2^R)}$ will tell almost no more information about $L_1^{F(q_1,q_2^L)}$ than $\widehat{L}_1^{D(q_2^L)}$ if

$C^I_{q_2^R}$ is coarser than $C^I_{q_2^L}$. For the same reason, $C^I_{q_2^R}$ cannot be too fine compared to $C^I_{q_1}$ since otherwise it will be difficult to save bits in the second WZ coding step. Thus we constrain the choices of quantizers to

$$C^I_{q_1} \ni C^I_{q_2^R} \ni C^I_{q_2^L} \ni \mathcal{C}(\infty, \infty), \tag{5.45}$$

where "$\ni$" means "finer than".

- In the original version of source splitting proposed by Rimoldi and Urbanke [46] for SW coding, where the source correlation is assumed to be known *a priori* at both the encoders and the decoder, only **one** classic source coding step and two WZ coding steps are involved. However, in our implementation of MT video coding using source splitting, it is not possible to obtain the exact correlation between the left and right sequences before compression. Hence it is necessary for the two encoders to first send "snapshots" of the two I-frames to the decoder to generate a rough estimate of the source correlation (in terms of disparity map) before WZ coding can be applied. This is why we have **two** classic source coding steps and two WZ coding steps.
- We also experiment with source splitting on the P-frames, but no sum rate gain is obtained. To explain, we note that it is easy for H.264/AVC to explore the remaining correlation among the 16 quantized DCT coefficients in the same 4×4 macroblock (by directly encoding the number of non-zero coefficients, number of trailing ones, etc.). For MT video coding, this is not trivial as it involves SW coding of non-i.i.d. sources. Consequently, our MT video coder ignores this in-source correlation and compresses the coefficients one position at a time. Fortunately, most of the sum rate savings in our first proposed MT video coding scheme (without source splitting) comes from the I-frames, and doing source splitting only on the I-frames already offers considerable flexibility in rate allocation (while outperforming separate H.264/AVC encoding).

CHAPTER VI

CONCLUSIONS

This dissertation focused on MT source coding problem, and consists of three parts: sum-rate loss, code designs, and applications to video sensor networks.

In the first part of this dissertation, we focused on the symmetric case of quadratic Gaussian MT source coding, where all sources are positively symmetric and all target distortions are equal. We gave the exact forms of the minimum sum-rate for both joint encoding and separate encoding problems, and thus the sum-rate loss between them. The supremum of the sum-rate loss for this special case is provided in exact form, and is shown to be increasing with the number of sources L in the order of $\frac{\sqrt{L}}{2}\log_2 e$ b/s. It is then conjectured that this supremum sum-rate loss is the supremum sum-rate loss over all jointly Gaussian source correlations and target distortions, for any given number of sources L.

In the second part of this dissertation, by extending our previous results on practical SW coding [29, 30, 49] and WZ coding [65], we have developed a general SWCQ framework for MT source coding and detailed practical code designs. Assuming ideal source coding (with independent dithering) and ideal SW coding, we have shown that our asymmetric design can achieve any point on the sum-rate bound of the rate regions for both the quadratic Gaussian direct and indirect MT source coding problems, while the symmetric design can approach most of the points. We have also provided an improved SWCQ design that can approach more points and has better performance. Our practical results are very close to the theoretical limits. Compared to asymmetric SWCQ that involves source splitting, symmetric SWCQ is conceptually simpler, because it only has one quantization step and one SW coding step, and more elegant, because all compression is done in one step that includes both classic entropy coding and syndrome-based channel coding for compression. However, our practical results using LDPC codes for the asymmetric scheme (with a 0.139

b/s gap to the sum-rate bound) performs slightly better than the symmetric scheme (with a 0.157 b/s gap to the sum-rate bound), because the asymmetric scheme benefits from the longer block length (10^6 bits) than the symmetric scheme (10^5 bits). Moreover, there are other extra losses in the symmetric SWCQ design, one of which comes from the assumption that (4.35) holds; another loss stems from the inefficiency of the symmetric SW code designs of [49] for (conditionally) non-uniform sources. Finally, we point out that TCQ and SWC coding in our proposed SWCQ framework are designed separately. This is proofably optimal at high rate (see Section IV). At low rate, a separate design is not optimal, and improved performance than those reported in Sectin 3 can be obtained by exploiting the *non-Gaussian* statistics of TCQ indices and employing non-linear estimation at the joint decoder (as done in [65] for Wyner-Ziv coding).

In the third part of this dissertation, building upon our experience with practical designs for quadratic Gaussian MT source coding, we have addressed MT video coding that targets at saving the sum rate over separate H.264/AVC coding. The main idea is to mimic H.264/AVC coding with a twist that instead of entropy coding, we explore the binocular redundancy by using disparity maps generated by stereo matching to form decoder side information for WZ coding. We proposed two MT video coders: the first (without source splitting) targets at the corner points of the MT sum rate bound, and second (with source splitting) aims at approaching any point on the MT sum rate bound. Results on rate savings for motion vectors in the low-rate regime and for I-frame and P-frame residual coefficients in the high-rate regime are given. We have represented the first work on practical MT video coding. It essentially relies on "asymmetric" SW coding and WZ coding, where one source is assumed to be available at the decoder as side information – the trick of source splitting is pulled to realize flexible rate allocation. This makes it easier in practical MT video coding, as we only need to focus on encoding one source at a time. For *simultaneous* SW coding of two sources, although the elegant idea of partitioning a single channel code was proposed

in [42] and successfully explored in [49] for arbitrary rate allocation between the two encoders for quadratic Gaussian MT source coding (after TCQ), it remains a challenging task to implement simultaneous MT video coding in practice. The main issue again lies in correlation modeling when dealing with practical video coding. Finally, for MT video coding with more than two terminals, since the theory is incomplete even with jointly Gaussian sources, there has not been any serious study yet.

REFERENCES

[1] A. Aaron and B. Girod, "Compression of side information using turbo codes, in *Proc. DCC-2002*, Snowbird, UT, March 2002, pp. 252–261.

[2] J. Bajcsy and P. Mitran, "Coding for the Slepian-Wolf problem with turbo codes," in *Proc. Globecom-2001*, San Antonio, TX, Nov. 2001, pp. 1400–1404.

[3] T. Bell, J. Cleary and I. Witten, *Text Compression*, Englewood Cliffs, NJ, Prentice Hall, 1990.

[4] T. Berger, "Multiterminal source coding", *The Inform. Theory Approach to Communications,* G. Longo, Ed., New York: Springer-Verlag, 1977.

[5] C. Berrou and A. Glavieux, "Near optimum error correcting coding and decoding: turbo-codes," *IEEE Trans. Communications*, vol. 44, pp. 1261-1271, Oct. 1996.

[6] S. Birchfield and C. Tomasi, "A pixel dissimilarity measure that is insensitive to image sampling," *IEEE Trans. PAMI*, vol. 20, no. 4, pp. 401–406, Apr. 1998.

[7] Y. Boykov, O. Veksler, and R. Zabih, "Fast approximate energy minimization via graph cuts," *IEEE Trans. PAMI*, vol. 23, pp. 1222-1239, Nov. 2001.

[8] J. Chen, X. Zhang, T. Berger, and S.B. Wicker, "The sum-rate distortion function and optimal rate allocation for the quadratic Gaussian CEO problem," *IEEE JSAC*, vol. 22, pp. 977-987, Aug. 2004.

[9] S. Cheng and Z. Xiong, "Successive refinement for the Wyner-Ziv problem and layered code design," *IEEE Trans. Signal Processing*, vol. 53, pp. 3269-3281, Aug. 2005.

[10] D. Comanicu and P. Meer, "Mean shift: A robust approach toward feature space analysis," *IEEE Trans. PAMI*, vol. 24, pp. 603–619, May 2002.

[11] J. Conway and J. Sloane, *Sphere Packings. Lattices and Groups*, New York, Springer, 1998.

[12] T. Cover and J. Thomas, *Element of Information Theory*, New York: Wiley, 1991.

[13] Z. Drezner and G. O. Wesolowsky, "On the computation of the bivariate normal integral", *Journal of statist. comput. simul. 35*, pp. 101-107, 1990.

[14] F. Dufaux, M. Ouaret, and T. Ebrahimi, "Recent advances in multiview distributed video coding," in *Proc. Mobile Multimedia/Image Processing for Military and Security Applications*, Orlando, FL, May 2007.

[15] P. F. Felzenszwalb and D. P. Huttenlocher, "Efficient belief propagation for early vision", *International Journal of Computer Vision*, Oct. 2006.

[16] M. Flierl and B. Girod, "Coding of multi-view image sequences with video sensors," in *Proc. ICIP'06*, Atlanta, GA, Oct. 2006.

[17] T. Flynn and R. Gray, "Encoding of correlated observations," *IEEE Trans. Inform. Theory,* vol. 33, pp. 773–787, Nov. 1987.

[18] K. Fukunaga, *Introduction to Statistical Pattern Recognition*, Academic Press, San Diego, 2nd Ed., 1990.

[19] R. Gallager, *Low Density Parity Check Codes*, Monograph, MIT Press, 1963.

[20] J. García-Frías and Y. Zhao, "Compression of correlated binary sources using turbo codes," *IEEE Commun. Lett.*, vol. 5, pp. 417–419, Oct. 2001.

[21] D. Geiger, B. Ladendorf, and A. Yuille, "Occlusions and binocular stereo," *Intl. J. Computer Vision*, vol. 14, pp. 211–226, 1995.

[22] X. Guo, Y. Lu, F. Wu, W. Gao and S. Li, "Distributed multiview video coding," in *Proc. SPIE*, vol. 6077, San Jose, CA, USA, Jan. 2006.

[23] T. S. Han and K. Kobayashi, "A unified achievable rate region for a general class of multiterminal source coding systems," *IEEE Trans. Inform. Theory*, vol. 26, pp. 277–288, May 1980.

[24] J. Jensen, "Bounds on the free distance of systematic convolutional codes", *IEEE Trans. Inform. Theory,* vol. 34, pp. 586–589, May 1988.

[25] H. Jin, A. Khandekar, and R. McEliece, "Irregular repeat-accumulate codes," in *Proc. 2nd Intl. Symp. Turbo Codes and Related Topics*, Brest, France, Sept. 2000, pp. 1–8.

[26] JVT reference software JM73, available at http://iphome.hhi.de/suehring/tml/download/old_jm/jm73.zip.

[27] V. Kolmogorov and R. Zabih,, "Multi-camera scene reconstruction via graph cuts," in *Proc. European Conf. Computer Vision*, Copenhagen, Denmark, May 2002, pp. 82–96.

[28] Z. Liu, S. Cheng, A. Liveris, and Z. Xiong, "Slepian-Wolf coded nested lattice quantization for Wyner-Ziv coding: high-rate performance analysis and code design", *IEEE Trans. Inform. Theory,* vol. 52, pp. 4358–4379, Oct. 2006.

[29] A. Liveris, Z. Xiong and C. Georghiades, "Compression of binary sources with side information at the decoder using LDPC codes," *IEEE Commun. Lett.*, vol. 6, pp. 440–442, Oct. 2002.

[30] A. Liveris, Z. Xiong and C. Georghiades, "Distributed compression of binary sources using parallel and serial concatenated convolutional codes," in *Proc. DCC-2003*,

Snowbird, UT, March 2003, pp. 193–202,.

[31] D. MacKay, "Good error-correcting codes based on very sparse matrices," *IEEE Trans. Inform. Theory*, vol. 45, pp. 399-431, March 1999.

[32] M. Marcellin, "On entropy-constrained trellis coded quantization," *IEEE Trans. Communications*, vol. 42, pp. 14–16, Jan. 1994.

[33] M. Marcellin and T. Fischer, "Trellis coded quantization of memoryless and Gaussian-Markov sources," *IEEE Trans. Communications*, vol. 38, pp. 82-93, Jan. 1990.

[34] J. R. Ohm, "Stereo/multiview encoding using the MPEG family of standards," in *Proc. SPIE Conf. Stereoscopic Displays and Virtual Reality Systems VI*, San Jose, CA, Jan. 1999, vol. 3639, pp. 242-253.

[35] Y. Oohama, "Gaussian multiterminal source coding," *IEEE Trans. Inform. Theory*, vol. 43, pp. 1912-1923, Nov. 1997.

[36] Y. Oohama, "The rate-distortion function for the quadratic Gaussian CEO problem," *IEEE Trans. Inform. Theory*, vol. 44, pp. 1057–1070, May 1998.

[37] Y. Oohama, "Multiterminal source coding for correlated memoryless Gaussian sources with several side information at the decoder," in *Proc. ITW-1999*, Kruger National Park, South Africa, June 1999.

[38] Y. Oohama, "Rate-distortion theory for Gaussian multiterminal source coding systems with several side informations at the decoder," *IEEE Trans. Inform. Theory*, vol. 38, pp. 2577-2593, July 2005.

[39] M. Ouaret, F. Dufaux and T. Ebrahimi, "Fusion-based multiview video coding," in *Proc. ACM International Workshop on Video Surveillance and Sensor Networks*, Santa Barbara, CA, Oct. 2006.

[40] V. Prabhakaran, D. Tse, and K. Ramchandran, "Rate region of the quadratic Gaussian CEO problem," in *Proc. ISIT-2004*, Chicago, IL, June 2004.

[41] S. Pradhan and K. Ramchandran, "Distributed source coding using syndromes (DISCUS): design and construction," *IEEE Trans. Inform. Theory*, vol. 49, pp. 626–643, March 2003.

[42] S. Pradhan and K. Ramchandran, "Generalized coset codes for distributed binning," *IEEE Trans. Inform. Theory*, vol. 51, pp. 3457–3474, Oct. 2005.

[43] R. Puri, A. Majumbar, P. Ishwar, and K. Ramchandran, "Distributed video coding in wireless sensor networks," *IEEE Signal Processing Magazine*, vol. 23, pp. 94-106, July 2006.

[44] J. Reichel, H. Schwarz, and M. Wien, "Joint scalable video model JSVM 4.2," ITU-T and ISO/IEC Joint Video Team, Document JVT-X208, June 2007, http://ftp3.itu.ch/av-arch/jvt-site/2007_06_Geneva/JVT-X208.zip.

[45] T. Richardson, M. Shokrollahi, and R. Urbanke, "Design of capacity-approaching irregular low-density parity-check codes", *IEEE Trans. Inform. Theory,* vol. 47, pp. 619-637, Feb. 2001.

[46] B. Rimoldi and R. Urbanke, "Asynchronous Slepian-Wolf coding via source-splitting", in *Proc. ISIT-1997*, Ulm, Germany, June 1997, pp. 271.

[47] D. Slepian and J. Wolf, "Noiseless coding of correlated information sources," *IEEE Trans. Inform. Theory*, vol. 19, pp. 471-480, July 1973.

[48] B. Song, O. Bursalioglu, A. K. Roy-Chowdhury, and E. Tuncel, "Towards a multi-terminal video compression algorithm using epipolar geometry", in *Proc. ICASSP'06*, Toulouse, France, May 2006.

[49] V. Stanković, A. Liveris, Z. Xiong, and C. Georghiades, "On code design for the general Slepian-Wolf problem and for lossless multiterminal communication networks," *IEEE Trans. Inform. Theory*, vol. 52, pp. 1495–1507, Apr. 2006.

[50] J. Sun, H. Shum, and N. Zheng, "Stereo matching using belief propagation", *IEEE Trans. PAMI*, vol.25, no. 7, pp. 787–800, 2003.

[51] M. Tagliasacchi, G. Prandi, and S. Tubaro, "Symmetric distributed coding of stereo video sequences," in *Proc. ICIP'07*, San Antonio, TX, Sept. 2007.

[52] D. Taubman and M. Marcellin, *JPEG2000: Image Compression Fundamentals, Standards and Practice*, Boston, Kluwer, 2001.

[53] S. Tavildar, P. Viswanath, and A. B. Wagner, "The Gaussian many-help-one distributed source coding problem," in *Proc. ITW-2006*, Oct., 2006, pp. 596-600.

[54] T. Tian, J. García-Frías, and W. Zhong, "Compression of correlated sources using LDPC codes", in *Proc. DCC-2003*, Snowbird, UT, March 2003.

[55] S. Tung, *Multiterminal Rate-distortion Theory,* Ph. D. Dissertation, School of Electrical Engineering, Cornell University, Ithaca, NY, 1978.

[56] G. Ungerboeck, "Channel coding with multilevel/phase signals," *IEEE Trans. Inform. Theory*, vol. 28, pp. 55-67, Jan. 1982.

[57] H. Viswanathan and T. Berger, "The quadratic Gaussian CEO problem," *IEEE Trans. Inform. Theory,* vol. 43, pp. 1549–1559, Sept. 1997.

[58] A. Wagner, S. Tavildar, and P. Viswanath, "Rate region of the quadratic Gaussian two-encoder source-coding problem," *IEEE Trans. Inform. Theory,* vol. 54, pp. 1938-1961, May 2008.

[59] T. Wiegand, G. Sullivan, G. Bjintegaard, and A. Luthra, "Overview of the H.264/AVC video coding standard," *IEEE Trans. Circuits and Systems for Video Tech.*, vol. 13, pp. 560-576, July 2003.

[60] J. K. Wolf, "Data reduction for multiple correlated sources," in *Proc. 5th Colloquium Microwave Communication*, Jun. 1973, pp. 287–295.

[61] A. Wyner, "Recent results in the Shannon theory," *IEEE Trans. Inform. Theory*, vol. 20, pp. 2-10, Jan. 1974.

[62] A. Wyner and J. Ziv, "The rate-distortion function for source coding with side information at the decoder," *IEEE Trans. Inform. Theory*, vol. 22, pp. 1-10, Jan. 1976.

[63] Z. Xiong, V. Stanković, S. Cheng, A. Liveris, and Y. Sun, "Source-channel coding for algebraic multiterminal binning," in *Proc. ITW-2004*, San Antonio, TX, Oct. 2004.

[64] H. Yamamoto and K. Itoh, "Source coding theory for multiterminal communication systems with a remote source," *Trans. IECE of Japan*, vol. E63, pp. 700–706, Oct. 1980.

[65] Y. Yang, S. Cheng, Z. Xiong, and W. Zhao, "Wyner-Ziv coding based on TCQ and LDPC codes," *IEEE Trans. Communications*, to appear.

[66] Y. Yang, V. Stanković, Z. Xiong, and W. Zhao, "Asymmetric code design for remote multiterminal source coding," in *Proc. DCC-2004*, Snowbird, UT, March 2004.

[67] Y. Yang, V. Stanković, Z. Xiong, and W. Zhao, "On multiterminal source code design," in *Proc. DCC-2005*, Snowbird, UT, March 2005.

[68] Y. Yang, V. Stanković, Z. Xiong, and W. Zhao, "Multiterminal source code design based on Slepian-Wolf coded quantization," in *Proc. 42nd Annual Allerton Conference on Communications, Control and Computing,* Monticello, IL, Oct. 2004.

[69] Y. Yang, V. Stanković, Z. Xiong, and W. Zhao, "On multiterminal source code design," *IEEE Trans. Inform. Theory*, vol. 54, pp. 2278-2302, May 2008.

[70] Y. Yang and Z. Xiong, "The supremum sum rate loss of quadratic Gaussian direct multiterminal source coding," in *Proc. UCSD Workshop on Information Theory and its Applications*, San Diego, CA, January 2008.

[71] C. Yeo and K. Ramchandran, "Distributed video compression for wireless camera networks," in *Proc. VCIP'07*, San Jose, California, Feb. 2007.

[72] R. Zamir, "The rate loss in the Wyner-Ziv problem," *IEEE Trans. Inform. Theory*, vol. 42, pp. 2073-2084, Nov. 1996.

[73] R. Zamir and T. Berger, "Multiterminal source coding with high resolution," *IEEE Trans. Inform. Theory,* vol. 45, pp. 106–117, Jan. 1999.

[74] R. Zamir and M. Feder, "Information rates of pre/post-filtered dithered quantizers", *IEEE Trans. Inform. Theory,* vol. 42, pp. 1340–1353, Sept. 1996.

[75] R. Zamir and M. Feder, "On universal quantization by randomized uniform/lattice quantizer," *IEEE Trans. Inform. Theory*, vol. 51, pp. 428–436, March 1992.

[76] R. Zamir, S. Shamai, and U. Erez, "Nested linear/lattice codes for structured multiterminal binning", *IEEE Trans. Inform. Theory,* vol. 48, pp. 1250–1276, June 2002.

APPENDIX A

PROOF OF LEMMA 6

Proof 5 *First, differentiating $\theta^{\nleftrightarrow}$ with respect to D, we have*

$$\frac{\partial \theta^{\nleftrightarrow}}{\partial D} = \frac{\partial \theta^{\nleftrightarrow}}{\partial t^{\nleftrightarrow}} \cdot \frac{\partial t^{\nleftrightarrow}}{\partial D} = \left(1 + \frac{t^{\nleftrightarrow}}{\sqrt{(t^{\nleftrightarrow})^2 + \frac{1}{L-1}}}\right) \cdot \left(\frac{(1-\rho)(1+(L-1)\rho)}{2(L-1)D^2\rho}\right) > 0, \quad \text{(A.1)}$$

hence $\theta^{\nleftrightarrow} \nearrow D\,|_{(0,1)}$ for fixed L and ρ. Then it is easy to verify that $\lim_{D\to 0} \theta^{\nleftrightarrow} = 0$ and $\lim_{D\to 1} \theta^{\nleftrightarrow} = \rho$, thus $\theta^{\nleftrightarrow} \in (0, \rho)$, and $\delta_L(\theta^{\nleftrightarrow}) \searrow D\,|_{(0,1)}$. Now consider the case when $D \le 1-\rho$, we have $R^{\Delta}_{L,\rho}(D) = -\frac{1}{2}\log_2 \delta_L(\theta^{\nleftrightarrow}) \nearrow D\,|_{(0,1)}$. Hence

$$\begin{aligned}
\sup_{\rho\in(0,1), D\in(0,1)} R^{\Delta}_{L,\rho}(D) &= \max\left\{ \sup_{\rho\in(0,1), D\in(1-\rho,1)} R^{\Delta}_{L,\rho}(D), \sup_{\rho\in(0,1), D\in(0,1-\rho]} R^{\Delta}_{L,\rho}(D) \right\} && \text{(A.2)}\\
&= \max\left\{ \sup_{\rho\in(0,1), D\in(1-\rho,1)} R^{\Delta}_{L,\rho}(D), \sup_{\rho\in(0,1)} R^{\Delta}_{L,\rho}(1-\rho) \right\} && \text{(A.3)}\\
&= \sup_{\rho\in(0,1), D\in(1-\rho,1)} R^{\Delta}_{L,\rho}(D) && \text{(A.4)}\\
&= \sup_{\rho\in(0,1), D\in[1-\rho,1)} \frac{1}{2}\log_2 \frac{\delta_L(\theta^{\nleftrightarrow})}{\delta_L(\theta^{\nleftrightarrow})}. && \text{(A.5)}
\end{aligned}$$

Denote $\mathscr{L}_L(\rho, D) = \frac{\delta_L(\theta^{\nleftrightarrow})}{\delta_L(\theta^{\nleftrightarrow})}$, we have

$$\begin{aligned}
&\frac{\partial \mathscr{L}_L(\rho, D)}{\partial D} && \text{(A.6)}\\
=\ &\frac{\partial\left[\frac{\delta_L(\theta^{\nleftrightarrow})}{\delta_L(\theta^{\nleftrightarrow})}\right]}{\partial D} && \text{(A.7)}\\
=\ &\frac{-L(L-1)(1-\theta^{\nleftrightarrow})^{L-2}(1-\theta^{\nleftrightarrow})^{L-2}}{\delta_L^2(\theta^{\nleftrightarrow})} && \text{(A.8)}\\
&\cdot\left[\theta^{\nleftrightarrow}(1-\theta^{\nleftrightarrow})(1+(L-1)\theta^{\nleftrightarrow})\frac{\partial \theta^{\nleftrightarrow}}{\partial D} - \theta^{\nleftrightarrow}(1-\theta^{\nleftrightarrow})(1+(L-1)\theta^{\nleftrightarrow})\frac{\partial \theta^{\nleftrightarrow}}{\partial D}\right]. && \text{(A.9)}
\end{aligned}$$

Setting $\frac{\partial \mathscr{L}_L(\rho,D)}{\partial D}$ *to zero, we have a unique solution in* $[1-\rho,1)$*, namely,*

$$D^\star_\rho \;=\; \begin{cases} \dfrac{(1+\rho)^2(1-\rho)}{1+2\rho} & L=2 \\ \dfrac{[(2(L-1)(L-2)\rho^2+2(2L-3)\rho+1)-\sqrt{1+4\rho+4\rho^2(L-1)}]}{2\rho(L-2)(2+(L-2)\rho)}(1-\rho) & L>2. \end{cases} \tag{A.10}$$

Then we compute

$$\theta^{\Rsh}\,|_{D=D^\star_\rho} \;=\; \frac{-1+\sqrt{1+4\rho+4\rho^2(L-1)}}{2\big(1+(L-1)\rho\big)} \triangleq \theta^{\Rsh}_{max}(\rho) \tag{A.11}$$

$$\theta^{\Rsh}\,|_{D=D^\star_\rho} \;=\; \frac{2\rho\big(1+(L-1)\rho\big)+1-\sqrt{1+4\rho+4\rho^2(L-1)}}{\rho(L-1)\big(2+(L-1)\rho\big)+1} \triangleq \theta^{\Rsh}_{max}(\rho) \tag{A.12}$$

Hence

$$\frac{\partial \mathscr{L}_L(\rho,D^\star_\rho)}{\partial \rho} \;=\; \begin{cases} \dfrac{-2}{\delta_2^2(\theta^{\Rsh}_{max}(\rho))}\Big[-\dfrac{\rho(1+2\rho)^2}{(1+\rho)^7}\Big] & L=2 \\ \dfrac{-L(L-1)(1-\theta^{\Rsh}_{max}(\rho))^{L-2}(1-\theta^{\Rsh}_{max}(\rho))^{L-2}}{\delta_L^2(\theta^{\Rsh}_{max}(\rho))}\cdot & \\ \qquad\Big[\mathscr{A}+\mathscr{B}\sqrt{1+4\rho+4\rho^2(L-1)}\Big] & L>2, \end{cases}$$

where $\mathscr{A}$ *and* $\mathscr{B}$ *are rational functions of* L *and* ρ*. We observe that for* $L=2$*,* $\frac{\partial \mathscr{L}_L(\rho,D^\star_\rho)}{\partial \rho}>0$ *for any* $\rho\in(0,1)$*. Moreover, it is not hard to verify that* $\mathscr{A}$ *and* $\mathscr{B}$ *satisfy the following conditions,*

$$\mathscr{B}<0, \quad \mathscr{A}^2-\mathscr{B}^2\times\big(1+4\rho+4\rho^2(L-1)\big)=-\frac{\rho(L-2)^2(2+(L-2)\rho)^2}{(1+(L-1)\rho)^7}<0, \tag{A.13}$$

which implies that $\frac{\partial \mathscr{L}_L(\rho, D^\star_\rho)}{\partial \rho} > 0$ *for any* $L > 2$ *and* $\rho \in (0,1)$*, hence*

$$\sup_{\rho\in(0,1), D\in(0,1)} R^{\Delta}_{L,\rho}(D) \tag{A.14}$$

$$= \sup_{\rho\in(0,1), D\in[1-\rho,1)} \frac{1}{2}\log_2 \frac{\delta_L(\theta^{\uparrow\downarrow})}{\delta_L(\theta^{\downarrow\uparrow})} \tag{A.15}$$

$$= \lim_{\rho\to 1} \frac{1}{2}\log_2 \mathscr{L}_L(\rho, D^\star_\rho) \tag{A.16}$$

$$= \lim_{\rho\to 1} \frac{1}{2}\log_2 \frac{\delta_L\big(\theta^{\uparrow\downarrow}_{max}(\rho)\big)}{\delta_L\big(\theta^{\downarrow\uparrow}_{max}(\rho)\big)} \tag{A.17}$$

$$= \frac{1}{2}\log_2 \frac{\delta_L\big(\lim_{\rho\to 1}\theta^{\uparrow\downarrow}_{max}(\rho)\big)}{\delta_L\big(\lim_{\rho\to 1}\theta^{\downarrow\uparrow}_{max}(\rho)\big)} \tag{A.18}$$

$$= \frac{1}{2}\log_2 \frac{\delta_L\big(\frac{2L+1-\sqrt{1+4L}}{2L^2}\big)}{\delta_L\big(\frac{-1+\sqrt{1+4L}}{2L}\big)} \tag{A.19}$$

$$= \frac{L-1}{2}\log_2 \frac{1-\frac{2L+1-\sqrt{1+4L}}{2L^2}}{1-\frac{-1+\sqrt{1+4L}}{2L}} + \frac{1}{2}\log_2 \frac{1+(L-1)\frac{2L+1-\sqrt{1+4L}}{2L^2}}{1+(L-1)\frac{-1+\sqrt{1+4L}}{2L}} \tag{A.20}$$

$$\overset{L\to\infty}{\rightsquigarrow} \frac{1}{2}\log_2\Big(1-\frac{1}{L}\Big)^{L-1} - \frac{L-1}{2\sqrt{L}}\log_2\Big(1-\frac{1}{\sqrt{L}}\Big)^{\sqrt{L}} - \frac{1}{2}\log_2\frac{1}{\sqrt{4L}} \tag{A.21}$$

$$\overset{L\to\infty}{\rightsquigarrow} \frac{\log_2 e}{2}(\sqrt{L}-1) + \frac{1}{2} - \frac{1}{4}\log_2 L. \tag{A.22}$$

APPENDIX B

PROOF OF THEOREM 2

Before proving Theorem 2, we first state the following lemma.

Lemma 9 *Define three jointly Gaussian random variables* (Z_1, Z_{21}, Z_{22}) *as*

$$Z_1 = Y_1 + Q_1, \quad Z_{21} = Y_2 + Q_{21}, \quad Z_{22} = Y_2 + Q_{22}, \tag{B.1}$$

where Q_1, Q_{21}, Q_{22} *are zero-mean independent Gaussian random variables that are also independent of* Y_1 *and* Y_2*. For any* $\epsilon > 0$*, there exists sufficiently large* n*, asymmetric SWCQ encoders* $\mathcal{E}_1$*,* $\mathcal{E}_2$*, and an asymmetric SWCQ decoder* $\mathcal{D}$*, such that the transmission rates* R_1 *and* R_2 *satisfy*

$$\begin{aligned} R_1 &< I(Y_1; Z_1) - I(Z_1; Z_{21}) + \epsilon, & \text{(B.2)} \\ R_2 &< I(Y_2; Z_{21}) + I(Y_2; Z_{22}) - I(Z_{22}; Z_1 Z_{21}) + \epsilon, & \text{(B.3)} \end{aligned}$$

with average distortions

$$\begin{aligned} E\Big\{\frac{1}{n}\sum_{i=1}^{n}(Y_{1,i} - \hat{Y}_{1,i})^2\Big\} &< E\left\{(Y_1 - E\{Y_1|Z_1, Z_{21}, Z_{22}\})^2\right\} + \epsilon, & \text{(B.4)} \\ E\Big\{\frac{1}{n}\sum_{i=1}^{n}(Y_{2,i} - \hat{Y}_{2,i})^2\Big\} &< E\left\{(Y_2 - E\{Y_2|Z_1, Z_{21}, Z_{22}\})^2\right\} + \epsilon. & \text{(B.5)} \end{aligned}$$

Proof 6 *This lemma is a direct consequence of results in [4, 35, 55, 58], hence the detailed proof is omitted here. However, we need to emphasize that the proof requires the linear coefficients* (α_c, β_c) *to be the minimum MSE coefficients in estimating* Y_2 *using* Z_1 *and* Z_{21}*, and* $(\alpha_1^A, \beta_1^A, \gamma_1^A)$ *(respectively,* $(\alpha_2^A, \beta_2^A, \gamma_2^A)$*) to be the minimum MSE coefficients of estimating* Y_1 *(respectively,* Y_2*) using* (Z_1, Z_{21}, Z_{22}).

Proof of Theorem 2: Without loss of generality, we assume that $\sigma_{y1}^2 = \sigma_{y2}^2 = \sigma_y^2$. Define $d_1^* = \frac{D_1^*}{\sigma_y^2}$ and $d_2^* = \frac{D_2^*}{\sigma_y^2}$. Then $\beta_{max} = 1 + \sqrt{1 + \frac{4\rho^2 d_1^* d_2^*}{(1-\rho^2)^2}}$. Let $(Z_1, Z_{21}, Z_{22}, Q_1, Q_{21}, Q_{22})$ be the same random variables as in Lemma 9, such that

$$\frac{E\{Q_1^2\}}{\sigma_y^2} = d_1 = \Big(\frac{\beta_{max}}{2d_1^*} - \frac{1}{(1-\rho^2)}\Big)^{-1}, \tag{B.6}$$

$$\frac{E\{Q_{21}^2\}}{\sigma_y^2} = d_{21} = \frac{\rho^2}{1 + d_1(1 - 2^{2R_1^*})} - 1, \tag{B.7}$$

$$\frac{E\{Q_{22}^2\}}{\sigma_y^2} = d_{22} = (\frac{1}{d_2} - \frac{1}{d_{21}})^{-1}, \text{ where } d_2 = \Big(\frac{\beta_{max}}{2d_2^*} - \frac{1}{(1-\rho^2)}\Big)^{-1}. \tag{B.8}$$

Then using (B.2) and (B.3) in Lemma 9, we have

$$R_1 < I(Y_1; Z_1) - I(Z_1; Z_{21}) + \epsilon = R_1^* + \epsilon, \tag{B.9}$$

$$R_2 < I(Y_2; Z_{21}) + I(Y_2; Z_{22}) - I(Z_{22}; Z_1 Z_{21}) + \epsilon = R_2^* + \epsilon. \tag{B.10}$$

The minimum MSE coefficients (α_c, β_c), $(\alpha_1^A, \beta_1^A, \gamma_1^A)$ and $(\alpha_2^A, \beta_2^A, \gamma_2^A)$ are

$$\begin{array}{lll} \alpha_c = \dfrac{\rho d_{21}}{\Omega}, & \beta_c = \dfrac{(1-\rho^2) + d_1}{\Omega}; & \\ \alpha_1^A = \dfrac{(1-\rho^2) + d_2}{\Omega^*}, & \beta_1^A = \dfrac{\rho d_1}{\Omega^*} \cdot \dfrac{d_2}{d_{21}}, & \gamma_1^A = \dfrac{\rho d_1}{\Omega^*} \cdot \dfrac{d_2}{d_{22}}; \\ \alpha_2^A = \dfrac{\rho d_2}{\Omega^*}, & \beta_2^A = \dfrac{(1-\rho^2) + d_1}{\Omega^*} \cdot \dfrac{d_2}{d_{21}}, & \gamma_2^A = \dfrac{(1-\rho^2) + d_1}{\Omega^*} \cdot \dfrac{d_2}{d_{22}}. \end{array} \tag{B.11}$$

where $\Omega = (1 + d_1)(1 + d_{21}) - \rho^2$ and $\Omega^* = (1 + d_1)(1 + d_2) - \rho^2$.

Then due to (B.4) and (B.5) in Lemma 9,

$$E\Big\{\frac{1}{n}\sum_{i=1}^{n}(Y_{1,i} - \hat{Y}_{1,i})^2\Big\} < E\left\{(Y_1 - \alpha_1^A Z_1 - \beta_1^A Z_{21} - \gamma_1^A Z_{22})^2\right\} + \epsilon = D_1^* + \epsilon \tag{B.12}$$

$$E\Big\{\frac{1}{n}\sum_{i=1}^{n}(Y_{2,i} - \hat{Y}_{2,i})^2\Big\} < E\left\{(Y_2 - \alpha_2^A Z_1 - \beta_2^A Z_{21} - \gamma_2^A Z_{22})^2\right\} + \epsilon = D_2^* + \epsilon. \tag{B.13}$$

Thus, we can approach any point on the sum-rate bound (2.9).

APPENDIX C

PROOF OF THEOREM 3

Proof 7 *The proof of Theorem 3 is similar to that of Theorem 2, hence we only provide the necessary parameters. Denote* $d^* = \frac{D^*}{\sigma_x^2}, n_1 = \frac{\sigma_{n_1}^2}{\sigma_x^2}, n_2 = \frac{\sigma_{n_2}^2}{\sigma_x^2}$*, and define* (Q_1, Q_{21}, Q_{22}) *as in Lemma 9 such that*

$$\frac{E\{Q_1^2\}}{\sigma_x^2} = d_1 = \frac{2}{(d^*)^{-1} - 1 + n_1^{-1} - n_2^{-1}} - n_1 \tag{C.1}$$

$$\frac{E\{Q_{21}^2\}}{\sigma_x^2} = d_{21} = \frac{1}{1 + n_1 + d_1(1 - 2^{2R_1^*})} - 1 - n_2 \tag{C.2}$$

$$\frac{E\{Q_{22}^2\}}{\sigma_x^2} = d_{22} = \left(\frac{1}{d_2} - \frac{1}{d_{21}}\right)^{-1}, \text{ where } d_2 = \frac{2}{(d^*)^{-1} - 1 + n_2^{-1} - n_1^{-1}} - n_2. \tag{C.3}$$

The minimum MSE coefficients are

$$\begin{aligned} &\alpha_c = \frac{d_{21}}{\Lambda}, \qquad \beta_c = \frac{(1+n_1)(1+n_2+d_1) - 1}{\Lambda}; \\ &\alpha_X^A = \frac{n_2 + d_2}{\Lambda^*}, \quad \beta_X^A = \frac{n_1 + d_1}{\Lambda^*} \cdot \frac{d_2}{d_{21}}, \qquad \gamma_X^A = \frac{n_1 + d_1}{\Lambda^*} \cdot \frac{d_2}{d_{22}}; \end{aligned} \tag{C.4}$$

where $\Lambda = (1 + n_1 + d_1)(1 + n_2 + d_{21}) - 1$ *and* $\Lambda^* = (1 + n_1 + d_1)(1 + n_2 + d_2) - 1$.

APPENDIX D

PROOF OF THEOREMS 4 AND 5

Proof 8 *By setting d_{21} in (B.7) to infinity, we can construct an asymmetric SWCQ coder $(\mathcal{E}_1^{\text{ı}}, \mathcal{E}_2^{\text{ı}}, \mathcal{D}^{\text{ı}})$ that achieves one corner point (denoted as $(R_1^{\text{ı}}, R_2^{\text{ı}})$) of the sum-rate bound for the direct MT problem. On the other hand, by setting d_{21} to d_2 in (B.8), we can construct another asymmetric SWCQ coder $(\mathcal{E}_1^{\text{ȷ}}, \mathcal{E}_2^{\text{ȷ}}, \mathcal{D}^{\text{ȷ}})$ that achieves the other corner point (denoted as $(R_1^{\text{ȷ}}, R_2^{\text{ȷ}})$). Hence any point on the sum-rate bound $\partial\hat{\mathcal{R}}_{12}^{BT}(D_1^*, D_2^*)$ can be achieved by using time sharing between $(\mathcal{E}_1^{\text{ı}}, \mathcal{E}_2^{\text{ı}}, \mathcal{D}^{\text{ı}})$ and $(\mathcal{E}_1^{\text{ȷ}}, \mathcal{E}_2^{\text{ȷ}}, \mathcal{D}^{\text{ȷ}})$. This proves Theorem 4.*

Similarly, by setting d_{21} in (C.2) to infinity or to d_2 in (C.3), the two corner points of the sum-rate bound $\partial\hat{\mathcal{R}}_{12}^{YI}(D^*)$ can be achieved. Hence any point on $\partial\hat{\mathcal{R}}_{12}^{YI}(D^*)$ can be achieved by time sharing, and Theorem 5 is proved.

APPENDIX E

PROOF OF LEMMA 7

Proof 9 *First, we need to invoke the regularity and symmetry conditions in designing a trellis* $\mathbb{T}$ *(i.e., the corresponding convolution code* $\mathcal{C}$*) [56]:*

1. *Four cosets* $(\mathcal{D}_0, \mathcal{D}_1, \mathcal{D}_2, \mathcal{D}_3)$ *should occur with equal frequency in the sense that*

$$\sum_{i=1}^{N_s} \sum_{m=0}^{1} \chi\big(\phi(i,m) = (*, c)\big) = N_s/2, \quad c = 0, 1, 2, 3, \tag{E.1}$$

   where the indicator function $\chi = 1$ *if the output part of the trellis mapping* ϕ *for state* i *and input* m *is* c*, and* $\chi = 0$*, otherwise.*

2. *Define* $\mathcal{B}_0 = \mathcal{D}_0 \cup \mathcal{D}_2$ *and* $\mathcal{B}_1 = \mathcal{D}_1 \cup \mathcal{D}_3$*. And denote the trellis output as* $c = \phi^o(i, m)$*, then for any* $1 \le i \le N_s$*,* $\mathcal{D}_{\phi^o(i,0)} \cup \mathcal{D}_{\phi^o(i,1)}$ *is either* $\mathcal{B}_0$ *or* $\mathcal{B}_1$*.*

3. *For any* $1 \le i \le N_s$*, let* j, k *be the two distinct states satisfying* $\phi^s(j, m_j) = i$ *and* $\phi^s(k, m_k) = i$*, where* $\phi^s(i, m)$ *denotes the next-state part of the trellis mapping, then* $\mathcal{D}_{\phi^o(j,m_j)} \cup \mathcal{D}_{\phi^o(k,m_k)}$ *is either* $\mathcal{B}_0$ *or* $\mathcal{B}_1$*.*

These conditions and the Σ*-uniformity of* X *ensure that each input vector* $\boldsymbol{m}$ *(thus coset index vector* $\mathbf{c}$*) appears with equal probability, i.e.,* $P(\boldsymbol{C} = \mathbb{T}(\boldsymbol{m})) = P(\boldsymbol{M} = \boldsymbol{m}) = 2^{-n}$ *for any* $\boldsymbol{m} \in \{0,1\}^n$ *(here the starting phase of TCQ is not considered). Hence* $P(\hat{X}_i \in \mathcal{D}_c) = \frac{1}{4}$ *for* $c = 0, 1, 2, 3$*.*

Now note that the quantization noise Q_i *must be in the range* $[-2, 2]$*. For a given pair of* (q_i, x_i)*, since* $q_i + x_i + v_i$ *must be a signal point* $j + 0.5$ *with* $j \in \mathbb{Z}$*, then* $x_i + v_i$ *can only take one value in the range* $[x - 0.5, x + 0.5)$*, i.e.,* $x_i + v_i = q_i + \lfloor x_i - q_i + 1 \rfloor - 0.5$*. Let*

$Y_i = X_i + V_i$, then $Q_i \to Y_i \to X_i$, hence

$$\begin{aligned} p_{Q_i|x_i}(q_i|x_i) &= \int_{y\in[x_i-0.5,x_i+0.5)} p_{Q_i|Y_i=y}(q_i|y)\cdot p_V(v_i)dy. \\ p_{Q_i|x_i}(q_i|x_i) &= \int_{y\in[x_i-0.5,x_i+0.5)} p_{Q_i|Y_i=y}(q_i|y)\cdot p_{Y|X_i=x_i}(y|x_i)dy \\ &= \int_{y\in[x_i-0.5,x_i+0.5)} p_{Q_i|Y_i=y}(q_i|y)dy \\ &= P(\hat{Y}_i \in \mathcal{D}_{\lfloor x_i-q_i+1\rfloor \bmod 4}|Y_i = q_i + \lfloor x_i - q_i + 1\rfloor - 0.5) \\ &= P(\hat{Y}_i \in \mathcal{D}_0|Y_i = q_i - 0.5), \end{aligned} \tag{E.2}$$

which is independent of x_i.

The last equation of (E.2) is due to the following proposition, which states a key property of a non-dithered trellis coded quantizer: statistical symmetry between cosets.

Proposition 1 *Assume $f_X(x)$ is Σ-uniform with respect to $\mathcal{D}$ (with step size 1). Consider a trellis coded quantizer $\mathcal{Q}_{\mathcal{D}}^{TCQ}$ with $\tilde{R} = 1$ and without dither. Let the quantized version of X^n be $\hat{X}^n = [\mathcal{Q}_{\mathcal{D}}^{TCQ}]^{-1}[\mathcal{Q}_{\mathcal{D}}^{TCQ}(X^n)]$, then for sufficiently large n,*

$$P(\hat{X}_i \in \mathcal{D}_c|X_i = x_i) = P(\hat{X}_i \in \mathcal{D}_{(c+j) \bmod 4}|X_i = x_i + j), \tag{E.3}$$

for $0 \le i \le n-1$, $0 \le c \le 3$, $j \in \mathbb{Z}$, $-2^R + 1.5 \le x_i, x_i + j \le 2^R - 1.5$.

Proof 10 *First, consider the following two input vectors*

$$\mathbf{x} = \{x_1, x_2, ..., x_n\}, \quad \mathbf{x}' = \{x_1 + 4i_1, x_2 + 4i_2, ..., x_n + 4i_n\}, \tag{E.4}$$

where $i_j \in \mathbb{Z}$, and $-2^R + 1.5 \le x_i, x_i + 4i_j \le 2^R - 1.5$, for $j = 1, 2, ..., n$. It is obvious that the Viterbi algorithm in TCQ produces the same coset index vector $\boldsymbol{C} = \mathbb{T}(\boldsymbol{M})$, and the codeword index vector of $\mathbf{x}'$ differs from that of $\mathbf{x}$ by $\boldsymbol{i} = \{i_1, i_2, ..., i_n\}$. Consider the set

$\mathcal{S}_j^i = \{\boldsymbol{c} = \mathbb{T}(\boldsymbol{m}) : \boldsymbol{m} \in \{0,1\}^n, c_i = j\}$ *for* $j = 0, 1, 2, 3$. *Since* X *is i.i.d., we have*

$$\begin{aligned} P_{\boldsymbol{C}}(\boldsymbol{c}|X_i = x_i) &= P_{\boldsymbol{C}}(\boldsymbol{c}|X_i = x_i + j) \text{ for any } \boldsymbol{c} = \mathbb{T}(\boldsymbol{m}) \\ \Rightarrow P(\boldsymbol{c} \in \mathcal{S}_c^i|X_i = x_i) &= P(\boldsymbol{c} \in \mathcal{S}_c^i|X_i = x_i + j) \\ \Rightarrow P(\hat{X}_i \in \mathcal{D}_c|X_i = x_i) &= P(\hat{X}_i \in \mathcal{D}_c|X_i = x_i + j), \end{aligned} \tag{E.5}$$

for $0 \le i \le n-1$, $0 \le c \le 3$, $j \in 4\mathbb{Z}$, $-2^R + 1.5 \le x_i, x_i + j \le 2^R - 1.5$. *Hence we can assume that* $x_i \in [0, 4]$ *without loss of generality. Then* Σ*-uniformity implies that* X *is i.i.d.*

Fix $c = 0$ *and* $j = 1$ *with* $i >> 1$. *We need to show that* $P(\hat{X}_i \in \mathcal{D}_0|X_i = x_i) = P(\hat{X}_i \in \mathcal{D}_1|X_i = (x_i + 1) \bmod 4)$ *for any* $x_i \in [0, 4]$. *Let* $\boldsymbol{c}^* = \{c_1^*, c_2^*, ..., c_n^*\} \in \mathcal{S}_1^i$, *then consider two input vectors* $\mathbf{x} = \{x_1, x_2, ..., x_i, ..., x_n\}$ *and* $\mathbf{x}' = \{x_1 + c_1^*, x_2 + c_2^*, ..., x_n + c_n^*\} \bmod 4$. *Suppose* $\mathbf{x}$ *corresponds to a coset index vector* $\boldsymbol{c}$, *then* $\mathbf{x}'$ *must correspond to coset index vector* $\boldsymbol{c} \oplus \boldsymbol{c}^*$ *(and vice versa), where* $\oplus$ *denotes item-wise binary addition (XOR). Since the mapping* $\boldsymbol{c} \to \boldsymbol{c} \oplus \boldsymbol{c}^*$ *from* $\mathcal{S}_{c_i}^i$ *to* $\mathcal{S}_{c_i \oplus c_i^*}^i$ *is one-to-one, it follows that*

$$\begin{aligned} P(\hat{X}_i \in \mathcal{D}_0|X_i = x_i) &= \sum_{\boldsymbol{c} \in \mathcal{S}_0^i} P_{\boldsymbol{C}}(\boldsymbol{c}|X_i = x_i) \\ &= \sum_{\boldsymbol{c} \in \mathcal{S}_{0\oplus 1}^i} P_{\boldsymbol{C}}(\boldsymbol{c}|X_i = (x_i + 1) \bmod 4) \\ &= P(\hat{X}_i \in \mathcal{D}_1|X_i = (x_i + 1) \bmod 4). \end{aligned} \tag{E.6}$$

This result can be easily generalized to $c = 0, 1, 2, 3$ *and* $j = 1, 2, 3$. *Thus the proposition is proved.*

APPENDIX F

PROOF OF THEOREM 6

Proof 11 *Assume that Quantizer II in Fig. 8 is the dithered trellis coded quantizer $\mathcal{Q}_{21}$ which uses an ESS of size 2^{R+1}, with $\tilde{R} = 1$ and step size Δ_{21}. Thus, the ESS $\mathcal{D} = \{-2^R + \Delta_{21}/2, -2^R + 3\Delta_{21}/2, ..., 2^R - \Delta_{21}/2\}$ is partitioned into 4 cosets, each with 2^{R-1} points. Then due to Proposition 1, $P(\hat{Y}_{2,i} \in \mathcal{D}_c | Y_{2,i} = y_{2,i}) = P(\hat{Y}_{2,i} \in \mathcal{D}_{(c+j) \bmod 4} | Y_{2,i} = y_{2,i} + j\Delta_{21})$, for $0 \le i \le n-1$, $0 \le c, j \le 3$, and $(-2^R + 1.5)\Delta_{21} \le y_{2,i}, y_{2,i} + j\Delta_{21} \le (2^R - 1.5)\Delta_{21}$. Denote the trellis bit vector of $\mathcal{Q}_{21}$ as $\boldsymbol{m}_{21} = \{m_{21,0}, m_{21,1}, ..., m_{21,n-1}\}$, and the codeword vector $\mathbf{w}_{21} = \{w_{21,0}, w_{21,1}, ..., w_{21,n-1}\}$. Now if we directly transmit the trellis bit vector $\boldsymbol{m}_{21}$ using one b/s (since $\tilde{R} = 1$) without SW coding, the practical transmission rate R_{21} satisfies*

$$\begin{aligned} R_{21} &= 1 + \frac{1}{n} H(\mathbf{W}_{21} | \boldsymbol{M}_{21}, V_{21}^n) = 1 + \frac{1}{n} H(\mathbf{W}_{21} | \boldsymbol{C}_{21}, V_{21}^n) \\ &\le 1 + \frac{1}{n} \sum_{i=0}^{n-1} H(W_{21,i} | C_{21,i}, V_{21,i}) \\ &= 1 + \frac{1}{n} \sum_{i=0}^{n-1} \int_{-\Delta_{21}/2}^{\Delta_{21}/2} \frac{1}{\Delta_{21}} H(W_{21,i} | C_{21,i}, V_{21,i} = v_{21,i}) dv_{21,i}. \end{aligned} \tag{F.1}$$

Here $V_{21}^n = \{V_{21,i}\}_{i=0}^{n-1}$ is a length-n vector of i.i.d. random dithers, $\boldsymbol{C}_{21} = \mathbb{T}(\boldsymbol{M}_{21})$ is the coset index vector, and $C_{21,i} = \mathbb{T}_i(\boldsymbol{M}_{21})$ is the i-th coset index for $0 \le i \le n-1$.

Note that the conditional distribution of $Y_{2,i}$ given $C_{21,i}$ and $V_{21,i}$ completely determines the conditional entropy $H(W_{21,i} | C_{21,i}, V_{21,i} = v_{21,i})$ in (F.1). We have

$$p(Y_{2,i} = y_{2,i} | C_{21,i} = c_{21,i}, V_{21,i} = v_{21,i}) \tag{F.2}$$

$$= p(Y_{2,i} = y_{2,i} + v_{21,i} | C_{21,i} = c_{21,i}, V_{21,i} = 0) \tag{F.3}$$

$$= \frac{p(Y_{2,i} = y_{2,i} + v_{21,i}) \cdot P(C_{21,i} = c_{21,i} | Y_{2,i} = y_{2,i} + v_{21,i})}{P(C_{21,i} = c_{21,i})}. \tag{F.4}$$

An example of the conditional distribution $p(Y_{2,i} = y_{2,i}|C_{21,i} = c_{21,i}, V_{21,i} = v_{21,i})$ *is shown in Fig. 29.*

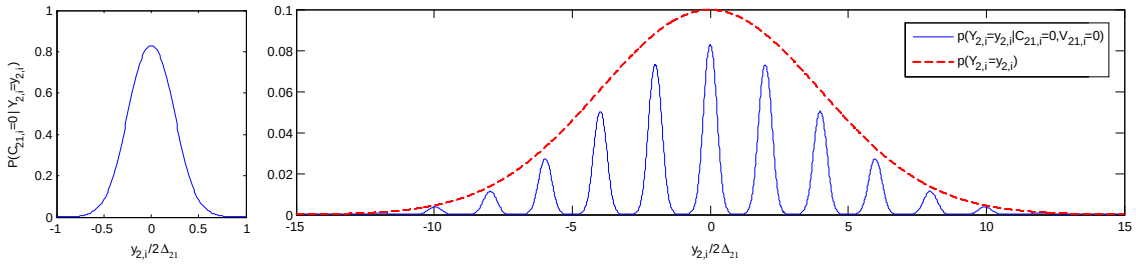

Fig. 29. Conditional distribution $p(Y_{2,i} = y_{2,i}|C_{21,i} = c_{21,i}, V_{21,i} = v_{21,i})$ *for* $c_{21,i} = 0$ *and* $v_{21,i} = 0$.

Next we consider the first WZ coding component which quantizes Y_1^n *and compresses the quantization output* $I_1 = \mathcal{Q}_1(Y_1^n)$ *to* R_1 *b/s. Let the ESS step size of the employed dithered TCQ be* Δ_1. *Similar to (F.1) and (F.4), we have*

$$\begin{aligned} R_1 &= 1 + \frac{1}{n} H(\mathbf{W}_1|\boldsymbol{M}_1, \hat{Z}_{21}^n, V_1^n) = 1 + \frac{1}{n} H(\mathbf{W}_1|\boldsymbol{C}_1, \hat{Z}_{21}^n, V_1^n) \\ &\le 1 + \frac{1}{n} \sum_{i=0}^{n-1} H(W_{1,i}|C_{1,i}, \hat{Z}_{21,i}, V_{1,i}) \\ &= 1 + \frac{1}{n} \sum_{i=0}^{n-1} \int_{-\Delta_1/2}^{\Delta_1/2} \frac{1}{\Delta_1} H(W_{1,i}|C_{1,i}, \hat{Z}_{21,i}, V_{1,i} = v_{1,i}) dv_{1,i}, \end{aligned} \tag{F.5}$$

$$\begin{aligned} & p(Y_{1,i} = y_{1,i}|C_{1,i} = c_{1,i}, \hat{Z}_{21,i} = \hat{z}_{21,i}, V_{1,i} = v_{1,i}) \\ = \; & p(Y_{1,i} = y_{1,i} + v_{1,i}|C_{1,i} = c_{1,i}, \hat{Z}_{21,i} = \hat{z}_{21,i}, V_{1,i} = 0) \\ = \; & \frac{p(Y_{1,i} = y_{1,i} + v_{1,i}|\hat{Z}_{21,i} = \hat{z}_{21,i}) \cdot P(C_{1,i} = c_{1,i}|Y_{1,i} = y_{1,i} + v_{1,i}, \hat{Z}_{21,i} = \hat{z}_{21,i})}{P(C_{1,i} = c_{1,i}|\hat{Z}_{21,i} = \hat{z}_{21,i})} \\ \overset{(\star)}{=} \; & \frac{p(Y_{1,i} = y_{1,i} + v_{1,i}|\hat{Z}_{21,i} = \hat{z}_{21,i}) \cdot P(C_{1,i} = c_{1,i}|Y_{1,i} = y_{1,i} + v_{1,i})}{P(C_{1,i} = c_{1,i}|\hat{Z}_{21,i} = \hat{z}_{21,i})}, \end{aligned} \tag{F.6}$$

where $V_1^n = \{V_{1,i}\}_{i=0}^{n-1}$ *is a length-*n *vector of i.i.d. random dithers, and* $(\star)$ *is true since the Markov chain* $\hat{Z}_{21,i} \to Y_{1,i} \to C_{1,i}$ *holds.*

Similar results can be obtained for the second WZ coding component which quantizes

Y_2^n and compresses the quantization output $I_{22} = \mathcal{Q}_{22}(Y_2^n)$ to R_{22} b/s:

$$R_{22} \leq 1 + \frac{1}{n}\sum_{i=0}^{n-1}\int_{-\Delta_{22}/2}^{\Delta_{22}/2}\frac{1}{\Delta_{22}}H(W_{22,i}|C_{22,i},\hat{Z}_{c,i},V_{22,i}=v_{22,i})dv_{22,i}, \tag{F.7}$$

$$\begin{aligned} & p(Y_{2,i}=y_{2,i}|C_{22,i}=c_{22,i},\hat{Z}_{c,i}=\hat{z}_{c,i},V_{22,i}=v_{22,i}) \\ = & \frac{p(Y_{2,i}=y_{2,i}+v_{22,i}|\hat{Z}_{c,i}=\hat{z}_{c,i})\cdot P(C_{22,i}=c_{22,i}|Y_{2,i}=y_{2,i}+v_{22,i},\hat{Z}_{c,i}=\hat{z}_{c,i})}{P(C_{22,i}=c_{22,i}|\hat{Z}_{c,i}=\hat{z}_{c,i})} \\ \overset{(\star\star)}{=} & \frac{p(Y_{2,i}=y_{2,i}+v_{22,i}|\hat{Z}_{c,i}=\hat{z}_{c,i})\cdot P(C_{22,i}=c_{22,i}|Y_{2,i}=y_{2,i}+v_{22,i})}{P(C_{22,i}=c_{22,i}|\hat{Z}_{c,i}=\hat{z}_{c,i})}, \end{aligned} \tag{F.8}$$

where $V_{22}^n = \{V_{22,i}\}_{i=0}^{n-1}$ is a length-n vector of i.i.d. random dithers, and $(\star\star)$ is true since the Markov chain $\hat{Z}_{c,i} \to Y_{2,i} \to C_{22,i}$ holds.

Equations (F.1) – (F.8) are based on the assumption of Σ-uniformity and are very difficult to compute in practice. However, at high rate, all the TCQ step sizes $\Delta_{21}, \Delta_1, \Delta_{22}$ tend to zero. Thus (see Fig. 29)

$$\begin{aligned} p(W_{21,i}=j|C_{21,i}=c_{21,i},V_{21,i}=v_{21,i}) &= p(Y_{2,i}+v_{21,i}\in\mathcal{W}_j|C_{21,i}=c_{21,i},V_{21,i}=v_{21,i}) \\ &\approx p(Y_{2,i}+v_{21,i}\in\mathcal{W}_j), \end{aligned} \tag{F.9}$$

where $\mathcal{W}_j = [(4j + c_i - 2^R + 0.5)\Delta_{21}, (4j + c_i + 2^R - 0.5)\Delta_{21}]$. Then

$$\begin{aligned} & H(W_{21,i}|C_{21,i}=c_{21,i},V_{21,i}=v_{21,i}) \\ = & \sum_{j=0}^{2^{R-1}} p(W_{21,i}=j|C_{21,i}=c_{21,i},V_{21,i}=v_{21,i})\log p(W_{21,i}=j|C_{21,i}=c_{21,i},V_{21,i}=v_{21,i}) \\ \rightsquigarrow & h(Y_{2,i}+v_{21,i}) - \log(4\Delta_{21}) \\ \rightsquigarrow & h(Y_{2,i}) - \log(4\Delta_{21}), \end{aligned} \tag{F.10}$$

where "$A \rightsquigarrow B$" means "A approaches B asymptotically", or $\lim_{\Delta_1\to 0,\Delta_2\to 0,\Delta_{21}\to 0}|A-B| = 0$.

On the other hand, assuming ideal SW coding in the sense that $\hat{Z}_{21}^n = Z_{21}^n$, due to the

definition of normalized second moment $G_{\mathcal{Q}_{21}}$, we have

$$d_{21} = \frac{1}{n}E(\|\hat{Z}_{21}^n - Y_2^n\|^2) = \frac{1}{n}E(\|Z_{21}^n - Y_2^n\|^2) = V^{2/n}G_{\mathcal{Q}_{21}} = (2\Delta_{21})^2 G_{\mathcal{Q}_{21}}. \tag{F.11}$$

Hence,

$$\begin{aligned} R_{21} &= 1 + \frac{1}{n}\sum_{i=0}^{n-1}\int_{-\Delta_{21}/2}^{\Delta_{21}/2}\frac{1}{\Delta_{21}}H(W_{21,i}|C_{21,i}=c_{21,i}, V_{21,i}=v_{21,i})dv_{21,i} \\ &\rightsquigarrow 1 + \frac{1}{n}\sum_{i=0}^{n-1}h(Y_{2,i}) - \log(4\Delta_{21}) \\ &\rightsquigarrow 1 + \frac{1}{2}\log(2\pi e\sigma_{y_2}^2) - \log(2\cdot\sqrt{d_{21}/G_{\mathcal{Q}_{21}}}) \\ &= \frac{1}{2}\log(\frac{\sigma_{y_2}^2}{d_{21}}) + \frac{1}{2}\log(2\pi e G_{\mathcal{Q}_{21}}). \end{aligned} \tag{F.12}$$

Similarly, we write

$$\begin{aligned} & p(W_{1,i}=j|C_{1,i}=c_{1,i}, \hat{Z}_{21,i}=\hat{z}_{21,i}, V_{1,i}=v_{1,i}) \\ = \; & p(Y_{1,i}+v_{1,i}\in\mathcal{W}_j|C_{1,i}=c_{1,i}, \hat{Z}_{21,i}=\hat{z}_{21,i}V_{1,i}=v_{1,i}) \\ = \; & \int_{\mathcal{W}_j}\frac{p(Y_{1,i}+v_{1,i}=\tau|\hat{Z}_{21,i}=\hat{z}_{21,i})\cdot P(C_{1,i}=c_{1,i}|Y_{1,i}=\tau)}{P(C_{1,i}=c_{1,i}|\hat{Z}_{21,i}=\hat{z}_{21,i})}d\tau \\ \approx \; & p(Y_{1,i}+v_{1,i}=\tau^*|\hat{Z}_{21,i}=\hat{z}_{21,i})\int_{\mathcal{W}_j}\frac{P(C_{1,i}=c_{1,i}|Y_{1,i}=\tau)}{P(C_{1,i}=c_{1,i})}d\tau \\ \approx \; & p(Y_{1,i}+v_{1,i}\in\mathcal{W}_j|\hat{Z}_{21,i}=\hat{z}_{21,i}). \end{aligned} \tag{F.13}$$

Then

$$
\begin{aligned}
& H(\mathbf{W}_{21,i}|C_i, \hat{Z}_{21,i}, V_{1,i} = v_{1,i}) \\
= & \int_{\mathbb{R}} \sum_{j=0}^{2^{R-1}} \Big[p(\mathbf{W}_{21,i} = j | C_i = c_i, \hat{Z}_{21,i} = \hat{z}_{21,i}, V_{1,i} = v_{1,i}) \\
& \qquad \cdot \log p(\mathbf{W}_{21,i} = j | C_i = c_i, \hat{Z}_{21,i} = \hat{z}_{21,i}, V_{1,i} = v_{1,i}) \Big] d\hat{z}_{21,i} \\
\rightsquigarrow & \int_{\mathbb{R}} \sum_{j=0}^{2^{R-1}} \Big[p(Y_{1,i} + v_{1,i} \in \mathcal{W}_j | \hat{Z}_{21,i} = \hat{z}_{21,i}) \log p(Y_{1,i} + v_{1,i} \in \mathcal{W}_j | \hat{Z}_{21,i} = \hat{z}_{21,i}) \Big] d\hat{z}_{21,i} \\
\rightsquigarrow & h(Y_{1,i} + v_{1,i} | \hat{Z}_{21,i}) - \log(4\Delta_1) \\
\rightsquigarrow & h(Y_{1,i} | \hat{Z}_{21,i}) - \log(4\Delta_1). \qquad \text{(F.14)}
\end{aligned}
$$

Hence

$$
\begin{aligned}
R_1 &= 1 + \frac{1}{n} \sum_{i=0}^{n-1} \int_{-\Delta_1/2}^{\Delta_1/2} \frac{1}{\Delta_1} H(\mathbf{W}_{21,i} | C_i, \hat{Z}_{21,i}, V_{1,i} = v_{1,i}) dv_{1,i} \\
&\rightsquigarrow \frac{1}{2} \log\left(\frac{\sigma^2_{Y_1|\hat{Z}_{21}}}{d_1}\right) + \frac{1}{2} \log(2\pi e G_{\mathcal{Q}_1}). \qquad \text{(F.15)}
\end{aligned}
$$

Similarly, R_{22} can be written as

$$
\begin{aligned}
R_{22} &= 1 + \frac{1}{n} \sum_{i=0}^{n-1} \int_{-\Delta_{22}/2}^{\Delta_{22}/2} \frac{1}{\Delta_{22}} H(\mathbf{W}_{22,i} | C_i, \hat{Z}_{c,i}, V_{22,i} = v_{22,i}) dv_{22,i} \\
&\rightsquigarrow \frac{1}{2} \log\left(\frac{\sigma^2_{Y_2|\hat{Z}_c}}{d_{22}}\right) + \frac{1}{2} \log(2\pi e G_{\mathcal{Q}_{22}}). \qquad \text{(F.16)}
\end{aligned}
$$

Finally, due to equations (B.9) and (B.10) in the proof of Theorems 2,

$$
\begin{aligned}
\frac{1}{2} \log\left(\frac{\sigma^2_{Y_1|\hat{Z}_{21}}}{d_1}\right) &\rightsquigarrow R_1^*, \\
\frac{1}{2} \log\left(\frac{\sigma^2_{y_2}}{d_{21}}\right) + \frac{1}{2} \log\left(\frac{\sigma^2_{Y_2|\hat{Z}_c}}{d_{22}}\right) &\rightsquigarrow R_2^*. \qquad \text{(F.17)}
\end{aligned}
$$

Therefore, (4.20) is true and the theorem proved.

APPENDIX G

PROOF OF THEOREM 7

Proof 12 *At high rate, there is no loss in transmitting the trellis bit-planes J_1^n and V_1^n using two b/s. Then the total transmission rate of our symmetric SWCQ scheme is $2 + \frac{1}{n}H(\mathbf{W}_1, \mathbf{W}_2|\boldsymbol{C}_1, \boldsymbol{C}_2, V_1^n, V_{21}^n)$ b/s. Now let (R_1', R_2') be one corner point of the sum-rate bound. By setting d_{22} to infinity, we have*

$$\begin{aligned} R_{21} + R_1 &= \left[1 + \frac{1}{n}H(\mathbf{W}_1|\boldsymbol{C}_1, V_{21}^n)\right] + \left[1 + \frac{1}{n}H(\mathbf{W}_2|\boldsymbol{C}_2, \hat{Z}_{21}^n, V_1^n)\right] \\ &= 2 + \frac{1}{n}H(\mathbf{W}_1, \mathbf{W}_2|\boldsymbol{C}_1, \boldsymbol{C}_2, V_1^n, V_{21}^n) \\ &= R_1' + R_2' + \frac{1}{2}\log(2\pi e G_{\mathcal{Q}_1}) + \frac{1}{2}\log(2\pi e G_{\mathcal{Q}_2}) + o(1) \\ &= R_1^* + R_2^* + \frac{1}{2}\log(2\pi e G_{\mathcal{Q}_1}) + \frac{1}{2}\log(2\pi e G_{\mathcal{Q}_2}) + o(1). \end{aligned} \tag{G.1}$$

Then the theorem readily follows.

VITA

Name	Yang Yang
Education	Doctor of Philosophy (August 2004 – December 2008)
	Major: Electrical Engineering
	Texas A&M University, College Station, TX 77843
	Master of Science (August 2002 – August 2004)
	Major: Electrical Engineering
	Texas A&M University, College Station, TX 77843
	Bachelor of Science (September 1998 – July 2002)
	Major: Electrical Engineering
	Tsinghua University, Beijing, P. R. China
Permanent address	Mail Box #316,
	Department of Electrical Engineering,
	Texas A&M University, College Station, TX 77843

The typist for this thesis was Yang Yang.